The role of metabolic enzymes in chromatin modifications and gene expression

Dissertation der Fakultät für Biologie

der Ludwig-Maximilians-Universität München

vorgelegt von

Anna Nieborak

München, 2020

This dissertation was completed at the Helmholtz Centre Munich

German Research Centre for Environment and Health (GmbH)

Institute of Functional Epigenetics

First examiner: Prof. Dr. Robert Schneider

Second examiner: Prof. Dr. Claude Becker

Date of submission: June 9, 2020

Date of oral examination: November 24, 2020

Eidesstattliche Erklärung

Ich versichere hiermit an Eides statt, dass die vorliegende Dissertation von mir selbstständig und ohne unerlaubte Hilfe angefertigt ist.

Erklärung

Hiermit erkläre ich, dass die Dissertation nicht ganz oder in wesentlichen Teilen einer anderen Prüfungskommission vorgelegt worden ist.
Ich erkläre weiter, dass ich mich anderweitig einer Doktorprüfung ohne Erfolg nicht unterzogen habe.

München, Juni 2020

_____

Anna Nieborak

Table of contents

Summary 1

Zusammenfassung 3

1. Introduction 5

1.1. Current definition of epigenetics 5

1.2. Chromatin architecture and dynamics 5
1.2.1. Historic overview of chromatin research 5
1.2.2. Nucleosome and higher order of eukaryotic chromatin 6
1.2.3. Role of histone post-translational modifications in chromatin functions 9
1.2.4. Role of DNA methylation in gene expression 12

1.3. Small metabolites are cofactors of chromatin modifications 13
1.3.1. Acetyl-CoA as the central player in histone acetylation 14
1.3.2. NAD^+-dependent chromatin modifications 16
1.3.3. Metabolic regulation of DNA and histone methylation 18
1.3.4. Roles of TCA cycle metabolites in chromatin methylation 21

1.4. Nuclear functions of metabolic enzymes 22

2. Aims of the study 24

3. Results 25

3.1. Establishing the system to investigate the effect of 'chromatin microdomains' by tethering the selected metabolic enzymes to the gene promoters 25
3.1.1. Designing dCas9-enzyme constructs 25
3.1.2. Testing gRNAs targeting various promoters in HEK293 cells 26
3.1.3. The effect of the presence of active metabolic enzyme at the promoter on the transcription of a downstream gene 28

3.2. Detecting the histone modifying activity co-purified with selected metabolic enzymes 33
3.2.1. Designing the MBP- and FLAG-2HA-enzyme constructs and expression tests in bacterial and mammalian systems 33
3.2.2. In vitro histone methyltransferase and acetyltransferase assays 35

3.3. Investigating the changes in histone PTMs and gene expression upon the depletion of selected metabolic enzymes 37
3.3.1. Establishing the protocol for efficient delivery of shRNA constructs using lentiviral systems 37
3.3.2. Validation of knockdown efficiency using shRNA constructs targeting selected metabolic enzymes 40
3.3.3. Analysis of histone PTMs in stable knockdown cell lines 42
3.3.4. Analysis of cytosine modifications in genomic DNA of stable knockdown cell lines 44
3.3.5. Targeted metabolomic profiling of selected knockdown cell lines 45
3.3.6. Genomic mapping of changes in histone PTMs 48
3.3.6.1. Validation of antibodies 49
3.3.6.2. Spike-in optimisation 51
3.3.6.3. ChIP-seq and RNA-seq analysis 53
3.3.7. PKM2 knockdown affects the expression of genes involved in oxidative stress response 56
3.3.7.1. Isoforms and oligomerisation state of *PKM* encoded proteins 56
3.3.7.2. PKM2 knockdown affects genes associated with oxidative stress 58
3.3.7.3. Upregulation of *TXNIP* and *ARRDC4* but not *DHRS2* in PKM2 knockdown can be mediated by MondoA : MLX transcription factors 60
3.3.7.4. *DHRS2* expression is induced by prolonged oxidative stress 62
3.3.7.5. Short-term depletion of PKM2 induces *TXNIP* but not *DHRS2* 64

3.4. Identification of nuclear interacting partners of investigated metabolic enzymes 65

4. Discussion 70

4.1. Localisation of metabolic enzymes at gene promoters promotes transcription 70

4.2. BHMT2 can interact with histone H3 methyltransferase 72

4.3. Potential role of MAT2A/B in RNA methylation 73

4.4. Identification of metabolic enzymes affecting histone PTM patterns 75

4.5. Depletion of ACSS2, MAT2B, PCCA and PKM2 affects DNA modifications 79

4.6. Depletion of ACSS2, PCCA and PKM2 change metabolic status of a cell 80

4.7. The link between PKM2 and oxidative stress response 83
4.7.1. Depletion of PKM2 in HEK293 cells affects its glycolytic function 83
4.7.2. Depletion of PKM2 correlates with upregulation of genes involved in redox balance 84
4.7.3. Upregulation of *TXNIP* and *ARRDC4* in PKM2 knockdown is mediated by MondoA : MLX transcription factors 85
4.7.4. Proposed mode of action of PKM2 knockdown 86

5. Materials 89

5.1. Bacterial strains 89

5.2. Cell lines 89

5.3. Guide RNA (gRNA)-encoding sequences 89

5.4. The RNAi consortium clone numbers (TRCN) 90

5.5. OriGene stock keeping unit (SKU) of synthetic open reading frames (ORFs) 90

5.6. Primer sequences 91
5.6.1. Primers for cloning 91
5.6.2. Primers for RT-qPCR 92
5.6.3. Primers for ChIP-qPCR 93

5.7. Antibodies 93

5.8. Buffers and solutions 94

5.9. Chemicals 97

6. Methods 100

6.1. Molecular biology methods 100
6.1.1. Heat shock transformation of chemically competent *E. coli* 100
6.1.2. Polymerase chain reaction (PCR) 100
6.1.2.1. Standard PCR 100
6.1.2.2. Quantitative PCR (qPCR) 101
6.1.3. Cloning 102
6.1.3.1. gRNA cloning 102
6.1.3.2. Site-directed mutagenesis 103
6.1.3.3. Gibson Assembly 105
6.1.4. Agarose gel electrophoresis 105
6.1.5. Sanger sequencing of purified DNA molecules 105

6.2. Biochemical methods 106
6.2.1. Dual luciferase assay 106
6.2.2. Preparative recombinant protein production in bacterial expression system 106
6.2.3. HeLa nuclear extract preparation 107
6.2.4. HEK293 nuclear fraction preparation 108
6.2.5. Quantification of protein concentration by Roti Nanoquant 109
6.2.6. Immunoprecipitation from nuclear fraction 109
6.2.7. RIPA total cell lysate preparation 110
6.2.8. Sodium dodecyl sulfate-polyacrylamide gel electrophoresis (SDS-PAGE) 110
6.2.9. Protein staining with Coomassie Brilliant Blue 111
6.2.10. Immunostaining (Western Blotting) 111

6.2.11. Co-purification of the histone writing activity from HeLa nuclear fraction with MBP-enzyme fusions 112
6.2.12. In vitro methyltransferase assay 112
6.2.13. Chromatin immunoprecipitation (ChIP) 113
6.2.13.1. Blocking protein A / protein G-coupled beads for ChIP-qPCR 113
6.2.13.2. Blocking protein A / protein G-coupled beads for ChIP-seq 114
6.2.13.3. Preparation of chromatin from HEK293 114
6.2.13.4. Preparation of *Drosophila* chromatin 115
6.2.13.5. Immunoprecipitation 116
6.2.14. Preparing ChIP samples for Next Generation Sequencing (NGS) 117
6.2.14.1. DNA library preparation 117
6.2.14.2. Size selection of DNA fragments 118
6.2.15. Preparing RNA samples for Next Generation Sequencing (NGS) 118
6.2.16. Preparation of genomic DNA for MS analysis 119
6.2.17. Intracellular crosslinking with disuccinimidyl suberate (DSS) 120

6.3. Cell culture methods 120
6.3.1. Eukaryotic cell growth conditions 120
6.3.2. Human cell standard transfection with plasmid DNA – small scale 121
6.3.3. Human cell transfection with plasmid DNA – large scale 122
6.3.4. Coating cell growth surface with poly-L-lysine 122
6.3.5. Lentiviral vector production using LENTI-Smart (Invivogen) 123
6.3.6. Human cell transduction with lentiviral particles 124
6.3.7. Harvesting cells for metabolomic analysis 124
6.3.8. siRNA transfection of human cells 125
6.3.9. Measurements of extracellular acidification rate (ECAR) and oxygen consumption rate (OCR) 126

7. Abbreviations 128

8. Acknowledgements 132

9. Bibliography 133

10. Curriculum Vitae 143

Summary

The eukaryotic genome is organised in the nucleus in a dynamic structure defined as chromatin, composed mainly of DNA and histone proteins. Alterations in chromatin architecture are crucial for many cellular processes such as transcription, DNA replication and DNA repair. Epigenetic mechanisms that enable cells to receive, respond to, and transmit information involve, to a large extent, post-translational modifications of histones and modifications of DNA. These marks can influence chromatin structure per se and serve as binding platforms for the downstream effector machineries. Each of these epigenetic modifications is a result of the activity of an enzyme that utilises one of several crucial metabolites during catalysis. Similarly, the removal of these marks also requires different metabolic intermediates. As a result, modifications of chromatin have the capacity of integrating the metabolic status of the cell, manifested by intracellular pools of various metabolites, with chromatin architecture and functions.

In this study I present different approaches to investigate the roles of metabolic enzymes involved in generation and conversion of epigenetically relevant metabolites in the context of chromatin. In the first approach, by tethering active and inactive metabolic enzymes to the gene promoter, I showed that the presence of acetyl-CoA synthetase ACSS2, betaine-homocysteine transferase BHMT2, fumarate hydratase FH and isocitrate dehydrogenase IDH2 at promoter regions positively affects transcriptional output. Secondly, in pull-down experiments in vitro I identified a metabolic enzyme as a novel putative interactor of a histone H3 methyltransferase. In the third approach I identified ACSS2, a regulatory subunit of methionine adenosyltransferase MAT2B, a subunit of propionyl-CoA carboxylase PCCA and the

pyruvate kinase PKM2 as important factors involved in establishment of various histone and DNA modifications. Using stable knockdown cell lines, I characterised changes in the transcriptome, genomic distribution of histone modifications and the profiles of multiple metabolites relevant for DNA and histone modifications in the cell lines with depletions of these enzymes. Based on these results I was able to suggest a potential link between global changes of metabolites and observed alterations in DNA modifications as well as propose a model of regulation of oxidative stress response caused by the depletion of PKM2. Moreover, using MS-based proteomics I identified putative nucleolar interactors of MAT2B and suggested a possible novel role of MAT2 in regulating rRNA maturation.

Altogether, I performed a thorough screening of metabolic enzymes whose activities can be essential factors in regulation of gene expression. The results of my thesis expand the current understanding of the links between metabolism, epigenetics and gene expression in human cells.

Zusammenfassung

Das eukaryotische Genom wird im Zellkern in einer dynamischen Struktur organisiert, die als Chromatin definiert ist und hauptsächlich aus DNA und Histonproteinen besteht. Änderungen in der Chromatinarchitektur sind entscheidend für viele zelluläre Prozesse wie etwa die Transkription, DNA-Replikation und DNA-Reparatur. Epigenetische Mechanismen, die posttranslationale Modifikationen von Histonen und DNA Modifikationen umfassen, ermöglichen es den Zellen extrazelluläre Informationen zu empfangen, darauf zu reagieren und sie zu übertragen. Diese Modifikationen können die Chromatinstruktur an sich beeinflussen und dienen aber auch als Bindungsplattformen für die nachgeschalteten Effektor-Maschinerien. All diese epigenetischen Modifikationen beruhen auf der Aktivität von Enzymen, die einen bestimmten Metaboliten als Substrat nutzen. In ähnlicher Weise erfordert das Entfernen dieser Markierungen verschiedene metabolische Zwischenprodukte.
Infolgedessen haben Modifikationen des Chromatins die Fähigkeit den zellulären Stoffwechselstatus, der sich in intrazellulären Pools verschiedener Metaboliten manifestiert, in die Chromatinarchitektur und -funktion zu integrieren.

In dieser Studie stelle ich verschiedene Ansätze vor, um die Rolle von metabolischen Enzymen bei der Erzeugung und Umwandlung epigenetisch relevanter Metaboliten im Kontext von Chromatin zu untersuchen. Im ersten Ansatz zeigte ich, dass die Rekrutierung der Acetyl-CoA-Synthetase ACSS2, der Betain-Homocystein-Transferase BHMT2, der Fumarat-Hydratase FH und der Isocitrat-Dehydrogenase IDH2 zu Promoterregionen die Transkriptionsleistung positiv beeinflusst. Zweitens identifizierte ich mittels in-vitro-Bindungsstudien ein metabolisches Enzym als neuen mutmaßlichen Interaktor einer Histon-H3-Methyltransferase. Im dritten Ansatz

identifizierte ich ACSS2, MAT2B – eine regulatorische Untereinheit der Methionin-Adenosyltransferase, PCCA – eine Untereinheit der Propionyl-CoA-Carboxylase und die Pyruvatkinase PKM2, als wichtige Faktoren, die an der Etablierung verschiedener DNA- und Histonmodifikationen beteiligt sind. Unter Verwendung stabiler Knockdown-Zelllinien, die eine Depletion dieser Enzyme aufweisen, charakterisierte ich Veränderungen im Transkriptom, der genomischen Verteilung verschiedener Histonmodifikationen und der Profile mehrerer Metabolite, die für DNA- und Histonmodifikationen relevant sind. Durch diese Ergebnisse konnte ich einen möglichen Zusammenhang zwischen den globalen Veränderungen verschiedener Metabolite und Veränderungen der DNA-Modifikationen feststellen. Weiterhin konnte ich ein Modell entwickeln, das beschreibt, wie die Reaktion auf oxidativen Stress durch die Depletion von PKM2 reguliert wird. Darüber hinaus identifizierte ich mithilfe von MS-basierter Proteomik mutmaßliche nukleolare Interaktoren von MAT2B und schlug eine mögliche neue Rolle von MAT2 bei der Regulierung der rRNA-Reifung vor.

Insgesamt führte ich ein umfassendes Screening von metabolischen Enzymen durch, die durch ihre Aktivitäten wesentlichen Anteil an der Regulation der Genexpression haben können. Die Ergebnisse meiner Arbeit erweitern das aktuelle Verständnis der Zusammenhänge zwischen Metabolismus, Epigenetik und Genexpression in menschlichen Zellen.

1. Introduction

1.1. Current definition of epigenetics

In early 1940s Conrad Waddington introduced the term ‘epigenetics’ defining it as ‘the branch of biology which studies the causal interactions between genes and their products which bring the phenotype into being’ [1], [2]. The meaning of ‘epigenetics’ evolved over the decades and while the discussion about the correct definition of it has not been closed, it is currently widely accepted in the scientific community to define ‘epigenetics’ as ‘the study of changes in gene function that are mitotically and / or meiotically heritable and that do not entail a change in DNA sequence’ [3]. In line with this definition, the wide body of current literature concerning mechanisms of aforementioned changes narrowed the term ‘epigenetic modifications’ mainly to covalent modifications of DNA and histone proteins.

1.2. Chromatin architecture and dynamics

1.2.1. Historic overview of chromatin research

The term ‘chromatin’ was proposed by Walther Flemming at the end of the 19th century as a name given to the stainable material within nuclei isolated from eukaryotic cells [4], [5]. The groundwork for the characterisation of the components of chromatin was laid approximately at the same time. In 1871 Friedrich Miescher described a phosphorus-rich acidic component of chromatin and called it ‘nuclein’ [5], [6]. Only several years later Albrecht Kossel defined the ‘histon’ (now ‘histone’) – proteinaceous structure that composes chromatin together with the acidic part previously

characterised by Miescher [5], [7]. The first half of the 20th century was the time of seminal discoveries in genetics, one of which was work of Oswald Avery, Colin MacLeod and Maclyn McCarty. They identified DNA as a carrier of genetic information, fully changing then anticipated notion that this function is assigned to proteins [8]. Since that discovery, it was speculated that histones perform merely a repressive role in gene expression. These suggestions were refined after a breakthrough discovery of Vincent Allfrey and Albert Mirsky who first described and correlated histone lysine (K) acetylation with gene transcription [9]. This suggested that histones are not only the structural scaffold for chromatin DNA but are involved in the regulation of gene expression and gave rise to the new field of research focused on numerous histone modifications. Following studies by Ada Olins and Donald Olins used advances of electron microscopy to show that chromatin is formed from repetitive subunits, later named 'nucleosomes' [10]. In 1980s the first crystal structure of the nucleosome core particle was determined [11]. Up until now, technological advances of the 21st century allowed to solve the structure of nucleosome core particle with the resolution of 2.4 Å [12].

1.2.2. Nucleosome and higher order of eukaryotic chromatin

A single copy of a human genome contains ~3.1 x 10^9 base pairs (bp) of DNA. The total length of linearised DNA from one human cell can reach 2 m. The fact that this DNA needs to be accommodated in a cell nucleus of a typical diameter ranging between 2 μm – 10 μm imposes the necessity to highly compact the genetic material of a cell. While tightly packed in a nucleus, particular fragments of the chromatin have to either (i) stay in a constantly active / repressed state or (ii) be able to adjust their transcription activity in response to the plethora of stimuli in order to sustain cellular

homeostasis. This tight regulation of gene expression is possible due to the highly ordered structure of chromatin. Nucleosomes, a structure consisting of 147 bp-long stretches of DNA wrapped around core histone octamers, represent the first level of chromatin organisation.

Histones are small, alkaline proteins highly evolutionary conserved in all eukaryotes what highlights that these proteins serve critical functions [13]. They can be broadly classified as core histones (H2A, H2B, H3, H4) and linker histones (H1). Core histones form two types of heterodimers: H2A-H2B and H3-H4, two copies of each form a complete histone octamer (Figure 1.1 a). Each core histone consists of (i) a globular domain with α-helical region forming a 'histone fold' motif facilitating interactions between histones within the relevant heterodimer and (ii) N- and C-terminal unstructured flexible tails protruding from the core of nucleosome [14], [15]. The lateral surface of a disk-shaped histone octamer is lined with positively charged amino acids that by interacting with the negatively charged DNA let it use the histone octamer as a 'spool' around which DNA is wrapped forming a nucleosome core particle [14]. Histones H1 can bind and protect the linker DNA close to the nucleosome entry-exit site that contributes to formation of the higher order of chromatin structure (Figure 1.1 b).

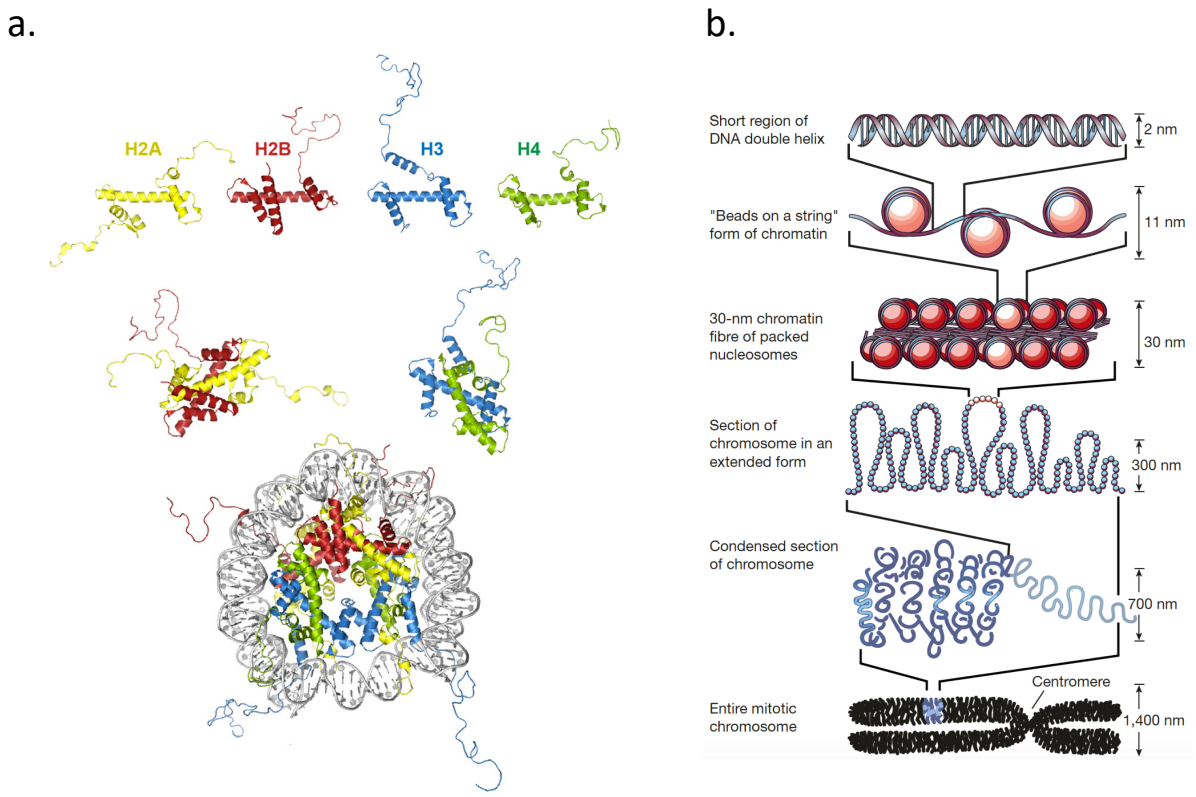

Figure 1.1 Hierarchical structure of chromatin; **a.** Model of nucleosome reconstructed from the crystal structure. Top: separate histone molecules with indicated α-helical 'histone folds'; Middle: H2A-H2B and H3-H4 heterodimers; Bottom: Histone octamer with two turns of DNA (in grey) wound around it. Figure adapted and modified from [16]; **b.** Increasing levels of DNA compaction within the chromatin structure. The lowest level is a nucleosome. Multiple nucleosomes are connected by short stretches of linker DNA (histones H1 are not shown). At the next level of organisation, the string of nucleosomes is folded into a fibre about 30 nm in diameter, these fibres are further folded into higher-order structures. The details of folding are uncertain at levels of structure beyond the nucleosome. Figure adapted from [17].

Arrangement of repetitive nucleosomes constitutes the first level of chromatin compaction forming a structure ~10 nm in width, resembling 'particles on a string' [10]. The next level of compaction is achieved by formation of ~30-nm-wide chromatin fibres. While the existence of these fibres is unquestionable, the exact structure and mechanisms of formation in vivo still remain elusive [18]. 30-nm fibres can be further condensed reaching the highest level of compaction during mitotic division. In the interphase of a cell cycle chromatin is not compacted uniformly. It can form highly condensed heterochromatin, generally devoid of protein coding genes, and looser, less compacted euchromatin more accessible to transcriptional machinery and thus, rich in protein coding genes [19], [20].

1.2.3. Role of histone post-translational modifications in chromatin functions

Histone post-translational modifications (PTMs) are usually small chemical groups covalently attached to various amino acid residues by enzymes broadly referred to as histone 'writers'. Most histone PTMs are reversible and can be removed by so-called 'erasers'. These modifications have been implicated in establishing different chromatin states and thus in regulation of chromatin-related processes e.g. gene expression, DNA replication and DNA repair [21]–[26]. The most extensively studied histone modifications are acetylation, methylation, phosphorylation and ubiquitination [26]–[29]. However, due to advances in mass spectrometry (MS) methods, in the last decades many novel modifications have been identified and most probably, the list of histone PTMs that we currently know is not complete [30]–[35].

Histone lysine acetylation is generally associated with active gene transcription and the activity of some histone acetyltransferases (HATs) was proved necessary for the gene transcription to occur [36], [37]. In general, acetylated histones shift the structure of chromatin towards more open conformation. This can be achieved either by changing the physical structure of the chromatin by the PTMs themselves or by recruiting additional factors that affect the dynamics and structure of chromatin. Among histone PTMs directly affecting chromatin structure, histone H4 acetylated at lysine 16 (H4K16ac) is so far the only acetylation mark on the histone tail that affects the compaction of nucleosomal arrays in vitro [38]. Acetylation of histones within their globular domains was shown to affect nucleosome stability, promote histone eviction and stimulate transcription in chromatin assembled in vitro [39], [40]. The majority of functions of acetylation within N-terminal histone tails are exerted by the additional

proteins (‘readers’), interacting with histones usually via acetyl-lysine binding bromodomains [41].

Protein methylation can occur on lysine, arginine and histidine residues but in histones, methylation of histidine is very rare. Lysine residues can be mono-, di- and trimethylated on their ε-amino groups and arginine residue can be mono- and symmetrically or asymmetrically di- methylated on their guanidyl group [42], [43]. The most extensively studied histone methylation sites include H3K4, H3K9, H3K27, H3K36, H3K79, H4K20, H3R2, H3R8, H3R17 and H4R3 [25], [28]. The function of histone methylation and the role it plays in gene expression depends both on the site that carries this PTM and the number of methyl groups attached to the modified residue. For example, monomethylation of histone H3 at lysine 4 (H3K4me1) is a chromatin signature of enhancers while H3K4me3 is highly enriched on active promoters [44], [45]. Adding to the complexity, the combinatorial patterns of histone methylation can mark different elements in chromatin e.g. poised enhancers characterised by co-occurrence of H3K4me1 and H3K27me3 or bivalent domains that silence genes while keeping them poised for activation, enriched in H3K27 and H3K4 methylations [46]–[48].

Methylation at H3K27 is very abundant. In mouse embryonic stem cells (mESC) around 50% of all H3K27 residues are dimethylated, 10-20% are trimethylated and 20% monomethylated [49]. H3K27me1 is associated with gene bodies of transcriptionally active genes and correlates with H3K36me3 that is a widely known mark of intragenic regions [50]. H3K27me3 is generally a mark of facultative heterochromatin linked to gene-specific silencing. Notably, in mESC this PTM was also assigned to bivalent promoters [51]. While the mechanism of establishing H3K27me1

mark remains elusive, di- and trimethylation of H3K27 is achieved through the action of EZH1 and EZH2 – two mutually exclusive enzymatic subunits of PRC2 complex [52], [53]. How PRC2 is initially recruited to chromatin is not clear. One of the models of this recruitment suggests that it is mediated by the additive effects of various weak interactions between multiple subunits of the PRC2 complex and chromatin components, including direct binding to DNA, interactions with long non-coding RNA (lncRNA), binding to histones and histone PTMs [54], [55]. Once PRC2-mediated di- and trimethylation of H3K27 is established, WD40 repeat domain of PRC2 structural subunit EED specifically binds H3K27me3 and thus provides an elegant model of propagation of this modification [56].

Di- and trimethylated H3K9 (H3K9me2/3) is found in transcriptionally inactive constitutive heterochromatin, such as pericentromeric and telomeric regions, both rich in repetitive elements [57]–[60]. In mammalian cells these PTMs are established by members of SET-domain containing family of proteins: SETDB1, GLP and G9a are responsible for mono- and dimethylation of H3K9 and SUV39H1 and SUV39H2 establish di- and trimethylated state of that residue [61]–[64]. H3K9me2/3 is bound by chromodomain of heterochromatin protein 1 (HP1) that subsequently recruits chromatin modifiers and leads to heterochromatin spreading [65]. Since HP1 interacts, among others, with SUV39H, a positive feedback loop of H3K9 methylation mediated by HP1 binding provides propagation of H3K9me2/3 to adjacent nucleosomes. Even though H3K9me2/3 is mainly studied in the context of constitutive heterochromatin, genome-wide mapping studies reported the role of this PTM also in cell type-specific regulation of gene silencing [66].

The catalogue of histone PTMs is ample and is continuing to expand. While the knowledge of roles of single modifications highly contributed to the current state of knowledge about chromatin structure and functions, it is well accepted that histone modifications do not act by themselves and their function must be investigated in a specific context. Due to the growing number of genome-wide studies, new chromatin functions are being assigned to the combinations of previously characterised modifications and thus shed more light to the global epigenetic regulation.

1.2.4. Role of DNA methylation in gene expression

Enzymatic methylation of DNA and RNA was discovered in the second half of the 20th century and since then, DNA hyper- and hypomethylation of particular genes have been correlated with their altered expression and occurrence of various cancers [67]–[69]. In all organisms where DNA methylation was reported, presence of this mark in promoter regions negatively correlates with gene expression [70]. In DNA, methyl group can be transferred to the C-5 position of pyrimidine ring of cytosine (5-mC) by DNA methyltransferases (DNMTs). Mammalian DNMTs can be broadly classified as de novo and maintenance methyltransferases. DNMT3A and DNMT3B are responsible for establishing de novo methylation patterns in early embryo development [71], [72]. Conversely, DNMT1 is a major enzyme in maintenance of the stable DNA methylation pattern after DNA replication [73]. For a long time, DNA methylation was considered enzymatically irreversible and the loss of 5-mC was anticipated to happen through ‘passive dilution’ upon DNA replication and DNA repair processes. The discovery of Tet-eleven translocation (TET) enzymes refined our current understanding of the 5-mC dynamics and showed that methyl group can be actively removed from DNA. Cytosine demethylation occurs in a series of iterative conversions of 5-mC to

5-hydroxymethylcytosine (5-hmC), 5-formylcytosine (5-fC) and 5-carboxycytosine (5-caC) that is subsequently removed via base excision repair (BER). Apart from being merely intermediate products of DNA demethylation, 5-hmC and 5-fC were suggested to be functional modifications. 5-hmC was reported to be enriched in gene bodies of active genes associated with neuronal differentiation [74]. Genome-wide mapping of 5-fC revealed its enrichment in active enhancers while structural studies suggested that this modification can retard polymerase II and thus, affect gene transcription [75]. The functional role of 5-caC remains elusive.

1.3. Small metabolites are cofactors of chromatin modifications

Covalent modifications of two main composites of eukaryotic chromatin, histones and DNA, are the key players in chromatin structure and function. Therefore, the abundance and activity of enzymes responsible for their placing and removal can constitute an essential factor regulating gene expression. Discovering mechanisms of action of various chromatin writers and erasers made it evident that to perform their role these enzymes require small metabolites generated in multiple cellular metabolic pathways. These metabolites play a role of cofactors (cosubstrates if they provide a group covalently attached to the chromatin component) or inhibitors of chromatin modifiers. Metabolic state of the cells is a resultant of availability of nutrients, presence of external stimuli and their intrinsic metabolic activity. Altogether this state is reflected by sets of metabolites whose abundance can affect chromatin modifiers and thus provide a link between metabolic status of a cell and chromatin modifications as well as gene expression (Figure 1.2).

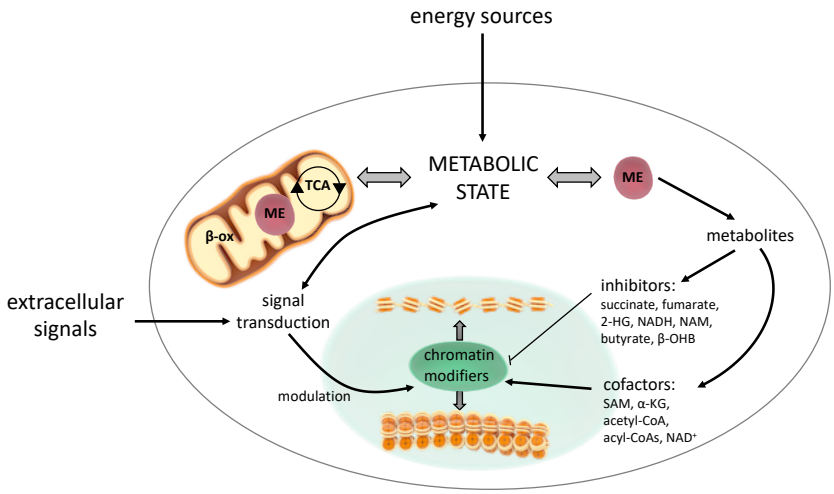

Figure 1.2 The crosstalk between metabolism and chromatin modifications. Cell supplied with external energy sources establishes a metabolic state shaped by metabolic enzymes (ME) that generate intermediary metabolites. These intermediates serve as cofactors and inhibitors of chromatin modifiers – hubs collecting intra- and extracellular signals – transferring information about the metabolic state to the chromatin level and affecting transcriptional events; TCA – tricarboxylic acid cycle; β-ox – β-oxidation; Figure adapted from [76]

1.3.1. Acetyl-CoA as the central player in histone acetylation

All HATs (as well as other lysine acetyltransferases), use acetyl-coenzyme A (acetyl-CoA) as a donor of acetyl groups for histone acetylation. Michaelis constant (K_m) of many HATs lies within the intracellular concentration of their cofactor making them attractive candidates for sensitive sensors of fluctuations of cellular acetyl-CoA [77], [78]. Notably, the side product of acetylation reaction, coenzyme A (CoA), serves as a competitive inhibitor of HATs, therefore it is not merely acetyl-CoA but rather acetyl-CoA : CoA ratio that determines the overall HAT activity. Acetyl-CoA is a central metabolic intermediate ‘collecting’ the information about the energetic status of a cell [79]. It is involved in many metabolic pathways including: energy production by bridging glycolysis and tricarboxylic acid (TCA) cycle through the activity of pyruvate dehydrogenase (PDH), fatty acid and steroid metabolism, catabolism of branched-chain amino acids (BCAA), synthesis of ketone bodies and

neurotransmitters [80]–[83]. Acetyl-CoA is mainly produced in mitochondria and subsequently exported to the cytosol in a form of citrate by a citrate-malate shuttle [84]. In the cytosol, citrate is re-converted to acetyl-CoA by ATP-citrate lyase (ACL). An alternative way of generation nucleocytosolic pool of acetyl-CoA is the activity of acetyl-CoA synthetase (ACSS2). It has been shown that depletion of acetyl-CoA-generating enzymes have impact on histone PTMs, however the exact residue that is affected by such metabolic perturbations can be cell line- or tissue-dependent. For example, knockdown of ACSS2 in murine neuronal cells leads to decreased acetylation of H3K9 and H3K27 [85]. In line with that, in human cells lines depletion of the E1α subunit of PDH or ACL affects global H2B, H3 and H4 acetylation [86], [87]. Even though acetyl-CoA can freely diffuse through nuclear pores, the plethora of pathways it can be used in can make such transport less efficient. Under certain cellular conditions, cytosolic ACL and ACSS2 can be translocated to the nucleus and provide a local supply of acetyl-CoA for histone acetylation [85], [87]. A striking evidence that all subunits of pyruvate dehydrogenase complex (PDC) can translocate from mitochondria to nucleus and re-establish enzymatically active complex, underlies the crucial role of in situ generated acetyl-CoA in the context of histone acetylation [86].

The impact of global fluctuations of acetyl-CoA has been thoroughly studied in budding yeast that, when grown in a chemostat with limited glucose, oscillate synchronously between oxidative (OX), reductive-building (RB) and reductive-charging (RC) phase collectively known as yeast metabolic cycle (YMC) [88]. Oscillations in intracellular acetyl-CoA follow the phases of YMC and reach the highest level at the transition from OX to RB. Of note, acetylation of multiple histone lysine residues mirrors the pattern of acetyl-CoA fluctuations. Global abundance of acetyl-CoA in mammalian cells does

not change periodically. However, it can drastically alter depending on the developmental stage and also in pathological state. Oncogenic metabolic reprogramming involving Akt kinase mediates the increase in cellular acetyl-CoA and globally affects H3 and H4 acetylation [89]. In mESC, due to the higher activity of threonine dehydrogenase (Tdh) the abundance of acetyl-CoA is significantly increased relative to embryoid bodies but so far the influence of that on histone modifications has not been investigated [90]. Altogether these discoveries implicate acetyl-CoA metabolism as one of the crucial factors regulating histone acetylation.

1.3.2. NAD^+-dependent chromatin modifications

Nicotinamide adenine dinucleotide is a redox cofactor that can exist in the oxidised and reduced form, NAD^+ and NADH respectively. NAD^+ is involved in catabolic processes that involve action of various dehydrogenases e.g. glycolysis, β-oxidation and catabolic TCA cycle activity. Electrons from different intermediates reduce NAD^+ to NADH which serves to supply mitochondrial electron transport chain and thus promote oxidative phosphorylation and ATP production. However, NAD^+ has also additional, chromatin related functions apart from its well-established role in cellular respiration.

Histone acetylation is a modification that can be enzymatically removed by histone deacetylases (HDACs) [91]. In humans there are at least 18 HDACs broadly grouped into 4 classes. Only one of them, class III named sirtuins after the yeast homologue protein Sir2, deacetylates histones in an NAD^+-dependent manner [92]. Another nuclear function of NAD^+ is linked to the activity of poly-ADP-ribose polymerases (PARPs) who use it as a co-substrate of ADP-ribosylation. By cleaving a bond between

nicotinamide and ADP-ribose, PARPs form a branched polymer of ADP-ribose at their target substrate. PARP1, the main consumer of cellular NAD^+, is sensitive to DNA damage and upon activation, extensively poly(ADP-ribosyl)ates itself, together with histones and other chromatin-associated proteins [93]–[96]. It is unlikely that these two predominant nuclear NAD^+-dependent activities compete for the availability of a common cofactor. In fact, K_m of PARP1 for NAD^+ is substantially lower than its nuclear concentration meaning that PARP1 is not a substrate-limited enzyme [97], [98]. However, it can effectively modulate the availability of NAD^+ to sirtuins and PARP2 and thus affect the activity of these enzymes [97], [99].

Production of NAD^+ in mammals can occur through de novo synthesis from tryptophan or via recycling of nicotinamide (NAM) – product of NAD^+-consuming enzymes (Figure 1.3 a). In a recycling salvage pathway NAM is first converted to nicotinamide mononucleotide (NMN) by the rate-limiting enzyme of the cycle – nicotinamide phosphoribosyltransferase (NAMPT), and subsequently to NAD^+ by nicotinamide mononucleotide adenylyltransferase (NMNAT). It was shown that the enzymes involved in the salvage pathway affect SIRT1 activity by regulating NAD^+ recycling. Knockdown of NAMPT in human vascular smooth muscle cells decreases their lifespan due to the impaired activity of SIRT1 [100]. Of note, the impact of nuclear NAD^+ production on histone acetylation was also reported. Global gene expression analyses in human MCF-7 cell line led to the identification of a group of genes commonly regulated by the exclusively nuclear isoform NMNAT1 and SIRT1. SIRT1-dependent recruitment of both enzymes to the promoters of these genes was shown to affect H4K16ac levels [101].

There are many lines of evidence suggesting that NAD^+ is one of the key molecules transferring information about metabolic status of a cell to chromatin. Variety of pathways this metabolite is involved in, together with metabolic modulation of inhibitors of NAD^+-utilising enzymes indicate that NAD^+ is a potential 'master regulator' of gene expression patterns established by the overall metabolic status of a cell.

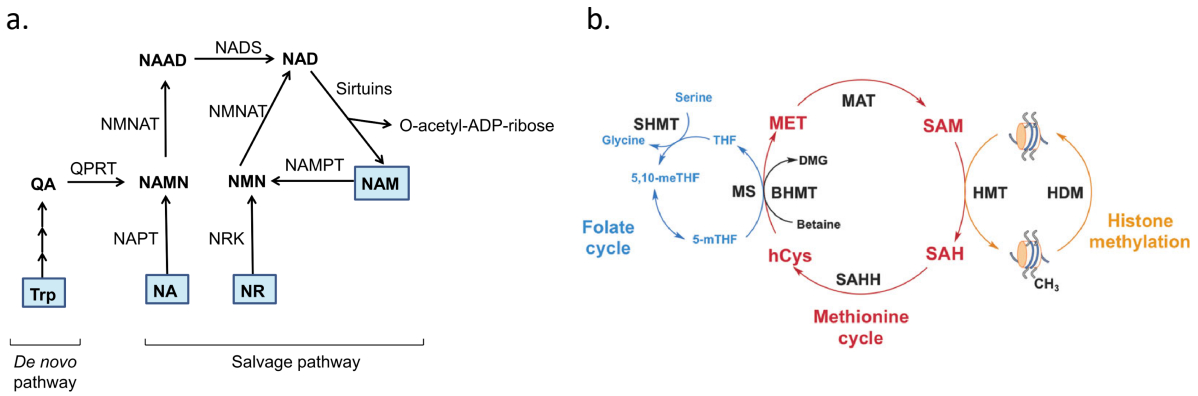

Figure 1.3 Metabolic pathways regulating production of two epigenetically relevant cofactors in mammals. Only parts involved in recycling of NAD^+ (in a.) and SAM (in b.) are described in the main text; **a.** Representation of de novo and salvage pathway of NAD^+ synthesis. In blue boxes are shown major precursors of NAD^+; NA – nicotinic acid, NAD – NAD^+, NAAD – nicotinic acid adenine dinucleotide, NADS – NAD synthase, NAM – nicotinamide, NAMN – nicotinic acid mononucleotide, NAMPT – NAM phosphoribosyltransferase, NAPT – NA phosphoribosyltransferase, NMN – nicotinamide mononucleotide, NMNAT – NMN adenylyltransferase, NR – nicotinamide ribose, NRK – NR kinase, Trp – tryptophan, QA – quinolinic acid, QPRT – quinolinate phosphoribosyltransferase; Figure adapted from [102] **b.** Connection between folate and methionine cycle and histone methylation. Methylation of other chromatin substrates is not shown; 5-mTHF – 5-methylentetrahydrofolate, 5,10-meTHF – 5,10-methylenetetrahydrofolate, BHMT – betaine-homocysteine methyltransferase, DMG – dimethylglycine, hCys – homocysteine, HDM – histone demethylase, HMT – histone methyltransferase, MAT – methionine adenosyltransferase, MET – methionine, MS – methionine synthase, SAM – S-adenosylmethionine, SAH – S-adenosylhomocysteine, SAHH – S-adenosylhomocysteine hydrolase, SHMT – serine hydroxymethyltransferase, THF – tetrahydrofolate; Figure adapted from [103]

1.3.3. Metabolic regulation of DNA and histone methylation

One-carbon (1C) metabolism is a series of metabolic pathways that are central to cellular functions, providing methyl groups for the synthesis of DNA, polyamines, amino acids, creatine, and phospholipids [104]. S-adenosylmethionine (SAM) is a central metabolite in 1C metabolism and a common cosubstrate in all methylation reactions. In mESC, metabolism of threonine (Thr), amino acid critically required for

pluripotency, and SAM are tightly coupled and regulate methylation status of H3K4 [105]. Depletion of Thr in the culture medium or partial depletion of Tdh results in decreased amount of cellular SAM and lower level of global H3K4me2/3. Notably, neither the level of H3K4me1 nor a set of other histone lysine methylations showed any alterations indicating high specificity and different sensitivity of various histone methyltransferases for SAM abundance. Similarly, studies in human HCT116 cell line led to the discovery that methionine restriction drastically reduced the cellular levels of several metabolites involved in SAM metabolism what significantly affected global histone methylation marks including trimethylation at H3K4, H3K9 and H3K27 [106].

Methionine cycle is essential for generation of SAM through the action of methionine adenosyltransferases (MATs) (Figure 1.3 b). After transferring the methyl group from SAM to the acceptor molecule, S-adenosylhomocysteine (SAH) is formed. Similarly to KATs and NAD^+-utilising enzymes, methyltransferases are also sensitive to inhibition by the side product of the reaction they catalyse. Accumulation of intracellular SAH in yeast cells, caused by genetic manipulation, induced toxicity and growth inhibition. However, this effect was fully reversed by supplementation of SAM suggesting that SAM : SAH ratio is the crucial parameter affecting the activity of methyltransferases [107]. In cells with fully functional methionine cycle, SAH is converted to homocysteine (hCys) that can either enter transsulfuration pathway to eventually generate cysteine (Cys), or serve as a methyl acceptor and complete the methionine cycle. Two enzymes can utilise hCys as their methyl group acceptor to synthesise methionine and complete the cycle. Betaine-homocysteine transferase (BHMT) is a zinc metalloenzyme highly expressed in liver, kidney and lens of the eye, that can use choline-derived betaine as a methyl donor [108]. Widely expressed methionine synthase (MTR) uses

5-methyltetrahydrofolate (5-mTHF) and generates tetrahydrofolate (THF) that is further converted in folate cycle to renew the 5-mTHF pool.

Proper functioning of the methionine cycle requires its well-orchestrated coordination with the folate cycle (Figure 1.3 b). Imbalance in various parts of 1C metabolism can lead to aberrant chromatin methylation. Studies in rodents reported double-sided effect of folate deficiency on global DNA methylation [109]. While hypomethylation could be explained by depletion of a methyl group donor, in some experimental setups upon folate deficiency global DNA methylation was increased what was linked to compensatory effects caused by the upregulation of DNMTs.

Studies on the effect of folate on histone methylation are sparse. While folate deficiency decreases the supply of methyl groups necessary for SAM synthesis, THF has protective effect on H3K4me1/2 demethylase LSD1. As a consequence, limited folate administration resulted in increased global H3K4me2 level [110].

Aberrant activity of MATs has a well-documented influence on histone methylation in many organisms. In immortalised mouse embryonic fibroblasts (iMEFs) depletion of catalytic subunit Mat2A reduced global abundance of H3K4me3 and H3K9me3 while it did not affect mono- and dimethylation status of these residues [111]. Interestingly, in this model Mat2A together with its regulatory subunit Mat2B was shown to be present at the promoter of *Cox-2* gene and provide an in-situ supply of SAM for H3K9 methyltransferase SETDB1 and thus repress the expression of *Cox-2*. In *Caenorhabditis elegans* knockdown of sams-1 (MAT homologue) reduced the global level of H3K4me3 but not H3K36me or H3K9me3 while double knockdown of sams-3 and sams-4 reduced the levels of H3K9me3, H3K27me3 and H3K36me3 [112], [113].

Similarly, in yeast knockout of MATs, the level of H3K4me3 but not H3K4me1/2, H3K36me3 and H3K79me3 was globally reduced. Of note, both of yeast MAT homologues as well as Set1 methyltransferase were found in a chromatin-associated complex SESAME regulating the expression of pyruvate kinase Pyk1, altogether showing the interplay between chromatin-associated metabolic activity and regulation of the expression of a metabolic gene [114].

Overall, imbalance in 1C metabolism can lead to various aberrations in chromatin functions. However, more research is needed to uncover the subtle interconnections between various parts of these pathways and chromatin methylation.

1.3.4. Roles of TCA cycle metabolites in chromatin methylation

Both DNA and histone methylation are reversible modifications. Demethylation of H3K4me1/2 is catalysed by flavin-dependent Lys-specific demethylases (LSD1 and LSD2) [115], [116]. Erasing of the majority of methylation marks present in chromatin is achieved by the activity of α-ketoglutarate (α-KG)- and Fe^{2+}-dependent dioxygenases (2-OGDOs): TET enzymes responsible for DNA demethylation and the jumonji C (JmjC) domain-containing histone demethylases. α-KG is involved in a plethora of cellular processes. It is a rate-limiting intermediate of TCA cycle and therefore, has a crucial role in energy metabolism. Moreover, it serves as a nitrogen scavenger and a source of amino acids. Additional influence on the homeostasis of immune system and regulation of senescence makes α-KG another important sensor of the overall metabolic state of a cell [117].

Availability of α-KG is necessary for proper functionality of 2-OGDOs. Notably, it has been shown that succinate and fumarate, other metabolites of TCA cycle, can competitively inhibit 2-OGDOs affecting DNA and histone demethylases [118], [119]. Aberrant activity of several enzymes of TCA cycle can alter the level of α-KG relative to inhibitors of 2-OGDOs. Mutations in succinate dehydrogenase (SDH) and fumarate hydratase (FH) observed in some tumours can lead to accumulation of succinate and fumarate, respectively [120], [121]. Ectopic expression of tumour-derived mutants of SDH and FH in HEK293T cells leads to the global increase of H3K4me1/3 and H3K9me2 and decrease of 5-hmC suggesting inhibition of the activity of histone and DNA demethylases [120]. Isocitrate dehydrogenases (IDHs) are enzymes converting isocitrate to α-KG. Gain-of-function mutations in cytosolic IDH1 and mitochondrial IDH2 are found in gliomas and acute myeloid leukaemia (AML) [122], [123]. These mutations cause the neomorphic activity of IDH that results in conversion of α-KG to 2-hydroxyglutarate (2-HG) – another competitive inhibitor of 2-OGDOs. In line with this, the neomorphic mutants of IDH enzymes lead to the increased levels of 5-mC manifested in defects of hematopoietic differentiation [123].

Overall, impaired activity of TCA cycle enzymes can affect the function of chromatin demethylases that has implications in aberrant gene expression and cellular functions.

1.4. Nuclear functions of metabolic enzymes

Canonical functions of many metabolic enzymes have been known for decades. Recent discoveries, mainly in the field of cancer research, revealed surprising activities of known metabolic enzymes outside of their well-established metabolic roles. Of

particular interest are the enzymes that upon certain stimulation translocate to the nucleus, where they contribute to transcriptional control by either providing metabolites for chromatin modifications, or serving as transcription factors.

All essential glycolytic enzymes have been found in the nucleus [124]. While many of them function as modulators of transcription factors, glyceraldehyde-3-phosphate dehydrogenase (GAPDH) and enolase (ENO) contain DNA-binding domains and have been implicated in protecting telomeres and regulating *c-Myc* gene expression, respectively [125], [126]. Nuclear localisation of several cytosolic enzymes involved in histone acetylation and methylation has also been reported [85], [87], [114]. Strikingly, several lines of evidence suggest that multiple mitochondrial enzymes crucial for the activity of chromatin modifiers (subunits of PDC, FH, SDH, IDH2), can be actively exported from mitochondria and imported to the nucleus [86], [127]–[131]. Unfolding mitochondrial proteins, their translocation through the inner mitochondrial membrane and subsequent refolding and nuclear import requires energetic effort that the cell needs to employ. The presence of such phenomenon clearly highlights the importance of ‘moonlighting’ roles of metabolic enzymes in the nucleus.

Altogether, newly discovered functions of nuclear metabolic enzymes provide advances in understanding an emerging metabolism-gene transcription axis, which includes epigenetic regulation.

2. Aims of the study

The main aim of this thesis was to investigate the role metabolic enzymes play in establishing chromatin (mostly histone) modifications and subsequently, in regulation of gene expression. I focused on metabolic enzymes that are responsible for establishing pools of metabolites that serve as cofactors, substrates or inhibitors of chromatin modifying enzymes (mainly writers and erasers).

Specifically, in my work I wanted to address the following points:

- establishing the system to investigate the effect of ‘chromatin microdomains’ by tethering the selected metabolic enzymes to the gene promoters,
- detecting the histone modifying activity co-purified with selected metabolic enzymes,
- investigating the changes in histone PTMs and gene expression upon the depletion of selected metabolic enzymes.

Altogether, this project should provide comprehensive insights into how the localisation and metabolic activity of cellular enzymes affect chromatin architecture, gene expression and cellular functions.

3. Results

3.1. Establishing the system to investigate the effect of ‘chromatin microdomains’ by tethering the selected metabolic enzymes to the gene promoters

3.1.1. Designing dCas9-enzyme constructs

Many metabolic enzymes are present in the nucleus even though their main metabolic role is assigned to a different cellular compartment. Some of the enzymes can be translocated to the nucleus upon certain stimulation and provide a direct in-situ supply of metabolites modulating the activity of chromatin modifiers. The list of metabolic enzymes present in the nucleus is not complete and their nuclear roles are often not completely understood.

To investigate if the presence of metabolic enzymes in close proximity to the promoter can affect the transcription of a downstream gene, I first decided to use catalytically inactive Cas9 (dCas9) fusions to tether the enzymes to the promoter using a single guide RNA (gRNA). I designed the fusion constructs that encode the enzyme of interest tagged with a FLAG-2HA tag at the N-terminus and fused to dCas9 using a flexible 16-residue ‘XTEN’ linker [132] (Figure 3.1 a). The constructs were generated by the cloning facility at IGBMC Strasbourg.

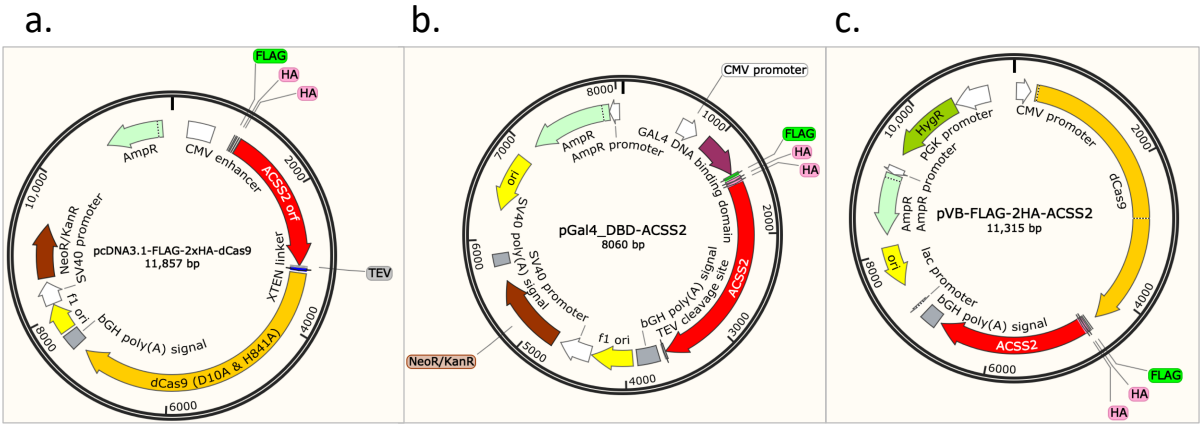

Figure 3.1 Examples of plasmid maps of the constructs generated for investigating tethering metabolic enzymes to the promoters. Only selected features are shown; **a.** pcDNA3.1-FLAG-2HA-enzyme-XTEN-dCas9 vector generated by the cloning facility at IGBMC, **b.** pGal4_DBD-FLAG-2HA-enzyme vector used in the HEK293 5xUAS-luc system; **c.** pVB-FLAG-2HA-enzyme vector used in mESC Sox1 system. Plasmid maps were generated using SnapGene® software.

3.1.2. Testing gRNAs targeting various promoters in HEK293 cells

I designed new and used published gRNAs targeting promoters of several genes that display different levels of expression in wild type HEK293 cells: *EGR1, NTF3* (low expression, prone to induction), *VEGFA* (medium expression, prone to both repression and activation), *CD71* (high expression, prone to repression) [133]–[135]. Choosing the gRNA that would enable me to investigate the activating role of the metabolic enzyme present at the promoter consisted of a 3-step validation procedure: (i) confirming the specificity of gRNA by chromatin immunoprecipitation (ChIP) with antibodies against HA or FLAG tag, (ii) confirming the lack of changes in transcription of the selected gene upon tethering dCas9 not fused to any metabolic enzyme (dCas9 solo) by RT-qPCR, (iii) confirming the activation of the selected gene by dCas9 fused to 3 x minimal VP16 transcriptional activation domain (VP48) [133]. The validation of gRNAs is summarised in Table 3.1.

Table 3.1 Validation of gRNAs tested in dCas9 tethering to the promoters; gRNA codes correspond to the internal DNA oligonucleotide numbers used for cloning; +: positive signal over control, -: negative signal comparable to control, +/-: inconclusive results, blank: not tested; marked in red are the results violating a given validation criterium

Target gene	gRNA code	Specific targeting (ChIP)	dCas9 affecting transcription of a target gene	Activation by dCas9-VP48
EGR1	45/46	-		
	47/48	+	-	-
	76/77	-		
	78/79	-	+/-	-
	80/81	-		
	126/127	-		
	128/129	-		
	166/167	+	+	-
	168/169	-	+/-	-
	170/171	-	+/-	-
	172/173		+	-
	174/175	+	+	-
	176/177	+	+	-
CD71	66/67	+	-	-
	68/69	+	-	-
	74/75	+	+	
	108/109	+	-	-
	124/125			-
VEGFA	213/214			-
	215/216			-
NTF3	217/218			-
	219/220			-

Several gRNAs showed promising results in ChIP experiments. However, neither of them was able to activate the target gene when used in combination with transcriptional activator dCas9-VP48. To define whether the lack of activation was caused by the 'insufficient tethering' of dCas9 to the target loci or by the weak activation potential of VP48 I used HEK293 cell line with stably integrated reporter cassette encoding 5 tandem Gal4 binding sites (5xUAS) followed by the human thymidine kinase (tk) promoter and firefly luciferase gene. I used two gRNAs targeting the UAS (g4-1 and g4-2) and dCas9 fused to the activating domain VP48 or VP64 (a stronger activator than VP48). In parallel I created the construct encoding the DNA binding domain of Gal4 (Gal4_DBD) fused to VP48. Gal4_DBD-VP48 fusion showed the

highest activation potential of all tested conditions both in RT-qPCR (data not shown) and in dual luciferase assay (Figure 3.2). However, when VP48 or VP64 was targeted via dCas9 and gRNAs the activation was very moderate.

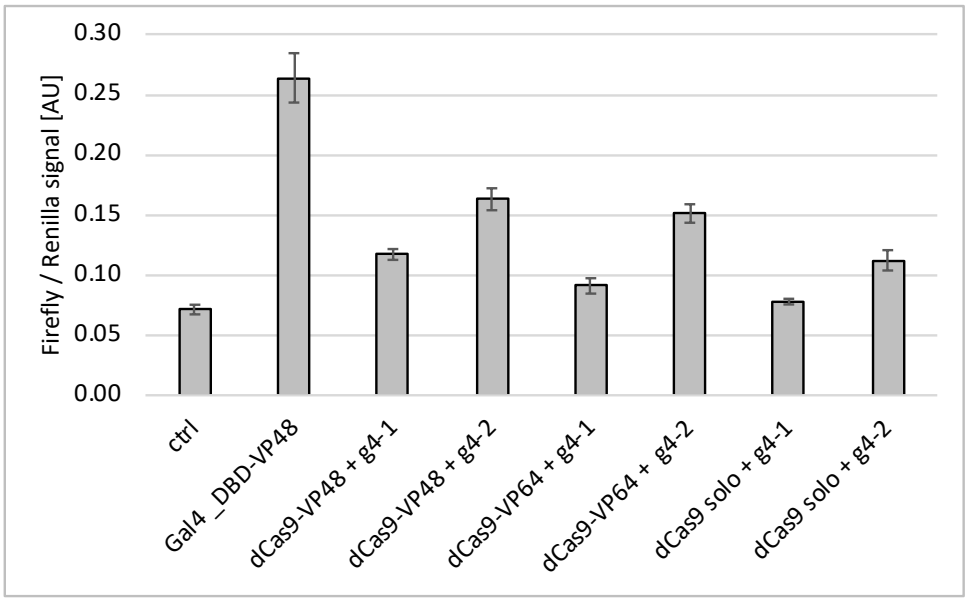

Figure 3.2 Dual luciferase assay in HEK293 with stably integrated firefly luciferase reporter cassette; cells transfected with gRNA 108/109 plasmid were used as a control; data show mean of 3 replicates ± SD

Based on the above, I decided that dCas9 system is not the most optimal approach to study tethering the metabolic enzymes to promoters in HEK293 cells. However, due to the fact that the relatively weak activator VP48 was able to significantly increase the transcription, and subsequently the activity, of firefly luciferase in 5xUAS-luc system, I decided to use that model in the subsequent experiments.

3.1.3. The effect of the presence of active metabolic enzyme at the promoter on the transcription of a downstream gene

Due to the fact that DNA sequences of all the metabolic enzymes in the vectors encoding fusions with dCas9 were flanked by the same sequences (FLAG-2HA at the 5’ end and TEV cleavage site at the 3’ end), I designed a common cloning strategy for

all Gal4_DBD-enzyme fusion constructs using Gibson Assembly approach [136]. After obtaining all the necessary tools (Figure 3.1 b) I performed a screening experiment by transfecting the reporter HEK293 5xUAS cell line with Gal4_DBD-enzyme fusions including Gal4_DBD followed by a stop codon (Gal4_DBD-stop) and Gal4_DBD-VP48 as a negative and positive control, respectively. Cells were simultaneously transfected with a constant, small amount of pRL plasmid encoding *Renilla* luciferase (ca. 1 pRL molecule per 50 Gal4_DBD plasmid molecules). The experiment was performed 3 times to obtain at least 2 biological replicates of each condition. The results of the screening are shown in Figure 3.3.

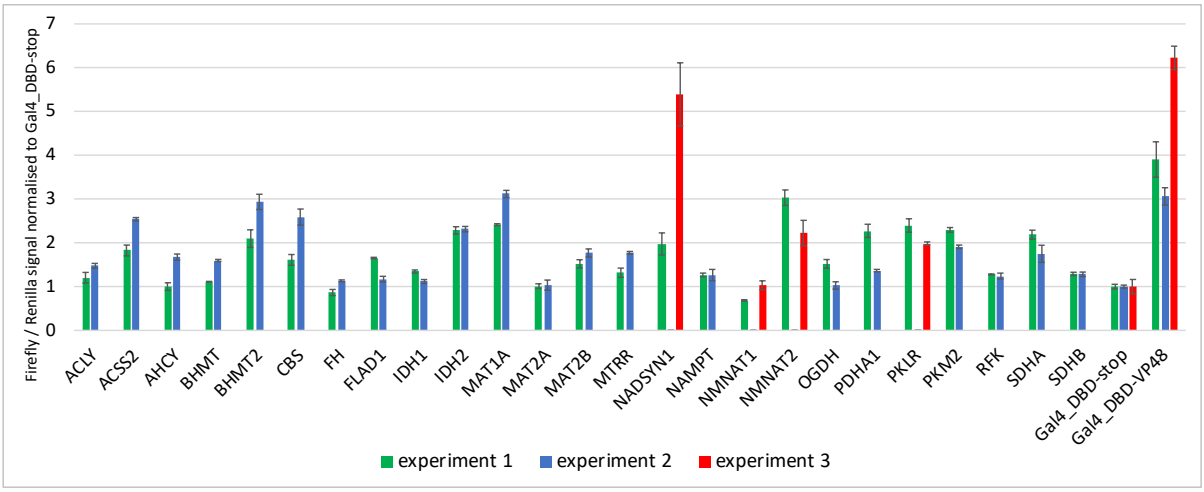

Figure 3.3 Firefly luciferase activity normalised to *Renilla* luciferase activity measured in cells transiently transfected with the indicated constructs and pRL plasmid for normalisation of transfection efficiency; data represented as fold change of control cells transfected with Gal4_DBD-stop (no protein fused to Gal4_DBD); data show mean of 3 replicates ± SD

Many of the metabolic enzymes fused to Gal4_DBD showed mild to moderate activation of firefly luciferase. While one should not exclude the possibility of activation of this gene by a steric hindrance caused by the presence of the protein (and its potential interactors) at the promoter, there was no correlation between the size of the fusion protein and its activation potential. Notably, both the smallest and the biggest fusion proteins, Gal4_DBD-RFK (34.5 kDa) and Gal4_DBD-ACLY (136.9 kDa) did not lead to the activation of firefly luciferase gene. In total, I identified 10 metabolic

enzymes whose presence at the promoter led to at least 2-fold increase of transcription (average of 2 experiments) of a downstream reporter gene.

HEK293 cells with the reporter cassette integrated in the unknown place in the human genome, possibly in multiple copies, constitute a rather artificial system, therefore my next goal was to confirm the activation potential observed in the dual luciferase assay in a system with the endogenous promoter as a target. For this I established a collaboration with the Stricker Lab (Helmholtz Zentrum München) who had used double gRNA dCas9 system to activate various genes in mouse embryonic stem cells (mESC). We used heterozygous mESC line where one locus of *Sox1* gene is replaced with GFP and the gRNA sequences previously validated by the Stricker Lab. Such system allowed us to use three different readouts: monitoring GFP-positive cells by flow cytometry and quantification of *Sox1* and *GFP* transcripts by RT-qPCR. In another round of Gibson Assembly cloning I generated a set of new custom pVB plasmids encoding dCas9 fused to metabolic enzymes and carrying hygromycin resistance (Figure 3.1 c), as the original dCas9 fusion plasmids (Figure 3.1 a) carried the resistance to geneticin that led to high toxicity in mESC. The changes in *Sox1* gene expression were consistently milder than in the HEK293 5xUAS-luc system, therefore I classified all the enzymes that upon tethering to the promoter caused the gene activation to reach 1.5 the level of control sample or more as positive candidates. 5 out of 11 metabolic enzymes tested, emerged as promising candidates positively regulating transcription. Interestingly, 4 of them were also activating transcription in HEK293 5xUAS-luc reporter cell line. The results of both screening approaches are presented in Table 3.2.

Table 3.2 Summary of screening of metabolic enzymes for their potential in gene activation in human (HEK293 5xUAS-luc) and mouse (mESC Sox1-GFP) cells; Results from 3 readouts used for mESC Sox1-GFP system are shown; marked in green are the results confirming activating potential of an enzyme. Gal4_DBD-stop was used as a control in HEK293 5xUAS-luc system, dCas9-solo was used as a control in mESC Sox1-GFP system; ND – no data

Enzyme	HEK293 5xUAS-luc	mESC Sox1-GFP		
	Firefly / *Renilla* signal	*GFP* mRNA	*Sox1* mRNA	GFP-positive cells
ACSS2	2.2	5.8	0.6	3.3
BHMT2	2.5	4.9	3	2.3
CBS	2.1	ND	ND	ND
FH	1.0	3.5	2.4	1.8
IDH2	2.3	4.7	1.9	3.8
MAT1A	2.8	ND	ND	ND
PKM2	2.1	3.5	0.5	2.7
SDHA	2.0	ND	ND	ND
control	1.0	1.0	1.0	1.0

Next, we addressed the question if the enzymatic activity of the metabolic enzyme is necessary for the transcription activation to occur. For this I designed mutants with the loss or change of the activity of the 5 enzymes selected from the Sox1-GFP screening. The mutants that I successfully cloned into pVB backbone are listed in Table 3.3.

Table 3.3 Point and deletion mutants designed for studying the effect of the activity of metabolic enzymes on gene activation upon tethering to the promoter; 2-HG – 2-hydroxyglutarate

Enzyme	Point mutant	Expected change in activity	Cloned	Deletion mutant	Expected change in activity	Cloned	Reference
ACSS2	T363K	loss		Δ361-365	loss	✓	[137]
BHMT2	S77F	loss	✓	Δ75-79	loss	✓	[138]
FH	R268H	loss	✓	Δ266-270	loss	✓	[139]
IDH2	R172K	neomorphic activity – production of 2-HG	✓	Δ170-175	loss	✓	[120]
PKM2	K270M	loss		Δ268-272	loss		[140]

Despite trying various cloning strategies, unfortunately I did not manage to assemble any of the mutant constructs for PKM2 and the point mutant of ACSS2. After several attempts, we decided to perform the experiment without the missing constructs. The results are presented in Figure 3.4.

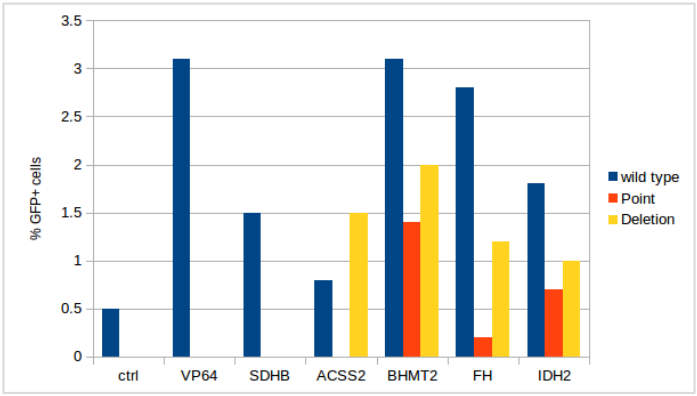

Figure 3.4 Percentage of GFP-positive cells in mESC Sox1-GFP system upon tethering of dCas9-metabolic enzyme fusions to *Sox1* promoter. SDHB was used as an additional negative control. The level of expression of each construct was checked by RT-qPCR and did not show drastic changes (data not shown). Figure made by the Stricker Lab

In this experiment fully active ACSS2 did not increase the number of GFP-positive cells. Probably this is due to the technical problem during the experiment, especially considering the fact that the ACSS2 deletion mutant, that should be devoid of any residual enzymatic activity, led to more GFP-positive cells. However, the loss of the wild type activity of BHMT2, FH and IDH2 at the *Sox1* locus led to its lower expression manifested by less GFP-positive cells indicating that the catalytical activity of these enzymes is necessary for them to contribute to the activation of transcription. Interestingly, deletion mutants showed higher activating potential than point mutants. Such behaviour can be caused by the structural disruption of the active site upon 5-amino acid deletion that can lead to the changed conformation of the enzyme and potentially affect the transcription by unforeseen steric effects.

Altogether, in this set of experiments I managed to establish the system to create a specific chromatin microenvironment by tethering metabolic enzymes to different gene promoters in human and mouse cell lines. Using the presented strategies, I identified several enzymes whose presence and / or activity in close proximity to TSS can increase the expression of the downstream gene.

3.2. Detecting the histone modifying activity co-purified with selected metabolic enzymes

3.2.1. Designing the MBP- and FLAG-2HA-enzyme constructs and expression tests in bacterial and mammalian systems

To investigate whether metabolic enzymes can interact with histone modifiers, I designed a pull-down approach followed by in vitro HAT and methyltransferase assays with tritium (^{3}H)-labelled acetyl-CoA or SAM, respectively (Figure 3.5).

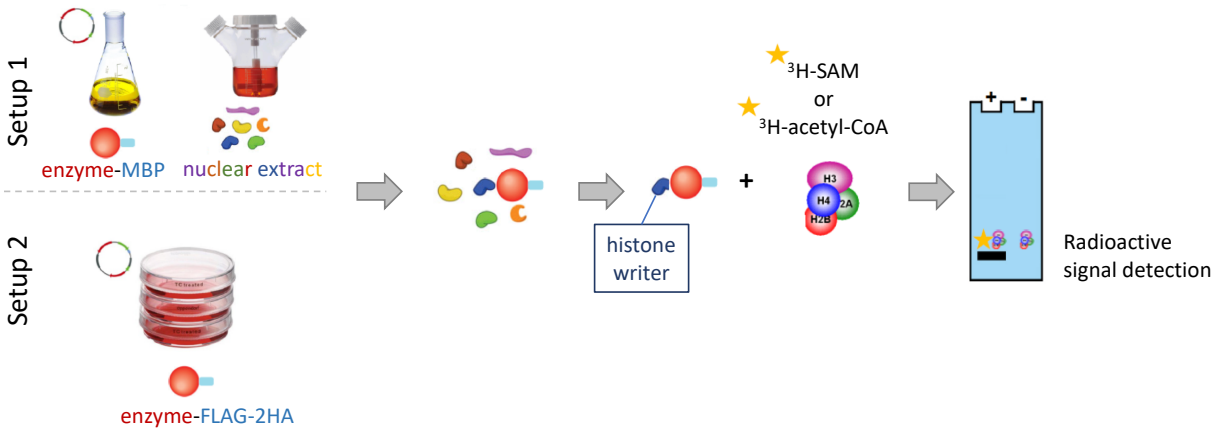

Figure 3.5 Schematic outline of the experiment to detect histone writing activity interacting with metabolic enzymes. In setup 1 MBP-tagged enzymes were expressed in *E. coli* and incubated with HeLa nuclear extract, in setup 2 the enzymes were expressed and purified from HEK293 cells. After pulling down proteins interacting with metabolic enzymes, they were incubated with histones and ^{3}H-labelled SAM or acetyl-CoA followed by detection of the radioactive signal.

To increase the chances of efficient bacterial expression and production of soluble recombinant proteins as well as to be able to subsequently use affinity chromatography for the protein purification, I decided to design the fusion of metabolic enzymes with maltose-binding protein (MBP) [141]. The constructs encoding metabolic enzymes were cloned into bacterial and mammalian expression vectors by IGBMC cloning facility.

Due to the fact that the DNA sequence of ORFs of human metabolic enzymes were not codon-optimised for bacterial expression system, I performed a small-scale expression test using 2 *E. coli* strains designed for efficient recombinant protein production induced by IPTG:

BL21 Gold (DE3) – characterised by high-level protein expression

Rosetta 2 (DE3) pLysS – default strain, characterised by lower protein expression than BL21 Gold (DE3), advantageous in expression of eukaryotic proteins due to the presence of tRNAs for 7 rare codons. The summary of MBP-enzyme fusion protein expression test is presented in Table 3.4.

Table 3.4 Summary of the expression test of recombinant metabolic enzymes in bacterial and mammalian expression systems; blank cells – expression not tested, M. w. – molecular weight

Enzyme	M. w. [kDa]	MBP-enzyme			FLAG-2HA-enzyme	
		M. w. fusion protein [kDa]	Expression in Rosetta	Expression in BL21	M. w. fusion protein [kDa]	Expression in HEK293
ACLY	121	163.5	yes		125	
ACSS2	79	121.5	yes		83	
AHCY	48	90.5	yes		52	
BHMT	45	87.5	yes		49	
BHMT2	40	82.5	yes		44	yes
CBS	61	103.5	yes		65	
FH	55	97.5	yes		59	
FLAD1	65	107.5	yes		69	
IDH1	47	89.5	yes		51	
IDH2	51	93.5	yes		55	yes
MAT1A	44	86.5	yes		48	
MAT2A	44	86.5	yes		48	
MAT2B	37	79.5	yes		41	
MTR	141	183.5	no construct		145	no construct
MTRR	80	122.5	no	no	84	
NADSYN1	79	121.5	no	no	83	yes
NAMPT	56	98.5	yes		60	
NMNAT1	32	74.5	yes		36	
NMNAT2	34	76.5	yes		38	
OGDH	116	158.5	no	no	120	yes
PCCA	80	122.5	no construct		84	no construct
PDHA1	43	85.5	no	no	47	
PKLR	62	104.5	yes		66	
PKM2	58	100.5	yes		62	
RFK	18	60.5	yes		22	
SDHA	73	115.5	no	no	77	yes
SDHB	32	74.5	yes		36	

The majority of metabolic enzymes were expressed in Rosetta expression system. None of the 5 fusions that were not expressed in Rosetta showed a better result in BL21. After the preliminary results of the in vitro methyltransferase assays (chapter 3.2.2), I also tested the expression efficiency of the most promising FLAG-2HA-enzyme fusions in HEK293 cells. As expected, all the tested human enzymes were overexpressed in mammalian system.

3.2.2. In vitro histone methyltransferase and acetyltransferase assays

After confirming the expression of the MBP-enzyme fusions expression in Rosetta system, I performed preparative recombinant protein production and purification. On the day of the assay, I incubated MBP-enzymes immobilised on the amylose resin with HeLa nuclear extract and performed an in vitro methyltransferase assay with histones and ^{3}H-labelled SAM as substrates. Due to the weak signal and high background of the radioactivity-based method, the experiment was performed at least 3 times for all MBP-fusions. The results of a representative experiment are presented in Figure 3.6 a.

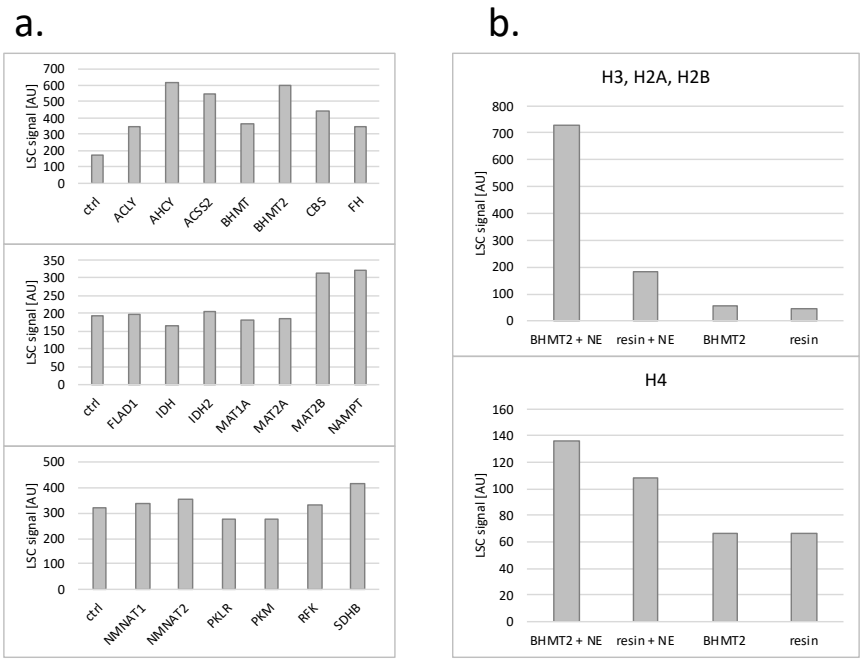

Figure 3.6 In vitro histone methyltransferase activity assay of nuclear proteins co-purified with recombinant MBP-enzymes; **a.** Quantification of the radioactive signal detected on total histones in one replicate of in vitro methyltransferase assay. Assay samples were analysed on 3 separate membranes. Signals from each membrane are plotted separately; **b.** Validation of histone methyltransferase activity co-purified with BHMT2. Cumulated radioactivity signal detected on histones H3, H2A and H2B was strongly elevated in the amylose resin-coupled BHMT2 sample pre-incubated with nuclear extract (BHMT2 + NE). A set of controls was used in presented experiment: amylose resin pre-incubated with nuclear extract (resin + NE), amylose resin-coupled BHMT2 not pre-incubated with nuclear extract (BHMT2) and amylose resin not pre-incubated with nuclear extract (resin). No drastic change was observed in radioactivity signal on histone H4; Data in panels a. and b. come from two separate experiments; LSC – liquid scintillation counting.

Out of 20 bacterially expressed recombinant enzymes, only BHMT2 was recurrently showing a consistently increased radioactivity signal on H3 over the control sample indicating that BHMT2 can physically interact with nuclear H3 methyltransferase. In vitro histone methyltransferase assay performed with MBP-BHMT2 protein without pre-incubation with HeLa nuclear extract led to the signal almost 13 times weaker than in the sample pre-incubated with the nuclear extract suggesting that intrinsic methyltransferase activity of BHMT2 did not affect histone methylation by itself (Figure 3.6 b). Tethering this enzyme to the promoter of *Sox1* and luciferase gene in mESC and HEK293, respectively, positively regulated transcription (chapter 3.1.3). Using these two independent approaches I identified BHMT2 as a metabolic enzyme involved in methionine synthesis that can play a role in chromatin modification and transcriptional regulation.

The next question I wanted to address was whether BHMT2, or any other enzyme from the list of my candidates, affects histone acetylation in an analogous in vitro assay. Unfortunately, protein acetylation, in contrast to methylation, occurs also non-enzymatically and is highly pH-dependent [142]. Because of that, I was not able to optimise the reaction conditions so that the signal could be distinguished from the background (data not shown).

Trials to co-immunoprecipitate H3 methyltransferase activity from total HEK293 cellular extract after transiently overexpressing FLAG-2HA-BHMT2 were also unsuccessful. Mass spectrometry (MS)-based proteomic analysis of the elution fraction of that experiment did not show any significantly enriched protein (data not shown). Therefore, as a next step I generated a stable HEK293 cell line overexpressing FLAG-2HA-BHMT2 and the future plan is to perform IP from nuclear fraction followed by MS analysis.

3.3. Investigating the changes in histone PTMs and gene expression upon the depletion of selected metabolic enzymes

3.3.1. Establishing the protocol for efficient delivery of shRNA constructs using lentiviral systems

To study the biological effects of depletion of the candidate metabolic enzymes in human cells, I first had to develop a strategy to reproducibly and efficiently knock down metabolic genes. To obtain a long-lasting depletion effect I decided to use shRNA-mediated knockdowns. The candidate enzymes whose roles I wanted to study are involved in various metabolic pathways and different candidates might play key roles in distinct disease models or cell types. However, performing a screening using different cell lines would require developing a high-throughput automated method, therefore I decided to use immortalised non-cancerous human HEK293 cell line as a model system.

To deliver plasmids encoding shRNA particles that lead to mRNA degradation in a sequence-specific manner, lentiviral vectors are used. To produce these vectors

HEK293T cells need to be transfected with necessary lentiviral genes, usually located on 3 or 4 plasmids (2nd or 3rd generation lentiviral system, respectively): psi (ψ) packaging sequence and transgene (or here: shRNA sequence) inserted between the lentiviral long terminal repeats (LTRs) for the integration in the genome of the target cell on the lentiviral expression plasmid; *pol*, *gag*, *rev* and (optional in 3rd generation system) *tat* genes and *rev*-response element (RRE) on the packaging plasmid(s) and the gene encoding the G protein of Vesicular Stomatitis Virus (VSV-G) on the envelope plasmid. HEK293T cells transfected with these plasmids release lentiviral particles to the culture medium that is subsequently used to transduce the target cells (here: HEK293).

I performed two rounds of optimisation of lentiviral vector production and target cell transduction using pLKO.1-puro based lentiviral expression plasmids from human MISSION shRNA library (Table 3.5).

Table 3.5 Summary of the optimisation of lentiviral vector production and target cells infection

<table>
<tr><td rowspan="3">Optimisation round</td><td colspan="5">Lentiviruses production</td><td colspan="2">Infection of HEK293 cells</td></tr>
<tr><td colspan="4">Protocol</td><td rowspan="2">Multinucleated HEK293T cells</td><td rowspan="2">Tested volumes of lentivirus supernatant [µL]</td><td rowspan="2">Maximal cell viability after 48 h puromycin selection</td></tr>
<tr><td>Transfection reagent</td><td>Volume of transfection reagent [µL]</td><td>Packaging plasmid</td><td>Envelope plasmid</td></tr>
<tr><td rowspan="4">1</td><td rowspan="2">Lipofectamine 2000</td><td>9</td><td rowspan="4">pCMV deltaR8.91</td><td rowspan="4">pMD2.G</td><td>Many</td><td rowspan="4">0, 1, 2, 4, 8, 16</td><td>0</td></tr>
<tr><td>12</td><td>Some</td><td>0</td></tr>
<tr><td rowspan="2">TurboFect</td><td>4</td><td>None</td><td>0</td></tr>
<tr><td>6</td><td>None</td><td>0</td></tr>
<tr><td>2</td><td colspan="5">LENTI-Smart Kit</td><td>Many</td><td>0, 1, 2, 4, 8, 16, 32, 64</td><td>70-90%</td></tr>
</table>

In the first round of optimisation, at the step of collecting supernatant from HEK293T culture, I observed the presence of fused multinucleated cells in the wells where cells were transfected with Lipofectamine 2000 what indicated that the transfection with this reagent was more efficient and more VSV-G protein was produced. However, the supernatant collected from the HEK293T culture lacked infectivity what manifested

itself with no resistance to puromycin after transduction of HEK293 cells. Since the transfection of HEK293T using Lipofectamine 2000 was efficient, most probably the used packaging plasmid lacked one or more necessary viral genes and lentiviral particles could not be assembled and released to the culture medium.

Assuming that the packaging plasmid was faulty, in the second round of optimisation I used commercially available mixture of packaging and envelope plasmids (LENTI-Smart, Invivogen). I produced lentiviral particles according to the manufacturer's instruction and titrated the lentiviral supernatant.

HEK293 cells treated with the lentiviral supernatant collected in the second round of optimisation showed significantly increased viability in the selection medium. To confirm that the optimised protocol led to the efficient knockdown of a target gene, I expanded cells from wells treated with 3 different lentiviral expression plasmids (targeting 3 different metabolic genes) and checked mRNA abundance of targeted genes by RT-qPCR (Table 3.6).

Table 3.6 Comparison of the knockdown efficiency of lentiviruses produced in the second round of optimisation and validated by the expression plasmid provider (Sigma-Aldrich); ND – no data

Clone TRC number	Target enzyme	mRNA expression compared to WT	
		Optimisation Round 2	Sigma-Aldrich
TRCN0000078425	PCCA	18.6 ± 1.9%	11%
TRCN0000036452	MAT2A	49.2 ± 3.1%	ND
TRCN0000196588	PKM2	2.6 ± 0.2%	1%

Knockdown efficiency of both expression plasmids that were previously validated was comparable to the efficiency reported by the provider. This indicated that the protocol that I established efficiently delivers DNA encoding shRNA to the target cells. Therefore, for all the subsequent shRNA-mediated knockdown experiments I followed the protocol developed in the second round of optimisation.

3.3.2. Validation of knockdown efficiency using shRNA constructs targeting selected metabolic enzymes

To generate stable cell lines with depletion of selected metabolic enzymes I selected the most promising shRNA clones for every enzyme based on the knockdown efficiency reported by Sigma-Aldrich (Figure 3.7 a-b). For the targets whose shRNAs were not previously validated, I arbitrarily chose one clone per enzyme. I transduced the cells according to the previously established protocol. Due to the metabolic perturbation caused by the depletion of cellular enzymes, some knockdown cell lines showed slower proliferation rate, therefore the total time of culture (from transduction to harvesting) varied from 16 to 30 days (Figure 3.7 c). Interestingly, only PKM2 knockdown (PKM2 kd) cell line showed altered morphology at the beginning of the post-transduction culture (Figure 3.7 d). Around day 20 after transduction, the cells regained their wild-type morphology suggesting that the PKM2-depleted cells had gone through the process of adaptation to the metabolic perturbation. The PKM2 mRNA abundance was more drastically reduced in the second round of optimisation than in the validation experiment (to 2.6% and 12% of WT abundance, respectively). Taking into account the fact that during the optimisation the cells were collected up to 7 days after transduction, in contrast to 30 days after transduction in the validation experiment, it is possible to speculate that during the prolonged culture, exogenous DNA integrated in the host genome gets silenced by promoter methylation via the mechanisms analogous to the impaired promoter methylation in multiple cancers [143].

a.

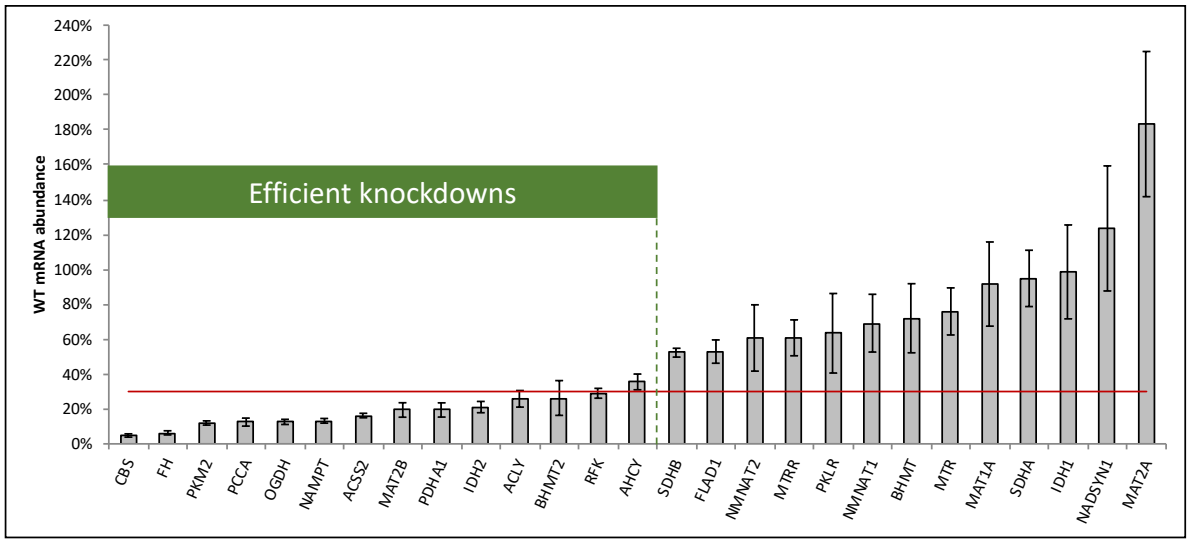

b.

Clone TRC number	Target enzyme	mRNA expression compared to WT	
		Screening in this study	Sigma-Aldrich
TRCN0000045359	CBS	4.8 ± 0.9%	14%
TRCN0000052466	FH	6.3 ± 1.2%	4%
TRCN0000196588	PKM2	12.0 ± 1.2%	1%
TRCN0000078425	PCCA	12.5 ± 2.3%	11%
TRCN0000028618	OGDH	12.6 ± 1.3%	13%
TRCN0000034522	MAT2B	19.4 ± 4.1%	8%
TRCN0000028627	PDHA1	19.4 ± 4.1%	5%
TRCN0000027225	IDH2	21.1 ± 3.2%	9%
TRCN0000078287	ACLY	25.8 ± 4.8%	5%
TRCN0000037602	RFK	29.0 ± 2.8%	3%
TRCN0000035406	MTRR	60.8 ± 10.3%	11%
TRCN0000028085	SDHA	94.8 ± 16.1%	4%

c.

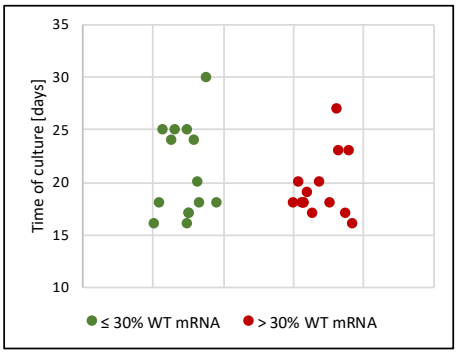

d.

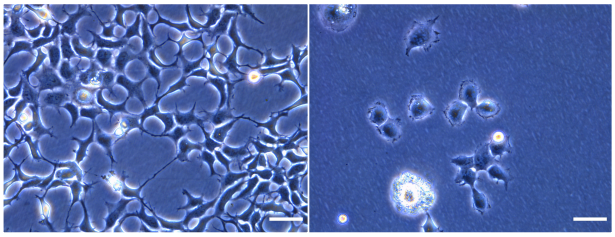

WT PKM2 kd

Figure 3.7 Validation of knockdown efficiency of selected shRNAs in HEK293 cells; **a.** RT-qPCR-based quantification of mRNA for target enzymes. Plotted are transcript abundances relative to housekeeping gene *B2M*. In red is shown the 30% WT mRNA abundance set as an arbitrary threshold of efficient knockdown; data show mean of 3 replicates ± SD; **b.** comparison of knockdown efficiency presented in this study with the values reported by the expression plasmid provider (Sigma-Aldrich); **c.** time of culture from transduction to harvesting. There was no significant difference in culture time of the efficient and not efficient knockdowns; **d.** Change in cell morphology of PKM2 kd 11 days after transduction. Scale bar – 100 μm

14 out of 27 selected shRNAs decreased the abundance of their target mRNAs to less or equal to 30% WT expression that was an arbitrarily chosen threshold for efficient knockdown. Not surprisingly, 10 out of 12 shRNAs whose efficiency was previously

reported, showed high efficiency of knockdown also in my experiment. Moreover, I validated the high efficiency of four more shRNAs, targeting NAMPT, ACSS2, BHMT2 and AHCY, that had not been reported before.

3.3.3. Analysis of histone PTMs in stable knockdown cell lines

To investigate whether the depletion of selected metabolic enzymes in HEK293 cells has an impact on histone PTMs I used MS-based proteomic approach. I collected the cells with validated knockdown efficiency and prepared them for histone extraction. The acid extraction of histones and preparation of samples for LC-MS analysis was performed by Dr. Andrey Tvardovskiy. The samples were processed in Core Facility Proteomics (Helmholtz Zentrum München) and analysed with the help of Dr. Andrey Tvardovskiy. The results are presented in Figure 3.8.

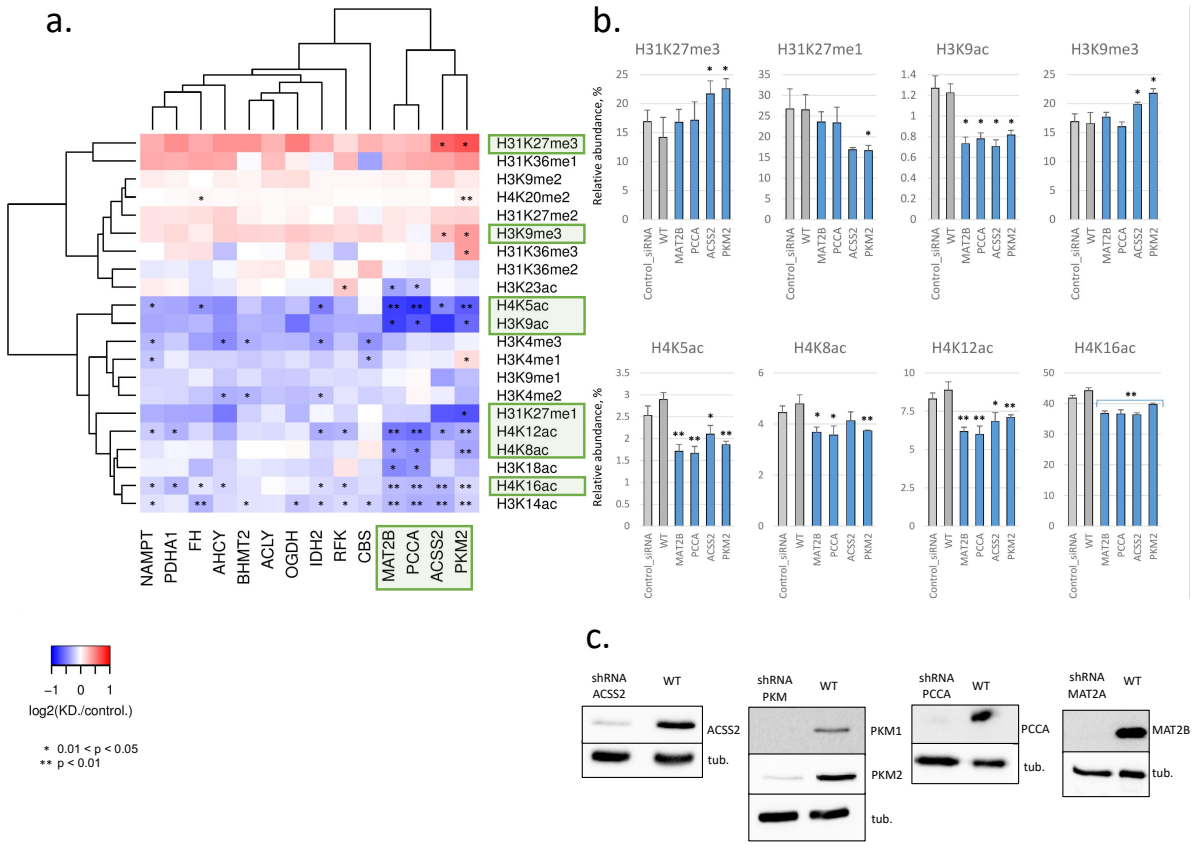

Figure 3.8 Knockdowns of selected metabolic enzymes lead to global changes in histone PTM patterns; **a.** Heatmap analysis of the changes in histone PTMs quantified by LC-MS, n = 3. P values were calculated from Student's two-tailed t-test and adjusted with Benjamini-Hochberg correction; The quantification of PTMs in knockdown cell lines marked in green is shown in panel b.; **b.** Quantification of relative abundance of selected PTMs for top candidate knockdown cell lines; **c.** Confirmation of knockdown efficiency of top candidate enzymes at the protein level; tub. – tubulin, WT – wild type

The relative abundance of multiple PTMs in WT cells were in agreement with previously reported data generated from the same cellular model [144]. The majority of knockdown cell lines that I studied did not cause any significant changes in global histone PTMs. However, in case of four cell lines (green box in Figure 3.8 a), the depletion of a single metabolic enzyme led to significant alterations in the histone PTM pattern. Interestingly, the trends of changes for histone acetylations were the same for all the cell lines what might suggest a common response mechanism of the cells to the perturbation affecting various metabolic pathways. All the knockdowns displayed decrease in H4 acetylation marks including K5 and K12 that are enriched at newly synthesised histones and K8 that was identified as one of the predictive marks of replication time [145], [146]. In ACSS2 kd and PKM2 kd I observed the increase in H3K9me3 and H3K27me3 that constitute the marks typical for constitutive and facultative chromatin, respectively [57]. Moreover, in these two knockdowns the gain of H3K27me3 was accompanied by the decrease of H3K27me1 levels. All four knockdowns displayed the downregulation of acetylation at H3K9 and H4K16 – the marks associated with transcriptionally active chromatin [38], [147]. Overall, the separate knockdowns of PKM2, ACSS2, MAT2B and PCCA in HEK293 cells caused a global depletion of active chromatin marks.

3.3.4. Analysis of cytosine modifications in genomic DNA of stable knockdown cell lines

Stable depletion of ACSS2, MAT2B, PCCA and PKM significantly altered the abundance of several histone PTMs. To investigate if such metabolic perturbance affects also the modifications of DNA, I extracted genomic DNA from the knockdown cell lines and performed MS-based quantification of 5-methyl-, 5-hydroxymethyl- and 5-formylcytosine (in collaboration with Dr. Mirko Wagner, LMU). The results are presented in Figure 3.9.

We did not observe any changes in global abundance of 5-mC meaning that global DNA methylation status was not impaired. Interestingly, all the knockdown cell lines displayed significant depletion of 5-hmC and 5-fC. These modifications are intermediate products of active DNA demethylation by TET enzymes, therefore I concluded that knockdowns of ACSS2, MAT2B, PCCA and PKM affect the activity of enzymes involved in the removal of methyl groups from DNA.

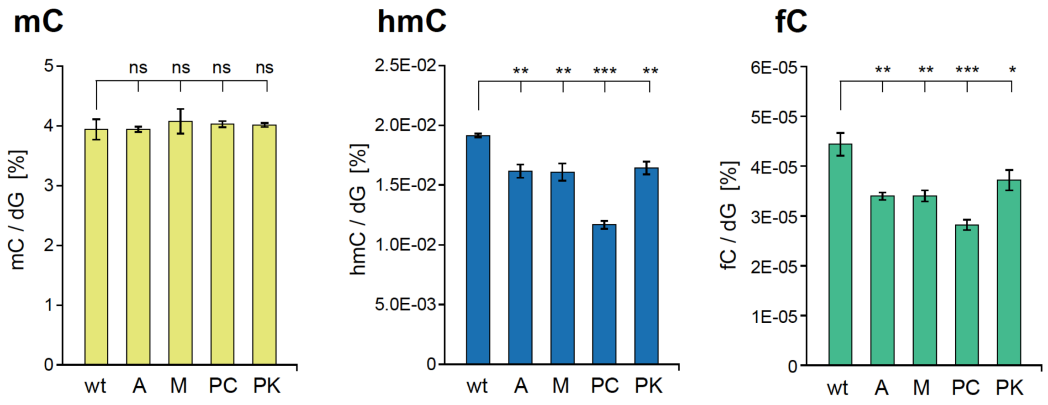

Figure 3.9 Quantification of global cytosine modifications in genomic DNA of knockdown cell lines. Shown are results for 5-methylcytoside (mC, in yellow), 5-hydroxymethylcytosine (hmC, in blue) and 5-formylcytosine (fC, in green); ns – not significant, wt – wild type, A – ACSS2 kd, M – MAT2B kd, PC – PCCA kd, PK – PKM2 kd; Values are given as modifications per 100 guanine bases. The results show mean of 3 biological and 2 technical replicates ± SD. For statistical analysis, Student's two-tailed t-test was used, * $p \leq 0.05$, ** ≤ 0.01, *** ≤ 0.001

3.3.5. Targeted metabolomic profiling of selected knockdown cell lines

Alterations in the abundances of histone PTMs and DNA modifications could be caused by the changes in the levels of cellular metabolites that are necessary for the writers and erasers to perform their function and establish the correct histone modification states. To elucidate whether the global changes that I observed in ACSS2 kd, MAT2B kd, PCCA kd and PKM2 kd are correlated with alterations in the abundance of epigenetically relevant metabolites, I decided to perform targeted MS-based metabolomic analysis of the studied knockdowns. Due to the fact that acetyl-CoA and SAM, being the co-substrates of histone acetyl- and methyltransferases respectively, were of my biggest interest, I aimed to find a platform that would enable me to quantify both metabolites in a single run. This task is not trivial due to the intrinsic chemical properties of acetyl-CoA which is prone to degradation upon ionisation in LC-MS approaches that are common for SAM quantification. After several tests performed in different metabolomic facilities, I established a collaboration with the Yanes Lab (Rovira I Virgili University) who were able to quantify these metabolites in a single LC-MS run. The whole set of metabolites detected and quantified by the Yanes Lab is shown in Figure 3.10.

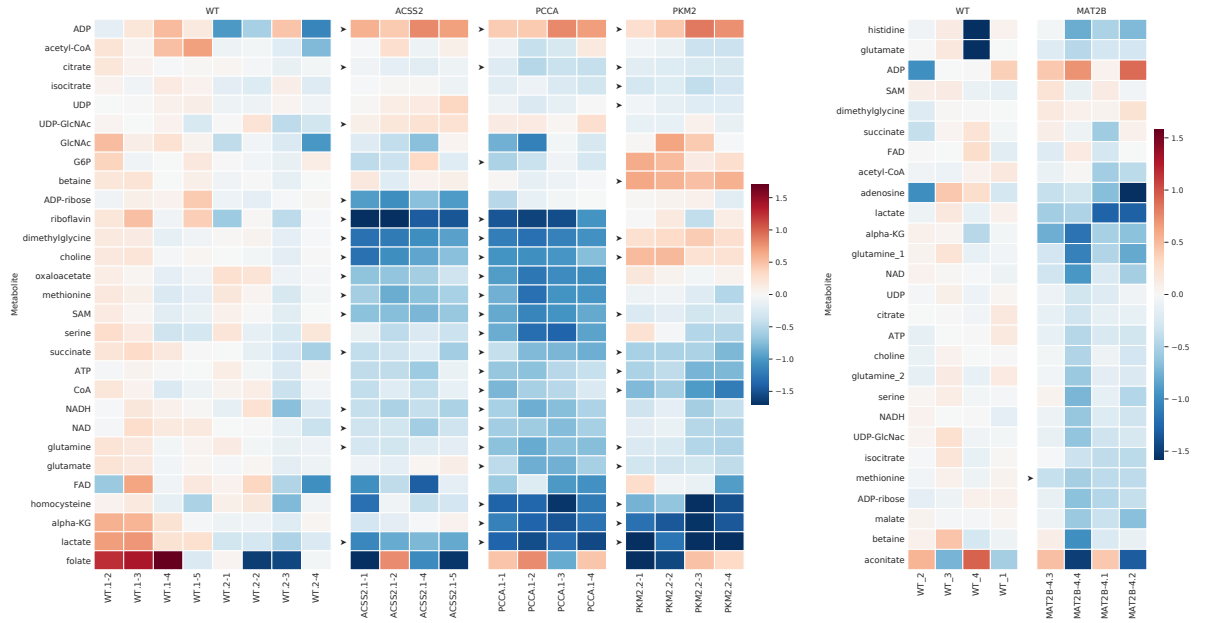

Figure 3.10 Heatmap analysis of LC-MS metabolomics in WT and knockdown cells. Colours indicate $\log_2$ fold changes in metabolite abundance. Due to the technical reasons, samples were quantified in 2 runs (ACSS2, PCCA, PKM2 knockdowns in run #1, MAT2B knockdown in run #2), each of which was compared to the WT sample analysed within the same run. 4 technical replicates of each knockdown were analysed. Metabolites indicated by the arrowheads were changed significantly with FDR ≤ 5%. P values were calculated from two-tailed Welch test with Benjamini-Hochberg correction.

The majority of metabolites quantified in this approach were downregulated relative to WT cells. The consistent exception observed in all investigated knockdown cell lines was upregulation of ADP (not significant in MAT2B kd), which together with downregulation of ATP, affected ATP : ADP ratio constituting a common sensor of cellular energy status [148].

I did not observe changes in global levels of acetyl-CoA. I reasoned that since it is a key metabolite involved in many cellular pathways, its abundance is tightly controlled and regulated to keep the pool of acetyl-CoA at the constant level even upon metabolic perturbation [79]. The other explanations could be linked to the subcellular compartmentalisation and potential post-harvesting artefacts [85]–[87], [149].

SAM, methionine and homocysteine, all involved in the methionine cycle, were downregulated in ACSS2 kd, PCCA kd and PKM2 kd. Surprisingly, MAT2B kd, directly involved in the methionine to SAM conversion, affected only the methionine level. Interestingly, PKM2 kd led to the significant upregulation of choline and its derivatives: betaine and dimethylglycine (DMG). Betaine-homocysteine methyltransferase (BHMT) uses betaine as a methyl donor for remethylation of homocysteine to methionine (with DMG as a side product) and thus contributes to the SAM recycling in the methionine cycle. However, since neither free SAM, nor methionine levels were upregulated in PKM2 kd, it suggests that in this knockdown the higher use of betaine as a methyl donor could at least partially mediate the observed gain of histone methylation. In this knockdown I also observed the downregulation of metabolites of TCA cycle: citrate, isocitrate, succinate and α-ketoglutarate, that consistently with the downregulation of lactate and a slight, yet not reaching statistical significance, increase of glucose-6-phosphate (G6P), reflects the expected perturbation in glycolysis and subsequently, TCA cycle.

In PCCA kd I observed downregulation of many metabolites involved in TCA cycle (citrate, oxaloacetate, succinate, α-ketoglutarate), methionine cycle (riboflavin, methionine, serine, SAM, homocysteine), and choline metabolism (choline, DMG). Knockdown of PCCA blocks the conversion of propionyl-CoA to methylmalonyl-CoA causing the mitochondrial accumulation of the former metabolite and its toxic derivatives: 3-hydroxypropionate, propionate and propionylcarnitine. These compounds affect multiple mitochondrial functions including TCA cycle, oxidative phosphorylation and glycine cleavage system that could explain the imbalance of related metabolites [150], [151].

The pattern of changes observed in ACSS2 kd resembled the one in PCCA kd. In this cell line the downregulation of TCA cycle metabolites can be caused by the shortage of acetate-derived acetyl-CoA supply (not detected in my analysis). The link between ACSS2 and 1C metabolism remains unclear.

Overall, the whole-cell metabolomic analysis did not allow me to fully explain the subtle and consistent changes in histone modification patterns in the investigated knockdown cell lines. Nevertheless, it shed light on the cellular pathways misregulated in the knockdown cell lines and pointed towards the need to investigate the links between the selected enzymes and metabolites that so far remain elusive. This analysis showed that even though the depletion of various enzymes manifests itself with similar changes in histone PTMs, the total metabolic state of these knockdowns represented by the abundances of metabolites, is different.

The trials to perform nuclear metabolome analysis, that would allow to quantify the abundance of cofactors in the compartment where the majority of histone writers and erasers perform their functions, were so far unsuccessful due to the technical challenges of sample preparation.

3.3.6. Genomic mapping of changes in histone PTMs

To elucidate whether the changes in histone PTMs constitute a genome-wide alteration or the marks are misregulated at particular genomic loci, I decided to conduct a ChIP-seq experiment using the antibodies raised against several marks that globally showed significant changes in MS-based screening and with H3K4me3 as an additional control for the IP since the antibody against this mark performed very well in

the previous ChIP experiments. To allow a comparison between the abundance of a given modification, or more broadly, between different chromatin states from various cell types or cells subjected to different treatments, spike-in approach should be applied [152]. In this modification of a standard ChIP-seq procedure a small and constant amount of reference chromatin from different species is added to the chromatin from the investigated cells. If the modification (or another ChIP target) of interest is not present in the reference species, a common strategy is to use two types of spike-in: reference chromatin and reference antibody e.g. commonly used *Drosophila* chromatin and antibody raised against *Drosophila*-specific histone H2Av. Since all the modifications that I wanted to investigate are present both in humans and in *Drosophila*, I decided to use the single spike-in approach [153].

3.3.6.1. Validation of antibodies

Anti-H3K9ac and anti-H3K27me3 antibodies were previously used in the Schneider Lab. H4K12ac and H4K5ac are the marks that are deposited on newly synthesised histones and were shown to co-reside in the same genomic regions, therefore for the ChIP I decided to choose one antibody that performs better in this application [154], [155]. Antibodies against H4K12ac and H4K5ac were not previously optimised, therefore I first tested (i) different amounts of each of them and (ii) the effect of extra washing step with lithium chloride (LiCl) that can improve the signal to noise ratio (Figure 3.11 a). In cases of both antibodies, the enrichment of ChIP signal at active h*ACTB* promoter over inactive h*NANOG* promoter was not dependent on the amount of used antibody but slightly improved in a procedure that included a more stringent LiCl wash. I achieved the highest h*ACTB* / h*NANOG* signal ratio for the anti-H4K12ac antibody, therefore I decided to use this antibody for the ChIP-seq experiment.

H3K9me3 is the modification that is enriched, among others, in highly compact, constitutive heterochromatin that upon standard sonication conditions is not released to the supernatant but stays in the pellet together with the cellular debris. Considering that in case of this mark, the amount of input chromatin might be the crucial factor, I tested (i) different amounts of input chromatin and (ii) the effect of a LiCl wash (Figure 3.11 b). In case of this antibody LiCl wash did not improve the specific signal. As expected, the higher mass of input chromatin slightly increased the above ratio.

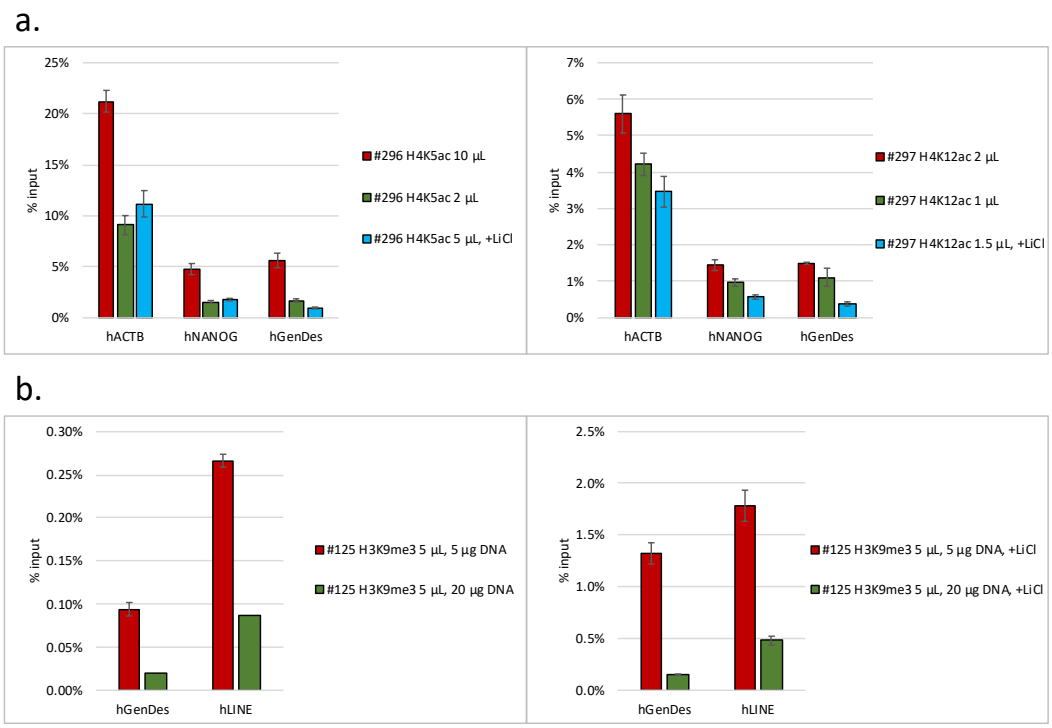

Figure 3.11 Validation of ChIP antibodies in human samples. Plotted are percentages of input recovered for different genomic amplicons after ChIP with indicated antibody. Data show mean of 2 replicates ± SD; **a.** Optimisation of anti-H4K5ac and anti-H4K12ac antibody use in ChIP. The highest h*ACTB* / h*NANOG* signal ratio (6.24) was observed for anti-H4K5ac antibody in a procedure including a LiCl wash (+LiCl); **b.** Optimisation of anti-H3K9me3 antibody use in ChIP. The highest h*LINE* / hGenDes ratio (4.29) was observed for the condition when 20 µg of chromatin DNA was used as the input; hGenDes – human DNA region devoid of genes ('gene desert'), h*LINE* – human long interspersed nucleotide element, #125, #296, #297 – internal numbers of used antibodies

To confirm that the chosen antibodies also perform well in ChIP of *Drosophila* S2 chromatin, I performed a test ChIP-qPCR with the antibodies previously tested with human chromatin. As shown in Figure 3.12, all tested antibodies performed well in the ChIP with *Drosophila* chromatin.

a.

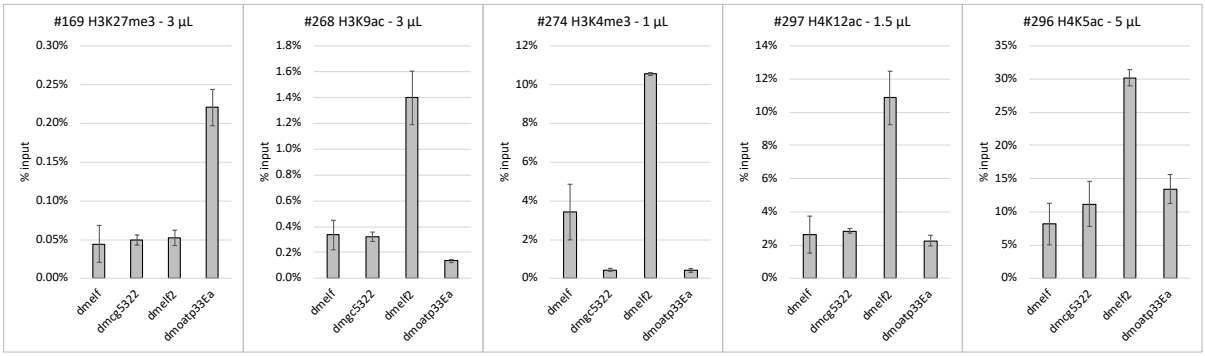

b.

	Type of control amplicon				
Amplicon	**H3K4me3**	**H3K27me3**	**H3K9ac**	**H4K5ac**	**H4K12ac**
dmelf	positive				
dmcg5322	negative				
dmelf2		negative	positive	positive	positive
dmoatp33Ea		positive	negative	negative	negative

Figure 3.12 Validation of ChIP antibodies in *Drosophila* samples; **a.** Plotted are percentages of input recovered for different genomic regions after ChIP with indicated antibody. Data show mean of 2 replicates ± SD; #169, #268, #274, #296, #297 – internal numbers of used antibodies **b.** Table defining types of control amplicons for different histone PTMs

3.3.6.2. Spike-in optimisation

To test if the spike-in approach with *Drosophila* chromatin would allow me to analyse ChIP-seq data quantitatively, I mixed two different amounts of *Drosophila* chromatin, equivalent of 5% and 15% of *Drosophila* nuclei (Dm5% and Dm15% respectively), with the constant amount of human chromatin. Considering the assumption that in spike-in ChIP, the proportion of reference chromatin (here: *Drosophila*) to target chromatin (here: human) should stay constant, such strategy mimicked the global, evenly distributed, genome-wide change in H3K4me3 in human cells. I did a trial ChIP-seq with well-performing anti-H3K4me3 antibody. The reads were aligned to the chimeric genome (hg38+dm6) generated specifically for this purpose. In the next step, for every condition I calculated the scaling factor α defined by: $\alpha = \frac{1}{N_d}$, where N_d is the number of reads aligned to *Drosophila* part of hg38+dm6 [152]. Normalisation of the read number using α equalised the signal in dm6 part of the chimeric genome in samples

with 3-fold difference of *Drosophila* chromatin (Dm5% and Dm15%) and consequently, decreased the signal in the hg38 part by the expected factor of 3 (Figure 3.13).

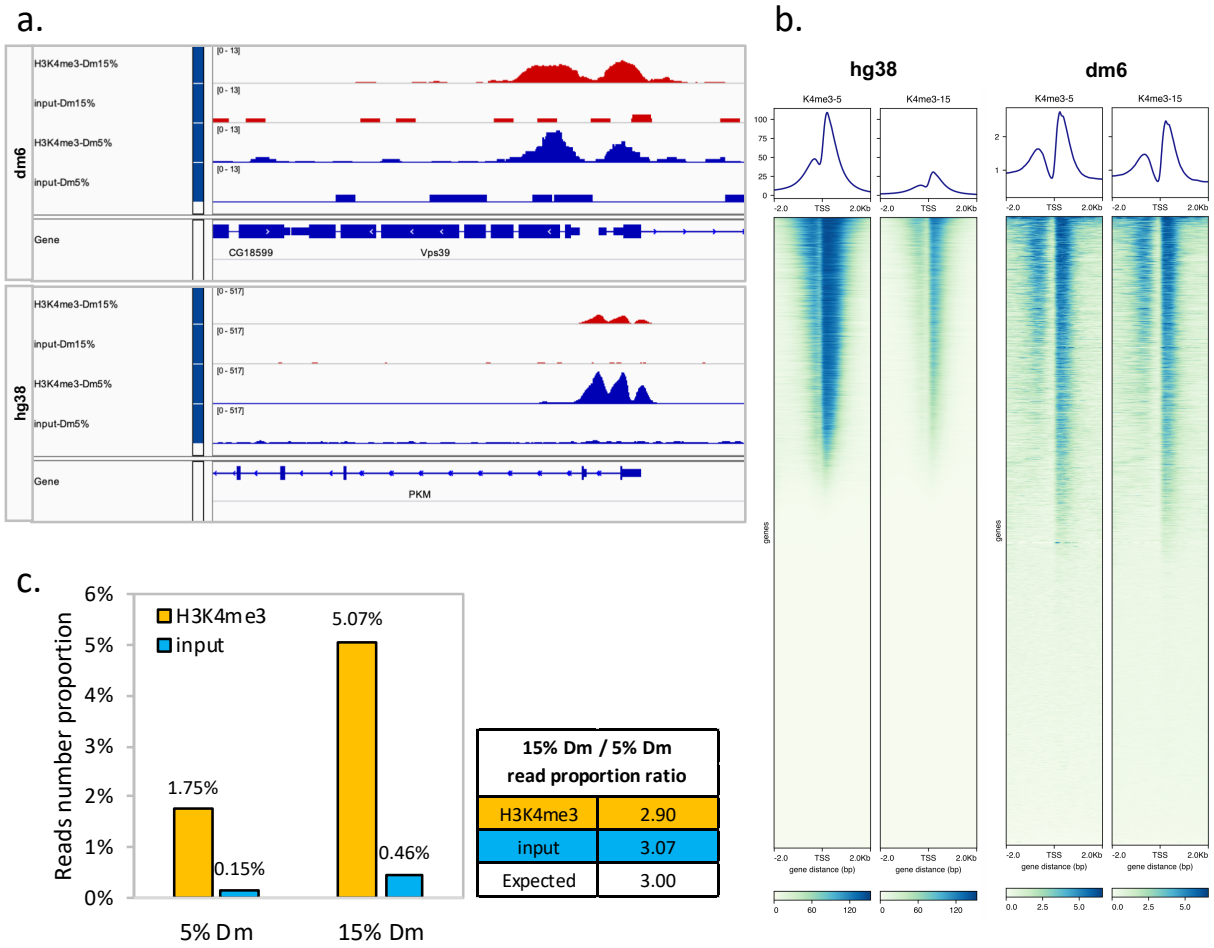

Figure 3.13 Quantitative analysis of H3K4me3 ChIP-seq in samples spiked-in with equivalents of 5% (Dm5%) or 15% (Dm15%) *Drosophila* nuclei; **a.** screenshots of *Drosophila* (dm6) and human (hg38) fragments of chimeric hg38+dm6 genome showing *Drosophila* and human promoters after α-normalisation. The signals in Dm5% and Dm15% samples in the dm6 part of the genome are comparable to each other while in the hg38 part the signal in Dm5% is visibly higher. All tracks within one screenshot are group autoscaled. **b.** Heatmaps of α-normalised read numbers across TSSs of all genes. Consistent with the screenshots in a. Dm15% sample (K4me3-15) shows decrease of the signal in human but not *Drosophila* promoters; **c.** Quantification of non-normalised reads aligned to *Drosophila* part of hg38+dm6.

Overall, this experiment showed that by using single spike-in with *Drosophila* chromatin as a reference in ChIP-seq from human cells I can quantitatively analyse genome-wide changes in the abundance of H3K4me3 mark in human cells. Unfortunately, in the subsequent experiments with other antibodies, simple α-normalisation was not working as expected. This might be caused by multiple

reasons including: (i) lower specificity of the antibodies, (ii) slightly different chromatin preparation coming from experiment-to-experiment variation (e.g. cell confluency, crosslinking time, formaldehyde concentration during crosslinking), (iii) different optimal ratio of *Drosophila* to human chromatin for various antibodies, (iv) unequal human to *Drosophila* chromatin ratio. Due to that, we decided to use the conventional ChIP-seq pipeline while still working on improving the performance of the spike-in approach for the other marks.

3.3.6.3. ChIP-seq and RNA-seq analysis

Depletions of ACSS2, MAT2B, PCCA and PKM2 caused global alterations in histone PTMs (chapter 3.3.3). To investigate the local changes of the abundance of these modifications in the genome I performed ChIP-seq with antibodies against globally changed histone marks: H3K9ac, H3K27me3, H4K12ac and H3K9me3. To complement the data and study changes in transcription, in my ChIP-seq experiment I included also antibody against H3K4me3, even though its abundance was not significantly changed in MS-based analysis, and performed RNA-seq analysis from the same knockdown cell lines.

As expected, combined analysis of RNA-seq and ChIP-seq signal revealed a positive correlation between the presence of the active marks (H3K4me3, H3K9ac, H4K12ac) and gene expression as well as a negative correlation between the repressive mark H3K27me3 and gene expression (Figure 3.14 a).

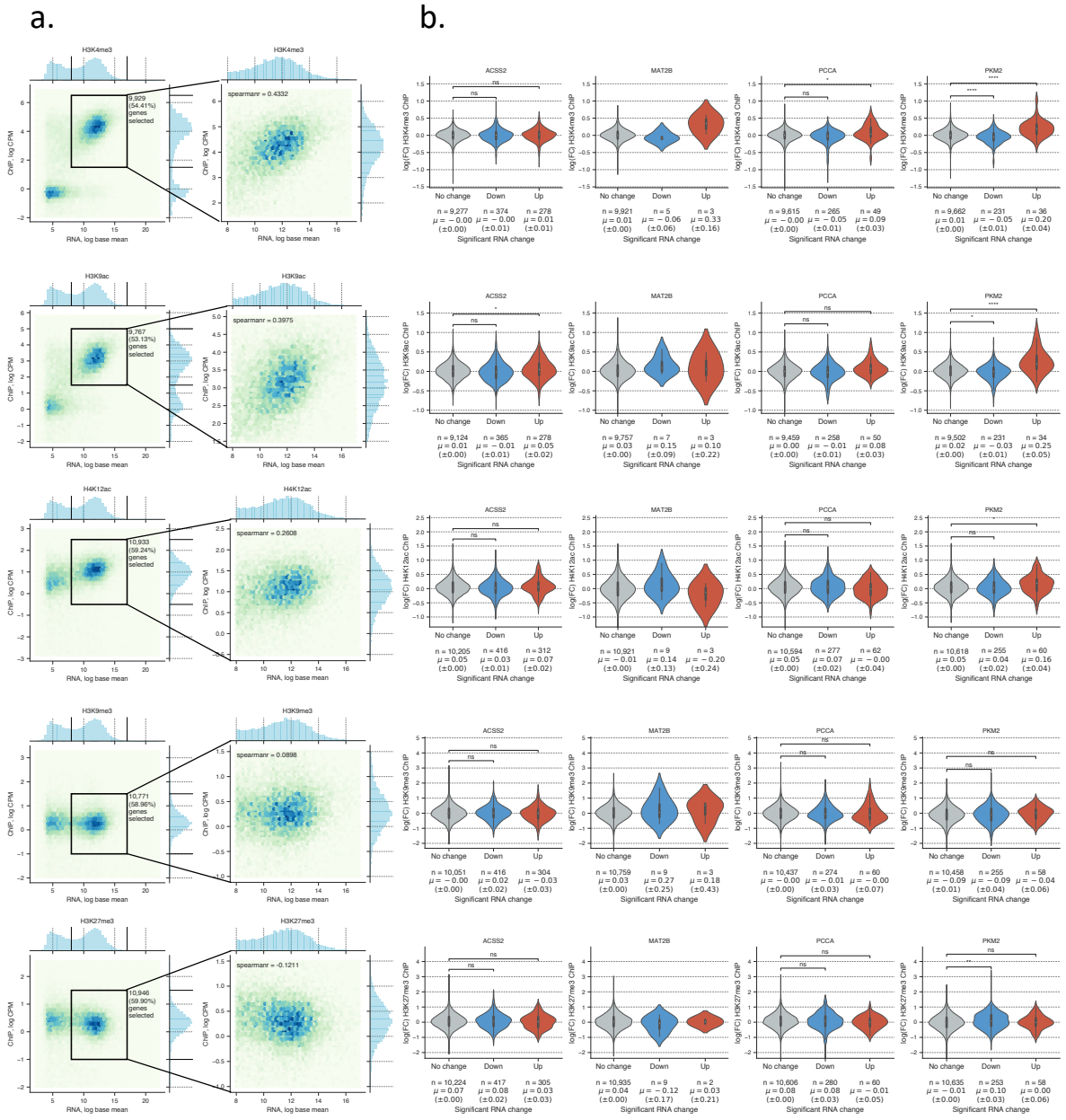

Figure 3.14 Correlation of changes in histone PTMs at gene promoters with their transcription; **a.** Spearman correlation between the abundance of indicated histone PTMs in the promoter region (TSS ± 3 kbp) and gene expression in WT. All the genes are presented in the left panel. The subset for which Spearman correlation was calculated is indicated by the boxes and presented in the right panel. Plotted are log_2 values of number of counts in RNA-seq (x axis) and log_2 values of number of counts per million reads (CPM) in ChIP-seq (y axis); **b.** Violin plots showing the log_2 fold change of the abundance of the indicated PTMs at gene promoters for groups of genes showing no change (in grey), downregulation (in blue) and upregulation (in red) in RNA-seq analysis of four investigated knockdown cell lines relative to WT. P values were calculated from two-sided Mann-Whitney U test with Bonferroni correction. Only classes with n ≥ 20 were tested; μ - mean (± standard error), n – number of genes, *p ≤ 5 x 10^{-2}, **p ≤ 1 x 10^{-2}, ***p ≤ 1 x 10^{-3}, ****p ≤ 1 x 10^{-4}

In the next step, we investigated whether the genes whose expression change in the knockdown conditions display alterations in the abundance of histone PTMs in their promoter regions (Figure 3.14 b). ACSS2 kd and PCCA kd showed low or not

significant correlations between the gain / loss of a given PTM and gene expression. In MAT2B kd the number of misregulated genes was too low to calculate the significance of investigated correlations. PKM2 kd showed a strong correlation between the abundance of H3K9ac and H3K4me3 and upregulation of gene transcription as well as milder, yet significant, correlation between the loss of the active marks or gain of H3K27me3 and downregulation of gene transcription. We then looked for the genes that gain or lose both H3K4me3 and H3K9ac and display up- or downregulation of transcription, respectively, in order to select the 'high confidence' genes whose promoter marks and expression are misregulated upon knockdown of PKM2 (Figure 3.15).

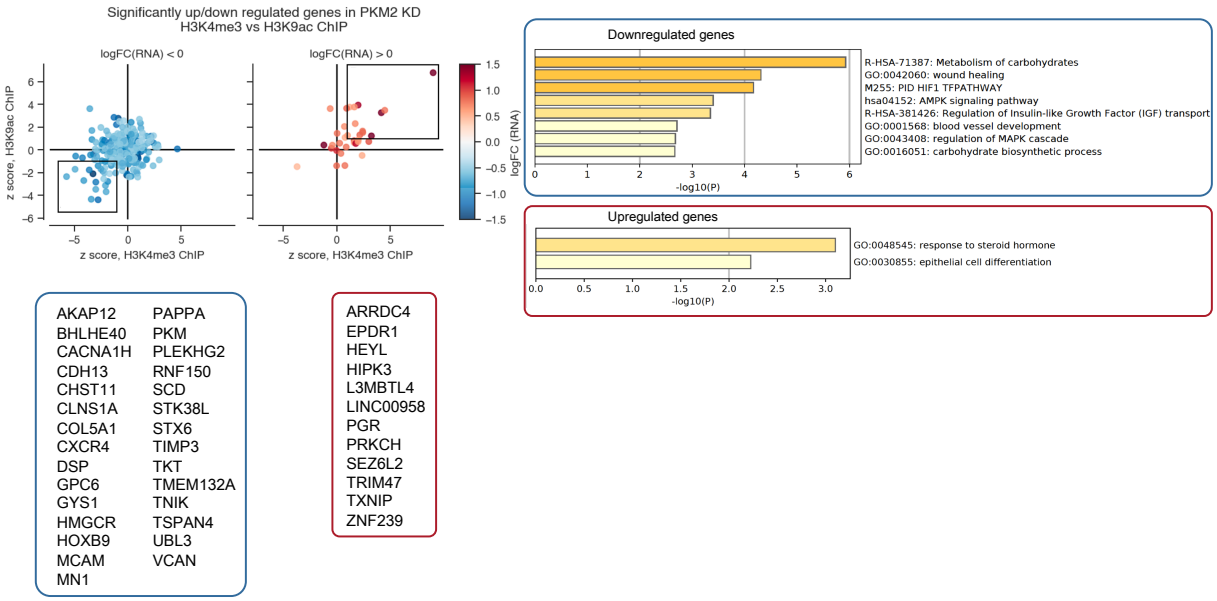

Figure 3.15 Identification of down- and upregulated genes showing depletion and increase of the abundance of active histone marks at their promoter upon PKM2 kd. Plotted are z scores of ChIP-seq fold change over WT cells for indicated histone PTMs and genes downregulated (in blue) and upregulated (in red) in RNA-seq. Genes indicated by the boxes are listed below the plots. GO terms analysis for the listed genes are shown in the right panel. The GO analysis was performed using Metascape resource [156].

Gene ontology (GO) analysis for the downregulated genes identified processes involved in metabolism of carbohydrates and AMPK signalling pathways that is in line with the role of PKM2 in glycolysis and glucose metabolism as well as with my results

of metabolomic analysis. We identified only several genes upregulated with high confidence and for these genes no metabolic processes were identified in GO analysis. However, among the upregulated genes there were two members of arrestin domain-containing family of proteins: *ARRDC4* and *TXNIP* previously reported to be involved in glucose homeostasis [157]. While in my further studies I focused on the subset of genes including these two candidates (chapters 3.3.7.2-3.3.7.5), we are also planning to investigate the functional role of other misregulated genes upon PKM2 depletion and aiming to find a link between metabolic changes and alterations of histone PTMs at the promoters of these genes.

3.3.7. PKM2 knockdown affects the expression of genes involved in oxidative stress response

3.3.7.1. Isoforms and oligomerisation state of *PKM* encoded proteins

PKM is a gene encoding two isoforms: PKM1 and PKM2 that differ in presence of mutually exclusive exons 9 and 10 in the spliced transcript. Exon 10-containing PKM2 can exist as a glycolytically active tetramer and glycolytically inactive dimer involved in nuclear protein phosphorylation, while exon 9-containing PKM1 exists only as a glycolytically active stable tetramer. Since the sequence of shRNA that I used for establishing stable knockdown cell line targets the part shared between the isoforms, I aimed to elucidate depletion of which isoform caused the observed phenotype. To address this question, I first analysed the abundance of all transcripts encoded by *PKM* gene in WT HEK293 cells (Figure 3.16 a). The most abundant transcript (PKM-202) constituting around 90% of all the *PKM* transcripts encodes PKM2 what stands in agreement with previously published data showing that in HEK293 PKM2 constitutes more than 95% of pyruvate kinase at the protein level [158].

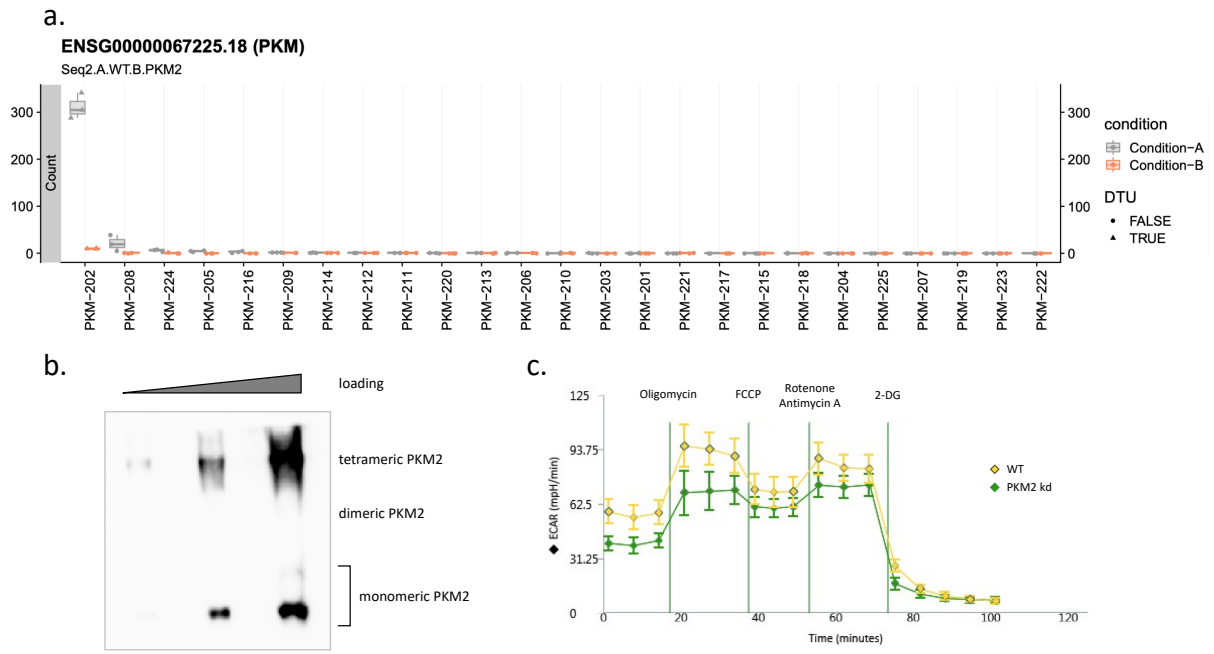

Figure 3.16 Inferring the role of *PKM* gene product in WT HEK293; **a.** Abundance of transcripts encoded by *PKM* in WT (Condition-A) and PKM2 kd (Condition-B) The most abundant transcript (PKM-202) encodes PKM2 isoform. The second most abundant transcript (PKM-208) does not encode protein. Significant Differential Transcript Usage (DTU) between WT and PKM2 kd was detected only for transcript PKM-202; **b.** Immunoblot of WT cells crosslinked with DSS and probed with isoform specific, anti-PKM2 antibody; **c.** Changes in the extracellular acidification rate (ECAR) upon sequential injections of compounds affecting electron transport chain (ETC) and glycolysis. PKM2 kd (in green) displayed lower acidification of the medium than the WT cells (in yellow) that was equalised after injection of glycolysis inhibitor 2-deoxyglucose (2-DG). Each data point shows mean of 15 replicates ± SD

As a next step, I investigated the oligomerisation state of the PKM2 isoform. For this I crosslinked the WT cells with disuccinimidyl suberate (DSS) and analysed the size of crosslinked mono- and oligomers (Figure 3.16 b). I detected a significant amount of tetrameric PKM2 indicating that in WT HEK293 cells this protein performs glycolytic function. Together with the observation that in the PKM2 kd cell line the total amount of PKM2 was significantly reduced (Figure 3.8 c and Figure 3.16 a) I concluded that the depletion of *PKM* transcripts severely affects the glycolytically active tetrameric PKM2. I further evaluated this inference by analysing extracellular acidification rate (ECAR) in the WT and PKM2 kd cells upon sequential injection of oligomycin (inhibitor of mitochondrial ATP-synthase), FCCP (dissipator of proton gradient), rotenone + antimycin A (inhibitors of complex I and III of electron transport chain (ETC)) and 2-deoxy-D-glucose (2-DG, inhibitor of glycolysis) (Figure 3.16 c).The conversion of

glucose to pyruvate, and subsequently lactate, results in a net production and extrusion of protons into the extracellular medium. This causes acidification of the medium that can be directly measured. From the beginning of the experiment, ECAR displayed by the PKM2 kd was lower than in the WT cells suggesting that in steady state (before injection of oligomycin) as well as upon injection of modulators of ETC, glycolysis was less efficient in the PKM2 kd. Notably, inhibition of glycolysis by 2-DG revealed that non-glycolytic acidification rate was equal in both analysed cell lines suggesting that the initial difference in ECAR could be caused by impaired glycolysis in PKM2 kd. However, it should be noted that this experiment did not account for the potential aberrations in glucose uptake. The changes in oxygen consumption rate (OCR) measured in parallel showed the expected pattern and were not drastically changed between WT and PKM2 kd suggesting that this knockdown does not cause aberrations in ETC (data not shown) [159].

3.3.7.2. PKM2 knockdown affects genes associated with oxidative stress

Analysis of ChIP-seq and RNA-seq data revealed that in PKM2 kd (but not in all the other knockdown cell lines), there was a consistent upregulation of *TXNIP*, *ARRDC4* and *DHRS2* encoding thioredoxin interacting protein, arrestin domain-containing protein 4 and dehydrogenase / reductase SDR family member 2, respectively (Figure 3.15 and Figure 3.17).

a.

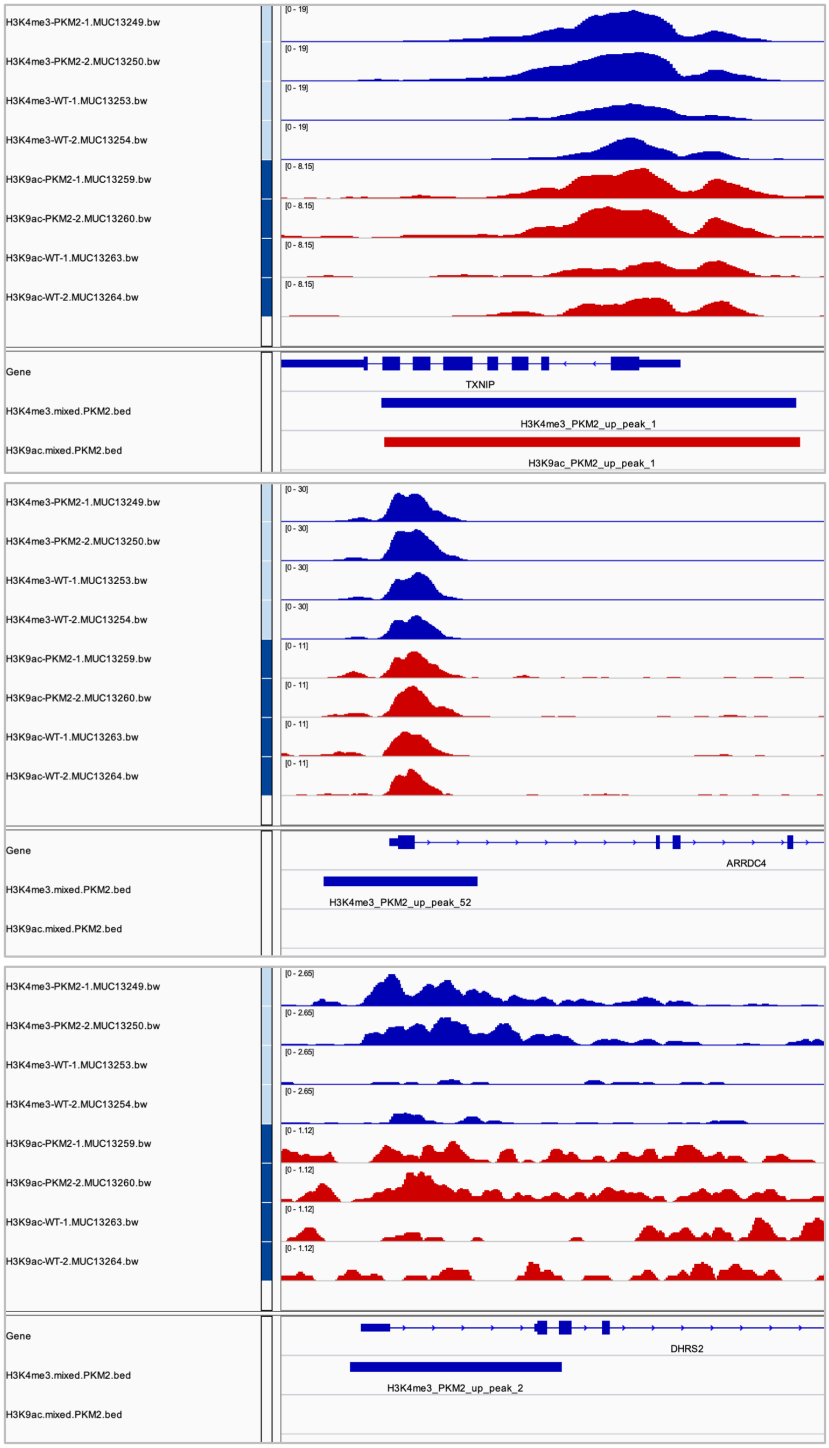

b.

Gene symbol	Expression fold change (log2)	Adjusted p value
TXNIP	3.38	3.18E-02

Gene symbol	Expression fold change (log2)	Adjusted p value
ARRDC4	1.61	2.20E-03

Gene symbol	Expression fold change (log2)	Adjusted p value
DHRS2	2.07	7.35E-08

Figure 3.17 Changes in histone PTMs at promoters of upregulated *TXNIP*, *ADDRC4* and *DHRS2* genes in PKM2 kd; **a.** screenshots of H3K4me3 (blue) and H3K9ac (red) ChIP-seq tracks in two replicates of PKM2 kd (two top tracks of every modification) and WT (two bottom tracks of every modification). Below the 'Gene' track the differential peaks are indicated. Peaks are ranked by increasing FDR; **b.** Fold mRNA abundance of relevant transcripts based on RNA-seq

TXNIP and ARRDC4 are members of arrestin domain-containing family of proteins and were shown to be the only members of this family highly upregulated in response to glucose by a complex of transcription factors MondoA : MLX suggesting that these transcription factors can be involved in transcription regulation in PKM2 kd [160]. TXNIP is the only protein in arrestin domain-containing family that plays a role in regulation of oxidative stress [161]. By binding thioredoxins (TXNs) via the cysteine residue necessary for reducing oxidised cysteines in other proteins, TXNIP blocks the activity of TXNs rendering the cell more susceptible to oxidative stress.

DHRS2 is an NADPH-dependent dicarbonylreductase belonging to the short-chain dehydrogenase / reductase (SDR) family. While SDR family proteins are responsible for conversion of a wide range of exo- and endogenous metabolites, the expression and enzymatic activity of DHRS2 was linked to metabolism of oxidative stress-induced α-dicarbonyls [162].

3.3.7.3. Upregulation of *TXNIP* and *ARRDC4* but not *DHRS2* in PKM2 knockdown can be mediated by MondoA : MLX transcription factors

TXNIP and *ARRDC4* have been previously shown to be regulated by the complex of transcription factors MondoA : MLX that binds to the carbohydrate response elements (ChoREs) within the promoters of these genes. To evaluate if *DHRS2* can be a novel target of MondoA : MLX, I analysed the promoter sequences of *TXNIP*, *ARRDC4* and *DHRS2* in order to detect potential binding sites of MondoA and MondoB (MondoA/B; both transcription factors share the binding motif) and MLX [163] (Figure 3.18 a). In the sequences within 500 bp upstream of TSSs MondoA/B and / or MLX binding sites were detected only for the promoters of *TXNIP* and *ARRDC4* suggesting that *DHRS2* is not

likely to be directly upregulated by MondoA : MLX. To corroborate that MondoA : MLX complex mediates the upregulation of *TXNIP* and *ARRDC4* in PKM2 kd, I performed ChIP-qPCR with antibodies against MondoA and MLX (Figure 3.18 b-d.). Due to the low complexity of the promoter of *DHRS2*, specific qPCR primers could not be designed for this region. As a negative control region I used the promoter of a housekeeping gene *ACTB* which does not contain ChoRE. As expected, both MondoA and MLX were significantly enriched at their target loci in comparison to *ACTB* promoter. Moreover, in PKM2 kd the enrichment of both transcription factors at the promoters of *TXNIP* and *ARRDC4* was slightly higher than in WT cells. This suggests that upregulation of *TXNIP* and *ARRDC4* observed upon PKM2 depletion can be driven by MondoA : MLX.

a.

Motif ID	-log10(P-value)	Seq name	Sequence	Logo	P-value	Start	End	Strand
MLXPL_HUMAN.H11MO.0.D	5.283	TXNIP_prom500	GCTCGTGCTGCCCTCGTGC		5.212e-6	71	89	+
MLXPL_HUMAN.H11MO.0.D	4.959	TXNIP_prom500	GCGCGTGGACACGGTGTGC		1.099e-5	157	175	+
MLX_HUMAN.H11MO.0.D	4.769	ARRDC4_prom500	TGTGCACGTGC		1.702e-5	286	296	+
MLXPL_HUMAN.H11MO.0.D	4.73	ARRDC4_prom500	GCACGTGCACAGGCCGTTT		1.862e-5	278	296	-
MLX_HUMAN.H11MO.0.D	4.662	ARRDC4_prom500	CGTGCACGTGC		2.178e-5	289	299	-
MLXPL_HUMAN.H11MO.0.D	4.104	ARRDC4_prom500	CCATGTGGACAGACAGTGG		7.870e-5	204	222	-

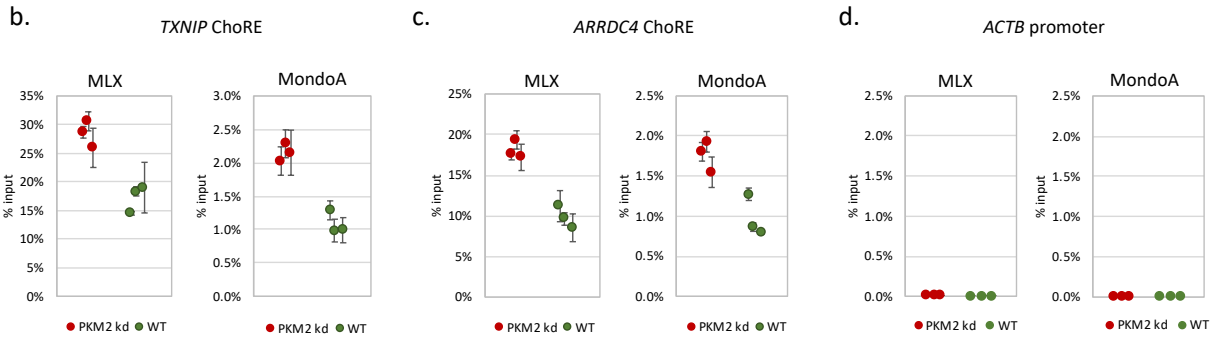

Figure 3.18 Transcription factors MondoA and MLX bind the promoters of *TXNIP* and *ARRDC4*; **a.** Binding sites of MondoA/B (MLXPL) and MLX detected in the promoters of *TXNIP* and *ARRDC4* (no binding sites were detected in *DHRS2* promoter). Analysis was done using MoLoTool available online with the P-value threshold = 1 x 10^{-4}; **b-d.** ChIP-qPCR enrichment of MondoA and MLX at the promoters of *TXNIP* (b.) and *ARRDC4* (c.) containing carbohydrate response elements (ChoREs) and *ACTB* (d.) devoid of ChoRE. Plotted are percentages of input recovered for indicated genomic regions and antibodies. Data show 3 independent IP samples for PKM2 kd and WT. Each data point shows mean of 3 replicates ± SD

3.3.7.4. *DHRS2* expression is induced by prolonged oxidative stress

TXNIP and DHRS2 are proteins encoded by two of the most upregulated genes in PKM2 kd and were previously shown to have a role in response to oxidative stress. To investigate whether *DHRS2* expression can be increased in response to oxidative stress in WT HEK293 cells, I treated the cells with GSH-conjugating reagent, diethyl maleate (DEM), and monitored the expression of *DHRS2* as well as the genes involved in thioredoxin antioxidant system over the course of time (Figure 3.19).

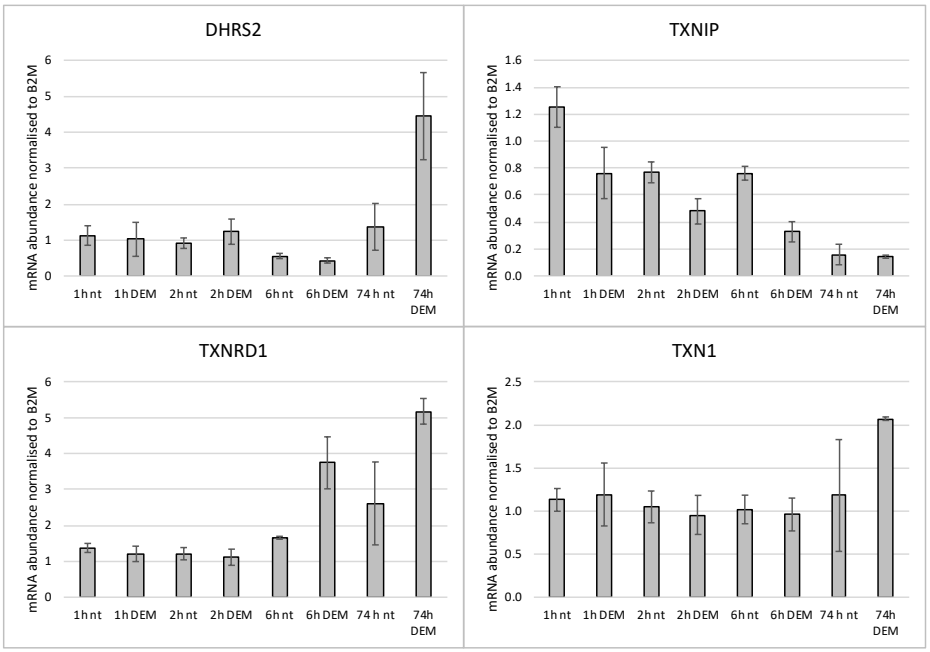

Figure 3.19 Representative experiment showing RT-qPCR-based quantification of mRNA of genes potentially involved in oxidative stress response in HEK293 cells upon treatment with 100 μM DEM in a 3-day time-course. Plotted are transcript abundances relative to housekeeping gene *B2M*. 2 hours before collecting the cells from the final timepoint, fresh medium with and without DEM was added to the treated and non-treated cells respectively; data show mean of 2 replicates ± SD; nt – non-treated cells

DHRS2 expression was not affected by up to 6 h of treatment with DEM but became significantly increased after prolonged, 3-day treatment. As expected, thioredoxin reductase 1 (*TXNRD1*) responsible for anti-oxidative function of thioredoxin system showed the same trend, yet with different kinetics. Its expression was elevated already after 6 h of treatment what suggests that the mechanisms of transcriptional activation

of *DHRS2* and *TXNRD1* are different. Interestingly, oxidative stress caused by GSH depletion downregulated *TXNIP* expression already after 1 h of treatment with DEM. This suggests that the upregulation of *TXNIP* observed in PKM2 kd is not likely to be the result of oxidative stress caused by reduced pool of GSH. The expression of thioredoxin 1 (*TXN1*) was not severely affected during the course of the whole experiment.

To address the question whether oxidative stress induced specifically by the inhibition of TXN1 activates *DHRS2* transcription, I analysed the mRNA levels of HEK293 cells treated with thioredoxin 1 inhibitor PX-12 (Figure 3.20).

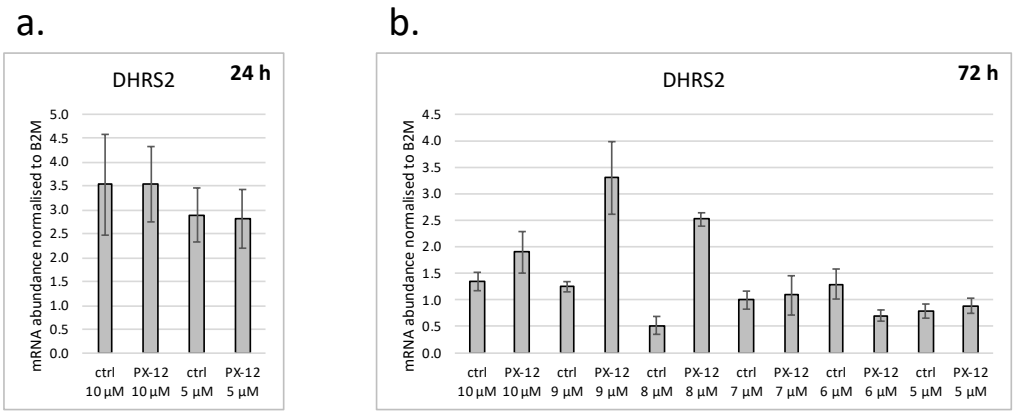

Figure 3.20 Representative experiment showing RT-qPCR-based quantification of mRNA of *DHRS2* in HEK293 cells treated with various concentrations of PX-12; **a.** 24-h treatment; **b.** 72-h treatment with a range of PX-12 concentration. Treatment with 8 μM PX-12 was repeated 3 times with consistent activation effect; data show mean of 2 replicates ± SD; ctrl – cells treated with DMSO, volume of DMSO in control samples was adjusted to its volume necessary to dissolve PX-12 stock to the desired concentration

After 24 h of treatment with 10 μM and 5 μM PX-12 I did not observe any changes in *DHRS2* expression. However, I observed that 10 μM PX-12 exerted toxicity to the cells. Since in the experiments with DEM, *DHRS2* expression was elevated only after prolonged treatment, in the next step I treated the cells with PX-12 for 72 h at the concentration 10 μM – 5 μM with 1 μM increment. Similarly to the response to DEM,

PX-12 at the concentration ≥ 8 μM increased *DHRS2* expression after prolonged treatment.

Overall, this set of experiments showed that *DHRS2* can be upregulated by oxidative stress caused by the prolonged inhibition of TXN1.

3.3.7.5. Short-term depletion of PKM2 induces *TXNIP* but not *DHRS2*

The abundances of histone PTMs and cellular metabolites as well as ChIP-seq and RNA-seq analysis of PKM2 kd were performed on a population of cells 3-4 weeks after lentiviral transduction. To shed more light on the kinetics of gene expression changes and elucidate whether *DHRS2* can be responsible for the process of long-term adaptation after depletion of PKM2, I performed a sequential siRNA-mediated knockdown and analysed expression of *TXNIP* and *DHRS2* 6 days after transfection (Figure 3.21).

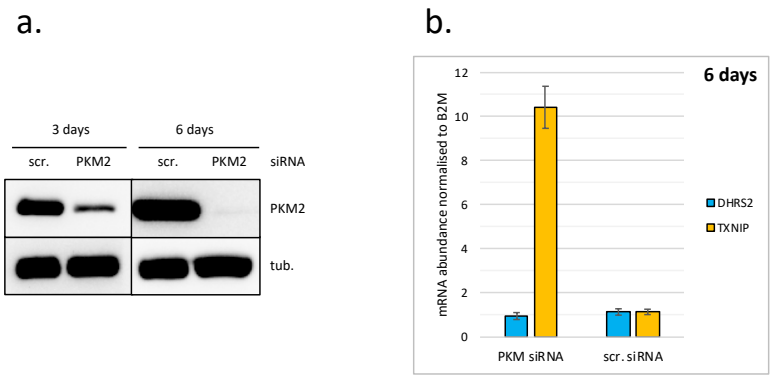

Figure 3.21 *TXNIP* is upregulated within 6 days after depletion of PKM2; **a.** Immunoblot showing the depletion and almost complete loss of PKM2 3 and 6 days after the first of two sequential transient transfections respectively, scr. – scrambled control, tub. – tubulin; **b.** RT-qPCR-based quantification of mRNA of *DHRS2* and *TXNIP* in the samples shown on the right side of a. (6 days), data show mean of 2 replicates ± SD

As expected, treatment with siRNA targeting PKM transcripts for 6 days led to almost complete loss of PKM2 (Figure 3.21 a). Knockdown efficiency at the level of protein

was more profound than the stable shRNA-mediated knockdown (compare with Figure 3.8 c). Such effect is not surprising taking into consideration that (i) for siRNA-mediated knockdown I used a pool of 4 siRNAs targeting different fragments of the transcript and (ii) the vector encoding shRNA after integration into the host genome can be subjected to epigenetic silencing. Notably, the almost complete ablation of PKM2 significantly induced *TXNIP* but not *DHRS2* (Figure 3.21 b). This shows that upon PKM2 knockdown *TXNIP* and *DHRS2* have different kinetics of induction and suggests that *DHRS2*, expressed upon prolonged depletion of PKM2, can play a role in long-term adaptation to the metabolic perturbation.

3.4. Identification of nuclear interacting partners of investigated metabolic enzymes

The nuclear localisation of ACSS2, PKM2 and MAT2B was previously reported [164]–[166]. To shed light into the potential nuclear function of the enzymes of my interest in HEK293 model, I performed the IP from the nuclear fraction followed by MS-based identification of the interacting proteins. I decided to conduct this experiment in the cells overexpressing the FLAG-2HA-tagged enzymes because the antibodies raised against the endogenous proteins performed poorly in the IP experiments. Due to the fact that to obtain the sufficient amount of nuclear extract for IP I needed to process a large number of cells grown in a high scale culture, instead of transfecting the cells transiently, I generated the 4 necessary stable cell lines. After transfecting the cells with the vectors encoding FLAG-2HA-enzymes and 2 weeks of selection with geneticin sulfate (G418), I monitored the expression of all 4 proteins by immunoblotting (Figure 3.22 a-c). It turned out that the cells stably transfected with the PCCA construct lost its expression suggesting that overexpression of this enzymes is not favourable

for the cells. All 3 other enzymes were stably overexpressed, therefore for the nuclear fraction preparation I used ACSS2, PKM2 and MAT2B stable cell lines and cells transiently transfected with PCCA. I confirmed the purity of nuclear fractions by comparing the abundance of tubulin in nuclear fractions and in the total cell extracts (Figure 3.22 d). Next, I performed the IP from the nuclear fraction against the FLAG-tag and I submitted the elution fractions enriched in the overexpressed enzymes for MS analysis (Figure 3.22 e).

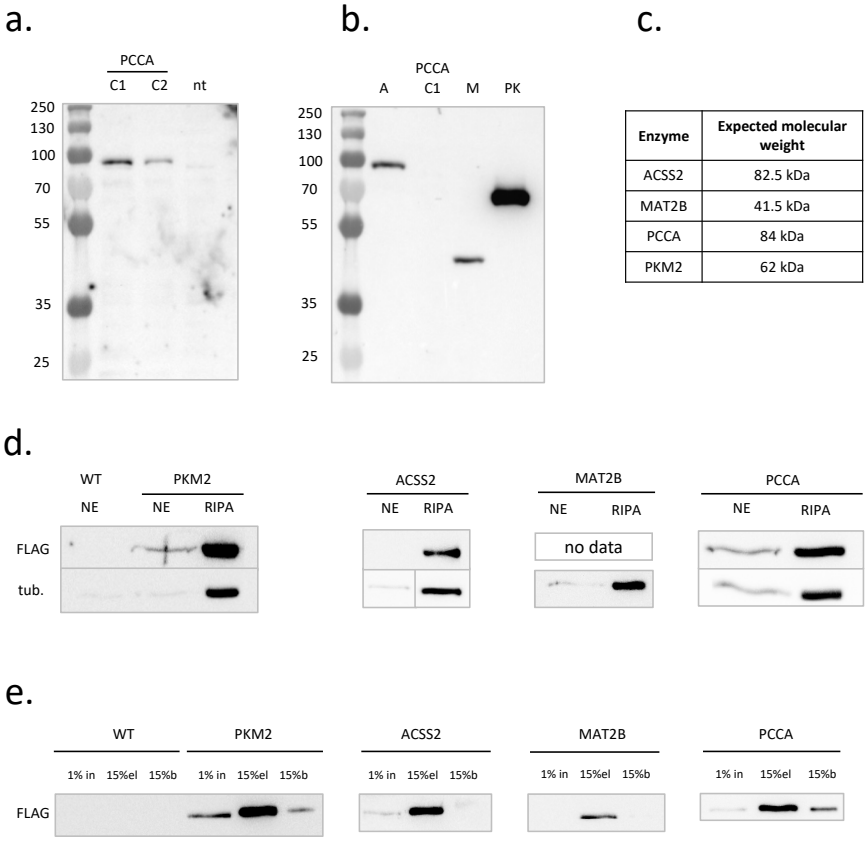

Figure 3.22 IP of the overexpressed metabolic enzymes from nuclear fraction; **a.** Immunoblot of the total cell extract samples from expression test of the self-assembled FLAG-2HA-PCCA construct in transient transfection; **b.** Immunoblot of the total cell extract samples from expression test of the stable cell lines after 14 days of selection with G418. In a. and b. anti-FLAG antibody was used; **c.** Expected molecular weights of the FLAG-2HA-tagged enzymes; **d.** Control for the contamination of nuclear with cytosolic fraction, **e.** Enrichment of immunoprecipitated enzymes in the elution fractions; 1% in – 1% input, 15%el – 15% elution fraction, 15%b – 15% anti-FLAG beads after elution, A – ACSS2, C1 or C2 – construct isolated from *E. coli* clone 1 or 2, M – MAT2B, NE – 20 μg nuclear extract, nt – non-transfected cells, PK – PKM2, tub. – tubulin, RIPA – 10 μg total cell extract, WT – wild type

The sample preparation and data analysis were done by the Core Facility Proteomics (Helmholtz Zentrum München). For protein identification Progenesis QI software was used. The results of the analysis are presented in Figure 3.23.

a.

Enzyme	Number of interactors	
	Replicate 1	Replicate 2
ACSS2	19	ND
MAT2B	163	69
PCCA	9	ND
PKM2	38	3

b.

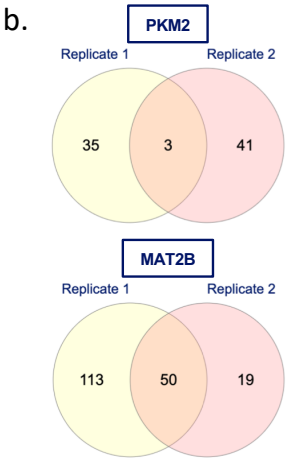

c.

Gene	Encoded protein
DDX21	Nucleolar RNA helicase
DKC1	H/ACA ribonucleoprotein complex subunit
EBNA1BP2	Probable rRNA-processing protein EBP2
HIST1H1E	Histone H1.4
HNRNPM	Heterogenous nuclear ribonucleoprotein M
KIF11	Kinesin-like protein
MAT2B	Methionine adenosyltransferase 2 subunit beta
NOP2	Probable 28S rRNA (cytosine (4447)-C(5))-methyltransferase
NUMA1	Nuclear mitotic apparatus protein 1
RBM28	RNA-binding protein 28
RPL10A	Ribosomal proteins
RPL11	
RPL12	
RPL13	
RPL13A	
RPL14	
RPL15	
RPL18	
RPL18A	
RPL21	
RPL23A	
RPL27	
RPL3	
RPL30	
RPL31	
RPL34	
RPL35A	
RPL4	
RPL5	
RPL6	
RPL7	
RPL8	
RPLP0	
RPLP2	
RPS14	
RPS16	
RPS18	
RPS2	
RPS23	
RPS25	
RPS3	
RPS3A	
RPS5	
RPS6	
RPS8	
RPSA	
RSL1D1	Ribosomal L1 domain-containing protein 1
SDHA	Succinate dehydrogenase, mitochondrial
TP53	Cellular tumour antigen p53
YBX1	Y-box-binding protein 1

d.

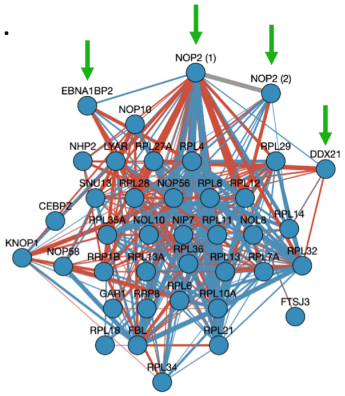

e.

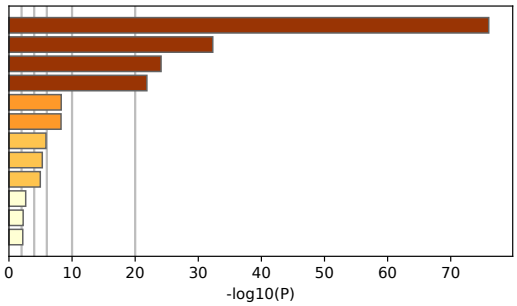

GO:0006614: SRP-dependent cotranslational protein targeting to membrane
GO:0042254: ribosome biogenesis
GO:0042273: ribosomal large subunit biogenesis
GO:0002181: cytoplasmic translation
GO:0042274: ribosomal small subunit biogenesis
GO:0003729: mRNA binding
GO:0008097: 5S rRNA binding
GO:0045296: cadherin binding
GO:0000470: maturation of LSU-rRNA
GO:0051225: spindle assembly
GO:0033044: regulation of chromosome organization
GO:0043487: regulation of RNA stability

Figure 3.23 Analysis of the nuclear interactors of the metabolic enzymes overexpressed in HEK293 cells; **a.** Number of interactors identified with more than 1 unique peptide enriched ≥ 5-fold over the control; ND – no data; **b.** Venn diagrams showing the numbers of shared hits between two biological replicates of IP; **c.** List of MAT2B nuclear interactors enriched in both biological replicates. In green are shown proteins marked with green arrows in d.; **d.** Screenshot of the complex predicted by the dataset

of nuclear proteins interacting with differently modified nucleosomes, data not published (manuscript in preparation), access kindly granted by Dr. Saulius Lukauskas; **e.** GO terms analysis of the biological processes enriched for the proteins listed in c. The analysis was performed using Metascape resource [156]

In the first replicate of the experiment only MAT2B and PKM2 showed interactions with histones and / or histone interacting proteins what could imply the involvement of these enzymes in the chromatin regulating processes. Surprisingly, MAT2B co-immunoprecipitated a set of proteins associated with ribosome biogenesis, RNA splicing, regulation of mRNA mediated processes and maturation of large subunit ribosomal ribonucleic acid. To validate the results, I performed the second biological replicate of nuclear IP for these two enzymes. The numbers of proteins enriched in the elution fraction over the WT cells are shown in Figure 3.23 a-b. Two replicates of PKM2 IP showed the overlap of only 3 proteins, one of which was the PKM1/2 itself (the particular isoforms were not identifiable). Interestingly, my experiments showed that MAT2B, a regulatory subunit of SAM synthetase, can physically interact with methyltransferase NOP2 as well as with putative rRNA processing protein EBNA1BP2 and nucleolar RNA helicase DDX21 that probably form a nucleolar complex (Figure 3.23 c-d). In total, 50 hits from the first replicate of MAT2B IP were also enriched in the second replicate. Gene ontology (GO) analysis of the biological processes enriched for the overlapping hits identified multiple processes involved in ribosomal biogenesis (Figure 3.23 e). Large subunit of human ribosome consists of 46 proteins and 3 rRNA molecules: 28S, 5.8S and 5S [167]. 28S and 5.8S rRNA are heavily post-transcriptionally modified [168]. One of the rRNA modifications, 5-methylcytosine (5-mC) is present only in two sites of human 28S rRNA and is characterised by the 100% abundance suggesting that this modification plays an important role in the structure or / and function of ribosomes. Studies in yeast identified Nop2 as a 25S rRNA C2870 methyltransferase. The activity of a human homologue NOP2 (NSUN1,

p120) on the corresponding cytosine on 28S rRNA (C4447) has not been confirmed yet. The observation that MAT2B can interact with multiple proteins involved in nucleolar rRNA maturation, including methylation, suggests the mechanism of the in-situ production of metabolic cofactor used for rRNA modification. To further investigate the interaction between MAT2B and NOP2 I established a HEK293 cell line stably overexpressing NOP2 and performed the reverse IP experiment. In the first replicate there was no enrichment of MAT2B in the elution fraction (data not shown). The further experiments that are currently ongoing as well as the outlook are described in the discussion.

4. Discussion

Research at the interface between epigenetics and metabolism has been growing dynamically in the last years. To provide advances in this still expanding field, in this PhD thesis I presented a thorough functional characterisation of selected metabolic enzymes whose activity is crucial for establishing the pools of epigenetically relevant metabolites. I established multiple connections between these enzymes and chromatin modifications, cellular metabolic state and gene expression. I addressed challenging questions regarding canonical and non-canonical functions, influence on chromatin modifications as well as the contribution of various metabolic enzymes to the overall cellular homeostasis.

Overall, in my work I identified betaine-homocysteine methyltransferase 2 (BHMT2) as a potential new player in establishing histone H3 methylation and affecting gene expression; discovered that ACSS2, MAT2B, PCCA and PKM2 contribute to the global levels of various chromatin modifications and uncovered a link between aberrant levels of PKM2 with oxidative stress response. Below I discuss these findings in more detail.

4.1. Localisation of metabolic enzymes at gene promoters promotes transcription

The nucleus of eukaryotic cells contains macromolecules at high concentration. This viscous medium restricts free diffusion of small metabolites that might slow down the transfer of the information from the cytosol [169]. Close coupling of metabolic enzymes and histone modifiers has been recently reported in the nucleus but this phenomenon

has not been systematically addressed [85]–[87], [111], [124], [126], [170]. Using two different approaches to tether metabolic enzymes to gene promoters, I identified a set of enzymes whose presence at promoter regions positively affects transcriptional output.

Activating potential of ACSS2 is consistent with previous observation of its colocalisation with acetylated histones (mainly H3K9ac, H4K12ac and H4K5ac) on active promoters in mouse neuronal cells [85]. My results suggest that this phenomenon might not be specific for one cell type or the organism.

BHMT2 has not been investigated in the transcriptional context before. This small (40 kDa) enzyme, highly expressed in liver and kidney, preferentially converts S-methylmethionine (SMM) to methionine – a direct precursor of SAM [138]. Given that to affect the activity of methyltransferases BHMT2 requires methionine adenosyltransferase (MAT), it is interesting to speculate that these three enzymes can form a complex to efficiently generate metabolite used by the chromatin writers. Such hypothesis stays in line with histone H3 modifying activity co-purified with BHMT2 (discussed in chapter 4.2). Interestingly, preliminary results of a master student under my supervision showed that BHMT2, when overexpressed in HEK293 cells, probably interacts with chromatin and this interaction is not direct but involves additional DNA-binding proteins.

FH and IDH2 are enzymes involved in TCA cycle converting fumarate to malate and isocitrate to α-ketoglutarate, respectively. Both reactions shift the ratio cofactor : inhibitor of 2-OGDOs, including many histone- and DNA demethylases, towards the former. Global loss of the FH activity and subsequent accumulation of

fumarate was previously linked to changes in histone and DNA methylation [120]. Similarly, neomorphic activity of IDH2 R172K was shown to lead to accumulation of 2-HG – competitive inhibitor of 2-OGDOs [122]. Shifting the balance of tuners of various histone and DNA demethylases regulating the abundance of repressive histone marks (e.g. KDM3, KDM4 for H3K9 methylation, KDM6, KDM7A for H3K27 methylation or KDM7B for both sites) and DNA methylation (TET enzymes), respectively, can be a potential explanation of reduced activation potential of the catalytically impaired enzymes that I observed in my studies [171]. However, the fact that an IDH2 deletion mutant, that does not directly cause an imbalance in the cofactor : inhibitor of 2-OGDOs ratio, reduces the activation potential after tethering to the promoter might suggest another mode of transcription regulation by this metabolic enzyme. Another potential explanation of the activating effect of FH is based on the assumption that out of its mitochondrial context, this enzyme can catalyse a reverse reaction (i.e. conversion of malate to fumarate). In fact, in human pancreatic cell line activation of AMPK promotes interaction of FH with the transcription factor ATF2 and the local production of fumarate by FH was linked to KDM2A inhibition and increase of H3K36me2 mark [131]. Which mechanism is mediating the effect in my experiments is not known. Future experiments involving ChIP with antibodies against various histone PTMs would shed more light on this aspect.

Overall, my work confirmed that presence of metabolic enzymes in chromatin microenvironment affects transcription and identified BHMT2 as a potential new player in regulation of gene expression.

4.2. BHMT2 can interact with histone H3 methyltransferase

Pull-down experiments with recombinant enzymes followed by in vitro histone methyltransferase assay identified BHMT2 as an enzyme physically interacting with H3 methyltransferase activity. By performing a set of controls I excluded the possibility that the observed H3 methyltransferase activity comes from the intrinsic methyltransferase activity of BHMT2 or co-purification of bacterial methyltransferase during the production of recombinant BHMT2 for the assay [172]. These results stay in line with the activation potential of BHMT2 upon tethering to the promoter (chapter 4.1).

Enzymes involved in one-carbon metabolism have been found in protein complexes localised on chromatin [114], [170]. The studies on BHMT2 are very limited and so far its activity has not been reported in the context of transcription. My work has laid the ground for deeper investigation of the roles of BHMT2 in chromatin functions. The lack of well-performing antibodies makes it difficult to assess the role, subcellular localisation and interacting partners of the endogenous protein, therefore the next goal of future experiments is to endogenously tag BHMT2 in a metabolically relevant cell type (liver- or kidney-derived) to be able to investigate the aforementioned aspects.

4.3. Potential role of MAT2A/B in RNA methylation

Analysis of changes in global histone PTMs in stable knockdown cell lines (chapters 3.3.3 and 4.4) revealed that individual depletions of 4 enzymes (or subunits of enzymes) led to profound alterations in histone modification patterns. In order to identify the potential nuclear interacting partners of the enzymes of interest, I performed the IP from the nuclear fraction of cells overexpressing the 4 selected candidate enzymes followed by MS-based protein identification.

RNA modifications have been known for several decades. Until now, more than 170 of them have been reported on all types of coding and non-coding RNA. The interplay between availability of nutrients and RNA modifications has been studied in the context of heavily modified tRNA as well as mRNA, however the metabolic impact on rRNA modifications is missing [173].

In my studies I identified MATII as a potential enzyme regulating 28S rRNA cytosine methylation. Immunoprecipitation (IP) from nuclear fraction of cells overexpressing MAT2B revealed its direct interaction with a set of nucleolar proteins involved in ribosome biogenesis. Among the proteins interacting with MAT2B I identified both structural ribosomal subunits and several accessory nucleolar proteins involved in maturation of rRNA necessary for assembly of fully functional ribosomes: RNA helicase DDX21, probable rRNA binding protein EBNA1BP2, and probable 28S rRNA methyltransferase NOP2. So far, I have not detected interaction of endogenous MATII subunits in the ‘reverse’ experiment with overexpression of exogenous NOP2. It might be explained by the preference of MAT2B to interact with endogenous NOP2 within nucleolus while the majority of exogenous NOP2 pulled down in the IP is present in the nucleoplasm. The other possibility is that MAT2B, when at endogenous concentration, interacts with NOP2 via rRNA molecule and the interaction is lost upon treatment of nuclei with Benzonase nuclease during preparation of nuclear extract. Currently I am aiming to address these questions by performing IP from nuclear fraction of (i) cell lines stably overexpressing FLAG-2HA-NOP2 without Benzonase treatment to keep RNA-mediated interactions intact and (ii) WT cells using antibody against endogenous NOP2.

The interaction of MATII with NOP2 within nucleolus could provide an efficient local supply of SAM necessary for rRNA methylation, the mechanism that is important especially in a dense, diffusion-limited and phase-separated structure of nucleolus [174]. The enzymatic activity of a yeast Nop2 methyltransferase as well as the exact residue it modifies in yeast 25S rRNA have been previously described [175]. Human NOP2 was shown to functionally complement yeast Nop2 deficient (nop2Δ) strain but the experiment showing that NOP2 is responsible for the methylation of homologous cytosine in human rRNA is still missing [176]. I am currently working on the analysis of RNA extracted from the human cells with NOP2 depletion with the aim to confirm its methyltransferase activity on the homologous residue. Yeast C2870 and its human homologue C4447 is localised within peptidyl-transfer centre (PTC) that in a fully functional ribosome is responsible for peptide bond formation and peptide release. In human cells 100% of C4447 is methylated what suggests that this modification is crucial for the ribosome structure and / or stability [168].

Altogether, my studies have a potential to establish the first link between the nuclear localisation and activity of SAM-generating enzyme and rRNA modification.

4.4. Identification of metabolic enzymes affecting histone PTM patterns

Analysis of 14 knockdown cell lines revealed that metabolic perturbation affects global abundance of histone PTMs. In the presented screening, separate depletions of 4 enzymes (or subunits of enzymes) caused the most profound effect and on these candidates I focused in my further studies.

ACSS2 (acyl-CoA synthetase short-chain family member 2) is a nucleocytosolic enzyme catalysing the synthesis of acetyl-CoA from acetate. The nuclear acetyl-CoA salvage pathway controlled by ACSS2 can regenerate acetyl-CoA from acetate at chromatin and therefore contribute to the stability of histone acetylation state [177]. Studies in murine neuronal cell lines previously reported chromatin localisation of ACSS2 and associated transient depletion of this enzyme with the reduction in global H3K27ac and H3K9ac [85]. In my experiment we observed the same change in the abundance of H3K9ac but since in wild type HEK293 cells H3K27ac is found on approximately 0.05% of nucleosomes, this modification was not detected by MS [144].

PCCA (propionyl-CoA carboxylase α chain) together with PCCB (propionyl-CoA carboxylase β chain) form a heterododecamer loosely attached to the inner mitochondrial membrane [150]. Deficiency of either subunit results in the loss of catalytic activity of PCC, the phenomenon causing a metabolic disease, propionic acidemia (PA). This disorder arises from accumulation of propionyl-CoA that instead of being converted to methylmalonyl-CoA and subsequently to succinyl-CoA to replenish TCA intermediates, gets converted to toxic compounds affecting mitochondrial metabolism. The activity of PCC has been previously shown to have an impact on histone PTMs. Propionate is a known inhibitor of HDACs and its accumulation in PA model led to increased histone acetylation in neuronal cells [178]. The fact that in my experiment the depletion of PCCA displayed the opposite direction of multiple histone acetylation changes suggests the presence of a different mechanism of regulation. Propionyl-CoA, whose cellular level is elevated in individuals with PA is also a co-substrate of histone propionylation, previously shown to be an active chromatin mark [179]. In mouse hypomorphic mutant of Pcca that has 2% of WT PCC activity, propionylation of H3K14 was elevated and that effect was reversed upon

re-introduction of fully active human PCCA. Unfortunately, due to the fact that preparation of histone samples for MS analysis involves chemical propionylation of unmodified lysine residues, the information about endogenous histone propionylation in my experiment could not be retrieved.

MAT2B is a non-catalytic subunit of MATII isozyme previously anticipated to play an inhibitory role in SAM synthesis [111]. However, recent kinetic studies refined the notion on the regulatory function of this subunit on the catalytically active MAT2A. According to the proposed model, when SAM level is high, MAT2B functions as an inhibitor of MAT2A by rendering it more susceptible to product inhibition [180]. At low methionine and SAM concentrations, MAT2B activates MAT2A by increasing its affinity for methionine. In contrast to studies involving MAT2A depletion, in my experiment I did not observe global alterations in histone methylation levels [111]. This was surprising especially considering the fact that a set of acetylation marks were reduced to the similar extent to the three other knockdown cell lines suggesting that the homeostasis of the cells was impaired. However, aberrations in the methionine cycle and subsequently, in SAM production do not necessarily have to be reflected in changes of histone methylation. Studies in yeast revealed that lipid methylation is the major consumer of SAM and serves as the most preferential ‘sink’ of methyl groups [181]. Therefore, it is plausible to speculate that impaired activity of methionine cycle caused by the misregulation of MATII is primarily reflected in aberrant lipid methylation.

Pyruvate kinase is the enzyme catalysing the last step of glycolysis. PKM2 (pyruvate kinase isoform M2) is one of 4 pyruvate kinase isoforms expressed in human cells. Isoforms L and R are tissue-specific products of *PKLR* gene while PKM1 and PKM2 are two isoforms encoded by *PKM* gene and result from alternative splicing [140].

Isoform M1 exists as a constitutively active tetramer not prone to allosteric regulation. PKM2 is the isoform characteristic for proliferating cells and its upregulation has been correlated with many cancers. It can exist as a glycolytically active tetramer or a less active dimer. The oligomerisation status of PKM2 is regulated allosterically. Fructose-1,6-bisphosphate (FBP), serine and SAICAR (intermediate product in purine synthesis) are factors promoting its tetramerisation while alanine and phosphotyrosine growth signalling prevent the formation of a tetramer [182]. Glycolytically inactive dimer can be translocated to the nucleus where PKM2 acts as a protein kinase that can phosphorylate H3T11 and transcription factor STAT3 among others [164], [165]. Phosphorylation of H3T11 by PKM2 was shown to promote dissociation of HDAC3 from chromatin and increase in H3K9ac level at promoters of specific genes. Depletion of histone acetylation marks observed in my experiment upon knockdown of PKM2 stays in line with the previously suggested model of nuclear activity of this enzyme.

In general, MS analysis of histone PTMs revealed that all the cell lines displayed globally lower levels of H3K9ac and H4K16ac commonly associated with active transcription. H4K5ac and H4K12ac, both significantly reduced in all the investigated knockdowns, are well-known transient markers of newly synthesised histones that are erased from chromatin within an hour after replication [183]. Lower abundance of these PTMs in non-synchronised cells might imply misregulation in the cell cycle, hypothesis that is further supported by the reduction of the abundance of H4K8ac identified in computational studies as a predictive mark of replication time [146]. Notably, several lines of evidence suggest that H4 acetylations have also functional roles in chromatin. For example, H4K5ac was reported to be an ‘epigenetic bookmark’ for increased transcriptional kinetics of post-mitotic re-activation while high H4K12ac was detected in transcribed regions what suggests its role in transcriptional elongation [147], [184].

The trends of histone PTMs changes observed in my experiment were the same in all investigated knockdown cell lines even though all the depleted enzymes are involved in various metabolic pathways. This might suggest a common cellular response to different metabolic perturbations. Investigating whether the changes observed in my experiment occur genome-wide or are associated with particular loci was a rationale for performing quantitative ChIP-seq analysis with marks globally altered in MS analysis. Unfortunately, so far this spike-in ChIP-seq approach has not been successful and still constitutes a question we want to address in the future.

4.5. Depletion of ACSS2, MAT2B, PCCA and PKM2 affects DNA modifications

Depletion of metabolic enzymes identified in histone PTM screening did not alter global DNA methylation levels. Such a result is inconsistent with the data from taxane-resistant breast cancer cell lines where downregulated expression of MAT2B was correlated with the decrease in the level of DNA methylation [185]. However, in that study the catalytic subunit MAT2A was also transcriptionally downregulated, therefore it is plausible that knockdown of MAT2B alone is not enough to exert the effect on DNA methylation. Even though in my experimental setup 5-mC levels were not affected by the knockdowns, the abundances of two intermediates of cytosine demethylation, 5-hmC and 5-fC, were significantly reduced. This could be linked to impaired functions of TET enzymes. The activity of TET enzymes is dependent on the presence of α-KG and can be inhibited by various metabolites, succinate and fumarate among others [118]. Interestingly, my metabolomic data showed that in all investigated knockdowns, the global level of both α-KG and succinate were reduced. Of note, these

metabolites can be present both in mitochondria and in the cytosol [186]. Due to this intracellular compartmentalisation of the pools of metabolites, the effective α-KG : succinate ratio in the nucleus might not be reflected by their global abundances. Therefore, to confirm the hypothesis that impaired demethylation causes the observed changes in the levels of 5-hmC and 5-fC, measurements of TET activity in the nuclear fraction extracted from the investigated knockdown cell lines are needed.

5-hmC and 5-fC affect the structure of DNA but several lines of evidence suggest that apart from their structural role, these modifications also have indirect influence on chromatin functions. Proteomic studies revealed a set of proteins interacting with both of these modifications established by TET enzymes and linked them with regulation of gene expression (5-hmC and 5-fC) and DNA damage response (5-fC) [74], [75]. Whether the local misregulation of DNA modifications other than 5-mC in my knockdown cell lines correlates with gene expression profiles is the question that we should address in the future.

4.6. Depletion of ACSS2, PCCA and PKM2 change metabolic status of a cell

Targeted metabolomic analysis of 3 out of 4 investigated knockdown cell lines revealed global changes in metabolic state of the cells, manifested by change in the abundances of many metabolites crucial for chromatin modifications. Various perturbations caused by the depletion of different metabolic enzymes elicited metabolic stress manifested by the decreased ATP : ADP ratio. Cells sense this energy status by AMP-activated protein kinase (AMPK) that in order to keep the cellular homeostasis, leads to the upregulation of catabolic processes (glucose and fatty acid uptake, glycolysis, fatty acid oxidation) and switching off ATP-consuming pathways (synthesis of proteins,

rRNA, fatty acids, triglycerides, phospholipids, sterols, hexosamines and gluconeogenesis) [187]. AMPK signalling controls a wide variety of cellular processes what can, at least partially, explain severe changes in metabolites involved in pathways not directly related to the enzyme, whose depletion caused the initial metabolic stress.

Even though the abundance of a group of metabolites was significantly altered, acetyl-CoA was not one of them. This effect was surprising considering the fact that one of the depleted enzymes was its direct producer, ACSS2. One possible explanation for that might be the compartmentalisation of acetyl-CoA-generating enzymes. In WT HEK293 cells ACSS2 is primarily localised in the nucleus (own observation based on immunofluorescence). It is plausible that depletion of ACSS2 affects mostly the nuclear pool of acetyl-CoA, effect that is globally masked by the non-changed cytosolic abundance of this metabolite. The other potential cause of the observed result implies post-harvesting artefacts. Metabolism of acetyl-CoA is very dynamic and can happen within seconds upon cell harvest. Immediately quenching the cell metabolism with cold organic solvents minimises the possibility of experimental artefacts [149]. However, the protocol for cell harvesting that I followed involved washing and centrifugation steps that might have led to the uncontrolled loss of information about intracellular abundance of acetyl-CoA in vivo.

Both ACSS2 and PCCA provide metabolites that supply the TCA cycle with its intermediates. As expected, depletion of these enzymes led to the reduction of levels of the metabolites of TCA cycle: citrate, oxaloacetate, succinate and α-KG (only in PCCA kd). Surprisingly, in these cell lines I observed pronounced depletion of many metabolites involved in 1C metabolism that constitutes a secondary effect caused probably by the response of cells to metabolic stress.

Knockdown of PCCA mimics the condition of a rare metabolic disorder, propionic acidemia. Impaired conversion of propionyl-CoA and subsequent accumulation of its toxic intermediates severely affects TCA cycle, oxidative phosphorylation and glycine cleavage system what altogether causes dramatic alteration in the overall metabolic status of the cells [150]. The fact that these changes were reflected both in global histone PTMs, and in DNA modification status emphasises the importance of properly functioning mitochondria in the regulation of chromatin functions.

Depletion of PKM2 led to the elevation of total cellular abundance of choline, betaine and DMG – three interrelated compounds in methyl metabolism [188]. Increased level of betaine, serving as an alternative to 5-mTHF donor of methyl groups in the methionine cycle, might be the reason why SAM and methionine are not as highly depleted as it is observed in PCCA kd and ACSS2 kd. Whether the replenishment of methyl groups by betaine can contribute to the observed increase in global H3K27me3 and H3K9me3 constitutes a question that could be addressed by isotope tracing of choline methyl groups. As expected, knockdown of PKM2 caused a drastic reduction in the abundance of lactate by blocking the final step of glycolysis, conversion of phosphoenolpyruvate (PEP) to pyruvate. However, branching of glycolysis into pentose-phosphate pathway (PPP), hexosamine biosynthesis pathway (HBP) and serine synthesis prevents glycolytic intermediates from accumulating to highly elevated concentration. This explains why the level of G6P, product of the first step of glycolysis, was not dramatically increased and potentially justifies a mild increase in N-acetylglucosamine (GlcNAc) [189].

4.7. The link between PKM2 and oxidative stress response

Many tumour cells undergo glycolysis even under highly oxygenated conditions, a phenomenon called aerobic glycolysis or Warburg effect [190]. Tetrameric PKM2 functions as a rate-limiting glycolytic enzyme converting PEP to pyruvate while its dimeric form has been linked to regulation of activity of certain transcription factors controlling expression of genes necessary for growth and proliferation [191]. PKM2 is overexpressed in many cancers and is associated with poor survival prognosis [192]. Many mechanisms of PKM2-mediated proliferation of tumour cells have been reported [193]–[195]. My work suggested the novel mechanism potentially leading to the activation of oxidative stress response upon suppressing glycolytic functions of PKM2.

4.7.1. Depletion of PKM2 in HEK293 cells affects its glycolytic function

Analysis of the abundance of *PKM* transcripts revealed that in WT HEK293 cells the transcript encoding PKM2 isoform is predominant and constitutes more than 90% of all *PKM* transcripts. PKM1 and PKM2 isoforms are encoded by the same gene and differ by the presence of mutually exclusive exon 9 and exon 10. That is why I reasoned that it is unlikely that these isoforms are differently regulated at the translational level and I used the transcript abundance as a proxy for protein abundance. shRNA targeting the product of *PKM* gene does not discriminate its isoforms what led me to the conclusion that in my knockdown experiment I mainly affect the activity of PKM2. Analysis of the oligomerisation status of PKM2 in WT cells as well as measurements of extracellular acidification rate in PKM2 kd cells, allowed me to specify that the shRNA-mediated knockdown affects predominantly the tetrameric form of PKM2 playing a crucial role in glycolysis. These results are in line with studies in T cells which

reported that in non-stimulated cells glycolytically active PKM2 tetramer is highly abundant while the nucleocytosolic, glycolytically inactive dimer is non-detectable [196].

4.7.2. Depletion of PKM2 correlates with upregulation of genes involved in redox balance

Analysis of RNA-seq and ChIP-seq results allowed me to identify genes misregulated upon depletion of PKM2. I observed the most prominent upregulation at the transcript level for genes involved in oxidative stress, namely *TXNIP* and *DHRS2*. The upregulation detected by RNA-seq was positively correlated with the gain of H3K9ac and H3K4me3 (marks of active promoters) near the TSSs of these genes.

Thioredoxin interacting protein (TXNIP) directly binds to a cysteine residue at the catalytic site of thioredoxins (TXNs) and thus impedes their reducing potential. This can result in increased redox stress [197]. Moreover, TXNIP has been shown to be a tumour suppressor that inhibits growth and hypertrophy and causes increased apoptosis [161]. Dehydrogenase / reductase SDR family member 2 (DHRS2) is an NADPH-dependent α-dicarbonyl reductase. Dicarbonyl compounds are generated during metabolic processes or oxidative stress and have been suggested to originate from carbohydrates, lipids and glycolytic intermediates what might be one of the signals eventually leading to the upregulation of DHRS2 in glycolytically impaired PKM2 kd [162], [198]. Notably, in endometrial cancer DHRS2 plays a protective role against oxidative stress-induced apoptosis and its upregulation was found to be caused by the upregulation of the transcription factor ETV5 [162]. Interestingly, in my

experiment PKM2 did not lead to the upregulation of ETV5 what suggests that in this model *DHRS2* expression might be regulated by a different mechanism.

My studies revealed that oxidative stress induced by chemical depletion of cellular glutathione (GSH) led to upregulation of *DHRS2* in WT HEK293 cells. Notably, depletion of GSH reduced the expression of *TXNIP* suggesting that upregulation of *TXNIP* observed in PKM2 kd is rather a cause and not a consequence of oxidative stress response triggered by other mechanism in these knockdown cells. This is in line with the observation that increased level of intracellular reactive oxygen species (ROS) results in lower *TXNIP* expression [199]. During further investigation of the relationship between the expression of these two redox-related genes I observed that prolonged chemical inhibition of TXN1, mimicking the upregulation of TXNIP, induced the expression of *DHRS2*. Altogether, my experiments suggest that upregulation of *TXNIP* leads to the increased expression of *DHRS2*.

4.7.3. Upregulation of *TXNIP* and *ARRDC4* in PKM2 knockdown is mediated by MondoA : MLX transcription factors

My analysis of RNA-seq data revealed that the expression of both *TXNIP* and *ARRDC4* is elevated in PKM2 kd relative to WT cells. TXNIP and ARRDC4 are two homologous members of arrestin domain-containing family of proteins implicated in glucose homeostasis [157]. Besides their structural homology, transcriptional regulation of both proteins is controlled by a complex of transcription factors MondoA : MLX that binds carbohydrate response elements (ChoREs) localised within the promoters of these genes [160], [189], [200]. As expected, in my experiment these transcription factors were enriched at the promoters of *TXNIP* and *ARRDC4* in PKM2 kd. Moreover, in this

knockdown cell line, due to impeded glycolysis the abundance of G6P, the product of the first step of glycolysis, was elevated. G6P is a potent inducer of nuclear translocation of MondoA : MLX by a mechanism that so far has not been elucidated, what explains the upregulation of the target genes by this complex [201].

Overall, my results suggested that in HEK293 the upregulation of *TXNIP* and *ARRDC4* upon depletion of PKM2 can be regulated by the activation of MonoA : MLX complex by glycolytic intermediates.

4.7.4. Proposed mode of action of PKM2 knockdown

Metabolic enzymes perform their roles in the context of specific pathways and their aberrant functions might have implications in other cellular processes. A series of experiments performed in cells in which the glycolytic activity of PKM2 is impaired, allowed me to propose the mechanism of regulation of oxidative stress response elicited by PKM2 depletion (Figure 4.1). According to this model, reduction of the abundance of PKM2 results in non-efficient glycolysis manifested by the accumulation of glycolytic intermediates. Elevated abundance of G6P, the product of the first reaction in this pathway, is sensed by the MondoA : MLX complex that translocates to the nucleus where it binds to ChoREs upstream of *TXNIP* and *ARRDC4*. Recruitment of additional factors promoting transcription, such as histone acetyltransferase p300, to promoter-bound MondoA : MLX activates transcription of the target genes [160], [202]. In the cytosol TXNIP protein binds and inhibits TXN1 that leads to the accumulation of oxidised proteins, the effect that mimics the action of the increase of intracellular ROS. Cellular oxidative stress response subsequently triggers the expression of *DHRS2* that

can play a protective role, for example by preventing oxidative stress-induced apoptosis.

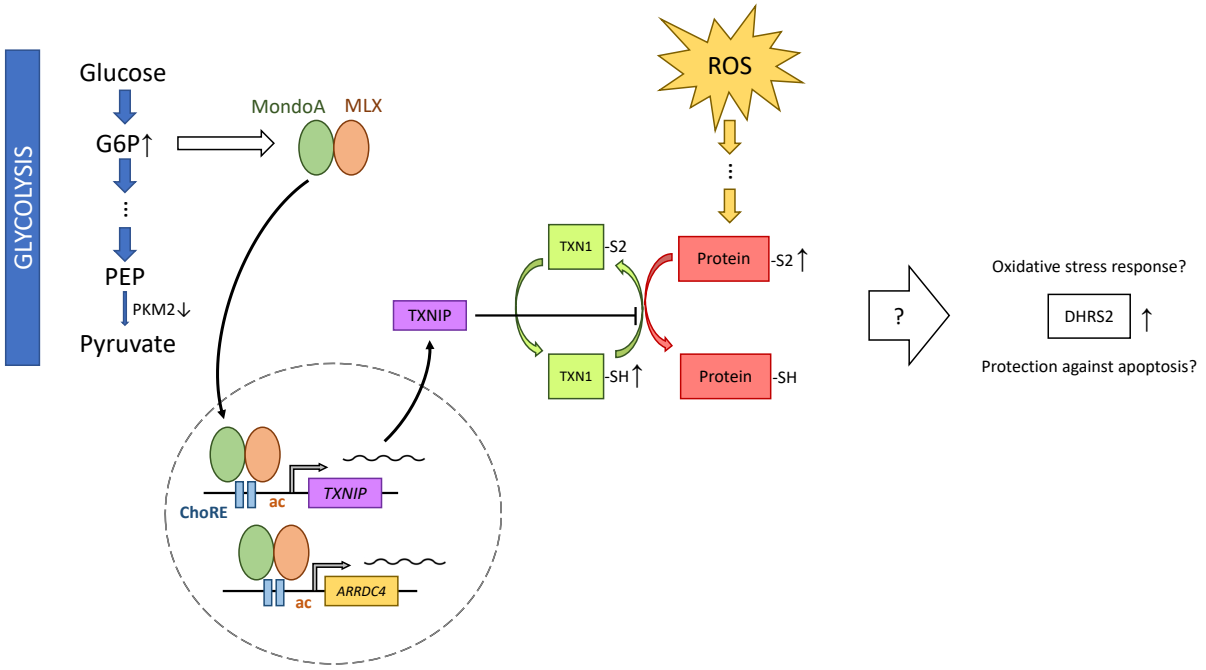

Figure 4.1 Proposed mechanism of regulation of cellular oxidative stress response by depletion of PKM2. Detailed description in the main text.

The proposed model provides the first link between impaired function of PKM2 and activation of the targets of MondoA : MLX complex as well as the correlation of such mechanism with increased expression of *DHRS2*. This regulatory axis can be of particular importance in the context of cancers and diabetes. PKM2 is a well-known target of various anticancer therapies [203]–[205]. By underlying the connection between PKM2 depletion and oxidative stress, my studies provide a rationale for designing multitarget therapeutic strategies. For example, development of specific pharmacological inhibitors of PKM2 that lead to elevated oxidative stress, could enhance the therapeutic effects of cisplatin-induced cell killing whose mechanism involves ROS production [206]. On the other hand, expression of *TXNIP* has been found to be dramatically increased in diabetic islets what results in apoptosis of pancreatic β-cells [207]. In this context protection against apoptosis is highly desirable.

Protective role of DHRS2 in diabetic model has not been investigated but constitutes an interesting hypothesis that should be addressed in the future.

5. Materials

5.1. Bacterial strains

Strain	Purpose	Genotype	Supplier
DH5α	Cloning	F- φ80*lacZ*ΔM15 Δ(*lacZYA-argF*)U169 *recA*1 *endA*1 *hsdR*17(r_K^-, m_K^+) *phoA supE*44 λ- *thi*-1 *gyrA*96 *relA*1	Thermo Fisher Scientific
BL21-Gold (DE3)	Protein expression	F– *ompT hsdS*(r_B^- m_B^-) *dcm*+ Tet^r *gal* λ(DE3) *endA* Hte	Agilent
Rosetta 2 (DE3) pLysS	Protein expression	F- *ompT hsdS*$_B$(r_B^- m_B^-) *gal dcm* (DE3) pLysSRARE2 (Cam^R)	Merck Millipore

5.2. Cell lines

Cell line	Description	Origin
HEK293	Human embryonic kidney 293	*H. sapiens*
HEK293T	Human embryonic kidney 293, contains the SV40 T-antigen	*H. sapiens*
HeLa	Human cervical cancer	*H. sapiens*
S2	Schneider 2	*D. melanogaster*

5.3. Guide RNA (gRNA)-encoding sequences

Gene	gRNA code	Sense strand	Antisense strand
EGR1	45/46	CTCCCCAAGTTCTGCGCGCT	AGCGCGCAGAACTTGGGGAG
	47/48	GCTCCCCAAGTTCTGCGCGC	GCGCGCAGAACTTGGGGAGC
	76/77	CCCACCACTCTTGGATGGGA	TCCCATCCAAGAGTGGTGGG
	78/79	TCACTCCGGGTCCTCCCGGC	GCCGGGAGGACCCGGAGTGA
	80/81	GTTCCAGACCCTTGAAATAG	CTATTTCAAGGGTCTGGAAC
	126/127	CGCCGGAACAGACCTTATTT	AAATAAGGTCTGTTCCGGCG
	128/129	CCACGGGCCGCGGCTACCGC	GCGGTAGCCGCGGCCCGTGG
	166/167	GGTGCCGGGCGCTGTCGGAT	ATCCGACAGCGCCCGGCACC
	168/169	TGTACGTCACGACGGAGGCG	CGCCTCCGTCGTGACGTACA
	170/171	CGGCCGGTCCTGCCATATTA	TAATATGGCAGGACCGGCCG
	172/173	CTTCAAATAGAGGCGGATCC	GGATCCGCCTCTATTTGAAG
	174/175	GTGACGTACATGGCCATATA	TATATGGCCATGTACGTCAC
	176/177	CGACTCGCCCTGGGCGCGGG	CCCGCGCCCAGGGCGAGTCG
CD71	66/67	CCGGGCGATCTGTCAGAGCA	TGCTCTGACAGATCGCCCGG
	68/69	TCCCCTCAGAGCGTCGGGATATC	GATATCCCGACGCTCTGAGGGGA
	74/75	CAGGAAGTGACGCACAGCCC	GGGCTGTGCGTCACTTCCTG
	108/109	AGGCCAGTGCGCCCATCGCG	CGCGATGGGCGCACTGGCCT
	124/125	CGCGATGGGCGCACTGGCCT	AAACCTGAGGCACGTACGCTCGCG

VEGFA	213/214	AAACCTGAGGCACGTACGCTCGCG	CCACTCTCGAAGACGCTGCTCG
	215/216	CCACTCTCGAAGACGCTGCTCG	CCACGCACACACTCACTCACCG
NTF3	217/218	CGGTGAGTGAGTGTGTGCGTGG	CTAACCCCTTCCGCGCCGCGCG
	219/220	CCACGCACACACTCACTCACCG	CGCCGGCCCGCGCCGCGCCGCG

5.4. The RNAi consortium clone numbers (TRCN)

TRCN clone number	Target gene
TRCN0000045359	CBS
TRCN0000052466	FH
TRCN0000196588	PKM
TRCN0000078425	PCCA
TRCN0000028618	OGDH
TRCN0000116177	NAMPT
TRCN0000045563	ACSS2
TRCN0000034522	MAT2B
TRCN0000028627	PDHA1
TRCN0000027225	IDH2
TRCN0000078287	ACLY
TRCN0000036169	BHMT2
TRCN0000037602	RFK
TRCN0000050018	AHCY
TRCN0000028071	SDHB
TRCN0000045595	FLAD1
TRCN0000035439	NMNAT2
TRCN0000035406	MTRR
TRCN0000194740	PKLR
TRCN0000035469	NMNAT1
TRCN0000036144	BHMT
TRCN0000035404	MTR
TRCN0000036419	MAT1A
TRCN0000028085	SDHA
TRCN0000027284	IDH1
TRCN0000045508	NADSYN1
TRCN0000036452	MAT2A

5.5. OriGene stock keeping unit (SKU) of synthetic open reading frames (ORFs)

OriGene SKU	Gene
SC128074	CBS
SC319415	FH
SC315792	PKM
SC127702	OGDH
SC111136	NAMPT
SC110397	MAT2B

SC119981	PDHA1
SC319226	IDH2
SC124281	BHMT2
SC113557	RFK
SC319344	AHCY
SC319204	SDHB
SC312888	NMNAT2
SC314547	MTRR
SC321691	PKLR
SC335019	NMNAT1
SC310239	FLAD1
SC110837	BHMT
SC309934	MTR
SC119881	MAT1A
SC319054	SDHA
SC116430	IDH1
SC113723	NADSYN1
SC116444	MAT2A

5.6. Primer sequences

5.6.1. Primers for cloning

Primer name	Sequence	Purpose	Cloning strategy
pcDNA3.1-FLAG-2HA_fwd	GCGGCCGCTCGAGTCTAG	NOP2 expression, PCCA expression	Gibson Assembly
pcDNA3.1-FLAG-2HA_rev	GGATCCTGCATAGTCCGGG	NOP2 expression, PCCA expression	Gibson Assembly
hNop2_ORF_fwd	TCCCGGACTATGCAGGATCCATGGG GCGCAAGTTGGAC	NOP2 expression	Gibson Assembly
hNop2_ORF_rev	CTCTAGACTCGAGCGGCCGCCTAA GATAGCAGCAGCTGGC	NOP2 expression	Gibson Assembly
PCCA_ORF_fwd	TCCCGGACTATGCAGGATCCATGGC GGGGTTCTGGGTC	PCCA expression	Gibson Assembly
PCCA_ORF_rev	CTCTAGACTCGAGCGGCCGCTCATT CCAGCTCCACGAGC	PCCA expression	Gibson Assembly
GA_VBbb_FLAG_for	GGCTGCAGGAGGCGGTGGAAGCGG GATGGACTACAAAGACGATGACG	Enzyme-dCas9 fusion + hygro resistance	Gibson Assembly
GA_VB_MCS_rev	ACAGTCGAGGCTGATCAGCGGGTTT GGGCCCTCTAGACTCGAG	Enzyme-dCas9 fusion + hygro resistance	Gibson Assembly
GA_VBbb_for	CCCGCTTCCACCGCCTCCT	Enzyme-dCas9 fusion + hygro resistance	Gibson Assembly
GA_VBbb_rev	AAACCCGCTGATCAGCCTCGACTGT	Enzyme-dCas9 fusion + hygro resistance	Gibson Assembly
EE148_FLAG_insert_SLIC_for	TGTAAAGCTTGACTACAAAGACGAT	Gal4_DBD-enzyme fusion	Gibson Assembly
EE148_TEV_insert_SLIC_rev	GGGCCCTCTAGCCCTGAAAATACAG	Gal4_DBD-enzyme fusion	Gibson Assembly
TEV_EE148_vec_SLIC_for	TTTTCAGGGCTAGAGGGCCCTATTC	Gal4_DBD-enzyme fusion	Gibson Assembly
FLAG_EE148_vec_SLIC_rev	CTTTGTAGTCAAGCTTTACAGTCAAC	Gal4_DBD-enzyme fusion	Gibson Assembly
pVB_BHMT2_del75-79_for	GAGGACAATATGGAAAGC	Deletion for BHMT2 catalytic mutant	Blunt-end joining
pVB_BHMT2_del75-79_rev	AAAAGTCTGCATGACATTTG	Deletion for BHMT2 catalytic mutant	Blunt-end joining
pVB_IDH2_del170-174_for	CATGGCGACCAGTACAAG	Deletion for IDH2 catalytic mutant	Blunt-end joining
pVB_IDH2_del170-174_rev	GGTGATGGGCTTGGTCCA	Deletion for IDH2 catalytic mutant	Blunt-end joining
pVB_FH_del266-270_for	GAGCTCGCAGCTGGAGGC	Deletion for FH catalytic mutant	Blunt-end joining

pVB_FH_del266-270_rev	GGCAGCTTTTATTCTTGTCATTGCATATTTTAC	Deletion for FH catalytic mutant	Blunt-end joining
pVB_ACSS2_del361-365_for	TCCTACGTCACCTATGGG	Deletion for ACSS2 catalytic mutant	Blunt-end joining
pVB_ACSS2_del361-365_rev	ACCAATGTCTGCCGTGCA	Deletion for ACSS2 catalytic mutant	Blunt-end joining
BHMT2_S77F_QC_for	TATTGTCCTCACTGGCGAAAAAGGTAAAAGTCTGCATGACATTTGATCC	Point mutation S77F in BHMT2	QuikChange
BHMT2_S77F_QC_rev	GGATCAAATGTCATGCAGACTTTTACCTTTTTCGCCAGTGAGGACAATA	Point mutation S77F in BHMT2	QuikChange
pVB_FH_R268H_GA_part1_for	TTCCTACTTGGCAGTACATCTACGTATTAGTCATCG	Point mutation R268H in FH	Gibson Assembly
pVB_FH_R268H_GA_part1_rev	GCTCATAGATATGTGGCATGGCAGCTTTTATTC	Point mutation R268H in FH	Gibson Assembly
pVB_FH_R268H_GA_part2_for	AGCTGCCATGCCACATATCTATGAGCTCGCAG	Point mutation R268H in FH	Gibson Assembly
pVB_FH_R268H_GA_part2_rev	TACGTAGATGTACTGCCAAGTAGGAAAGTCC	Point mutation R268H in FH	Gibson Assembly
IDH2_R172K_for	ACCATTGGCAAGCACGCCCAT	Point mutation R172K in IDH2	Blunt-end joining
IDH2_R172K_rev	GATGGGCTTGGTCCAGCC	Point mutation R172K in IDH2	Blunt-end joining

5.6.2. Primers for RT-qPCR

Gene	Forward primer	Reverse primer
CBS	GGCCAAGTGTGAGTTCTTCAA	GGCTCGATAATCGTGTCCCC
FH	GGAGGTGTGACAGAACGCAT	CATCTGCTGCCTTCATTATTGC
PKM	AAGGGTGTGAACCTTCCTGG	GCTCGACCCCAAACTTCAGA
PCCA	ACAGTGCTTAATGGTGTCCCG	ACGACATCTTCTGCTGCCAA
OGDH	GGCTTCCCAGACTGTTAAGAC	GCAGAATAGCACCGAATCTGTTG
NAMPT	CGGCAGAAGCCGAGTTCAA	GCTTGTGTTGGGTGGATATTGTT
ACSS2	TTGGGGCTTTGCACTCCATT	AGGCATCTGTAGTGATGAGAAGA
MAT2B	TTCACTGGTCTGGCAATGAAC	AGGGCTGTCAGTAATAGGTCTT
PDHA1	TGGTAGCATCCCGTAATTTTGC	ATTCGGCGTACAGTCTGCATC
IDH2	CGCCACTATGCCGACAAAAG	ACTGCCAGATAATACGGGTCA
ACLY	TCGGCCAAGGCAATTTCAGAG	CGAGCATACTTGAACCGATTCT
BHMT2	GATAGACCCGTGGCAGTTACC	AGCTCCATCGTCTTCAAGCTG
RFK	GGCATCCCCACAGCTAATTTTC	CACTTCCAACACTGGCCCAA
AHCY	TAGCAGGCTATGGTGATGTGG	ATGGGGTCAATCTCGGTGATG
SDHB	ACCTTCCGAAGATCATGCAGA	GTGCAAGCTAGAGTGTTGCCT
FLAD1	GAAGGGACTATTCCAAAACCCAG	CCAAGCCTACGTCCAAAGTG
NMNAT2	ACGGTGATGCGGTATGAAGAG	CACCTCCATATCTGCCTCGTT
MTRR	ACAGCCCGCAAGTTTGTTAAG	CCAGTAACCCATACCGCAGG
PKLR	GCCCACACTGAAAGCATGTC	CTGGAGCCCCAATCAGGATG
NMNAT1	AGGAAGGTACACAGTTGTCAAAG	GATGACCCGGTGATAGGCAG
FLAD1	AGGTTTGCCGAGTCTCAGTTG	AGGGCACCAATGATAGCTTCT
BHMT	TGGAGAACAGGGGCAACTATG	CTGACTCACTCCTCCTGCTAC
MTR	CTTGGCCTACCGGATGAACAT	TGCCACAAACCTCTTAATTCCTG
MAT1A	ATCAGGGTTTGATGTTCGGCT	GCGTTGAGCTTGTGAGCAA
SDHA	ACTGTTGCAGCACAGCTAGAA	GCTCTGTCCACCAAATGCAC
IDH1	AGAAGCATAATGTTGGCGTCA	CGTATGGTGCCATTTGGTGATT

NADSYN1	GGAGTCTCCCGTCACTCAG	TCAGGTCCTGTATCATCCGAG
MAT2A	ACCAGAAAGTGGTTCGTGAAG	CAAGGCTACCAGCACGTTACA
DHRS2	CCTCTGGTAGGGAGCACTCT	CCAGCGCCACTACTGGATTA
TXNIP	GGTCTTTAACGACCCTGAAAAGG	ACACGAGTAACTTCACACACCT
TXN1	GTGAAGCAGATCGAGAGCAAG	CGTGGCTGAGAAGTCAACTACTA
TXNRD1	ATATGGCAAGAAGGTGATGGTCC	GGGCTTGTCCTAACAAAGCTG

5.6.3. Primers for ChIP-qPCR

Target locus	Forward primer	Reverse primer
hACTB	TAGAAGTCGCAGGACCACACT	TGGGTAGGTTTGTAGCCTTCAT
hGenDes	AATCACCTTGCATCTGTTTGG	AAAAGGAGAAACCCAGTGGAA
hNANOG	TGGGTTTGTCTTCAGGTTCTG	CTACTGACCCACCCTTGTGAA
hLINE	AAGATGGCCGAATAGGAACA	GATGAACCCGGTACCTCAGA
dmelf	TGTTAACAATCACGGCGCAT	AAACGACACCACAAAGCGAA
dmcg5322	TCGGGGATTGGTCTTATCGG	GGTTTATCGCCTCAAGTGCC
dmelf2	GCGATCGAAGCTCGTTTCTC	CGCCCTTACTCATGATTCCGA
dmoatp33Ea	TCGAGGTAGGTCTGTCCCAG	TGGAGTGGACAAAACCGAGG
hTXNIP_ChoRE	TCCAGAGCGCAACAACCAT	AAGCAGGAGGCGGAAACGT
hARRDC4_ChoRE	CGGAGATAACCCTGTTCCGC	CAGGCCGTTTACTGGCTGA

5.7. Antibodies

Antibody	Host species	Clonality	Application	Supplier	Catalogue number
Flag	Rabbit	polyclonal	WB, ChIP	Sigma-Aldrich	F7425
PKM2	Rabbit	monoclonal (D78A4)	WB	Cell Signaling	#4053
MAT2B, MAT II beta	Mouse	monoclonal (A-3)	WB	Santa Cruz	sc-390586
PKM1	Rabbit	monoclonal (D30G6)	WB	Cell Signaling	#7067
AceCS1	Rabbit	monoclonal	WB	Cell Signaling	#3658
PCCA	Rabbit	polyclonal	WB	Proteintech	21988-1-AP
Tubulin	Rat	monoclonal	WB	Abcam	ab6160
H3K27me3	Mouse	monoclonal	ChIP	Abcam	ab6002
K9me3	Rabbit	polyclonal	ChIP	Upstate (Millipore)	07-442
H3K9ac	Rabbit	polyclonal	ChIP	Abcam	ab4441
H3K4me3	Rabbit	monoclonal	ChIP	Millipore	17-614
H4K5ac	Rabbit	polyclonal	ChIP	Abcam	ab51997
H4K12ac	Rabbit	polyclonal	ChIP	Abcam	ab46983
HA	Rabbit	polyclonal	WB, ChIP	Abcam	ab9110
MLXIP	Rabbit	polyclonal	ChIP	Proteintech	13614-1-AP

MLX	Rabbit	Monoclonal (D8G6W)	ChIP	Cell Signaling	#85570

5.8. Buffers and solutions

Name	Composition
GA Mix 1	1.33 x ISO buffer
	0.033 U/µL Phusion polymerase (NEB)
	5.3 U/µL Taq DNA Ligase (NEB)
	0.005 U/µL T5 Exonuclease (NEB)
5 x ISO buffer	500 mM Tris-HCl pH 7.5
	50 mM MgCl2
	1 mM dNTP mix
	50 mM DTT
	25% (w/v) PEG 8000 25%
	5 mM NAD
1 x TAE buffer	40 mM Tris-HCl pH 8.2
	20 mM acetic acid
	1 mM EDTA
1 x PBS	10 mM Na2HPO4
	2 mM KH2PO4
	2.7 mM KCl
	137 mM NaCl
	adjusted to pH 7.4
Buffer A (HeLa nuclear extract)	10 mM HEPES-KOH pH 7.9
	1.5 mM MgCl2
	10 mM KCl
Buffer C (HeLa nuclear extract)	20 mM HEPES-KOH pH 7.9
	25% (w/v) glycerol
	420 mM NaCl
	1.5 mM MgCl2
	0.2 mM EDTA
	0.1% IGEPAL
	1 mM DTT
	1 x PIC
1 x SDS-PAGE running buffer	25 mM Tris
	192 mM glycine
	0.1% SDS
6 x Laemmli sample loading buffer	60 mM Tris-HCl pH 6.8
	47% (v/v) glycerol
	416 mM SDS
	603 mM DTT

Coomassie Brilliant Blue stain	2% Coomassie Brilliant Blue
	40% methanol
	10% acetic acid
Coomassie destaining solution	50% (v/v) H2O
	40% (v/v) methanol
	10% (v/v) acetic acid
1 x transfer buffer	25 mM Tris
	192 mM glycine
	20% ethanol
Ponceau S solution	0.1% (w/v) ponceau S
	1% acetic acid
1 x TBS	50 mM Tris-HCl pH 7.6
	150 mM NaCl
MBP column buffer	20 mM Tris-HCl pH 7.4
	200 mM NaCl
	1 mM EDTA
IPH buffer	50 mM Tris-HCl pH 8.0
	150 mM NaCl
	0.5% IGEPAL
	5 mM EDTA
	1 mM DTT
	1 x PIC
Buffer C (MV)	20 mM HEPES-KOH pH 7.9
	420 mM NaCl
	20% (v/v) glycerol
	2 mM MgCl2
	0.2 mM EDTA
	0.1% IGEPAL
	1 x PIC
Buffer C* (MV)	20 mM HEPES-KOH pH 7.9
	300 mM NaCl
	20% (v/v) glycerol
	2 mM MgCl2
	0.2 mM EDTA
	0.1% IGEPAL
	1 x PIC
1.5 x MS elution buffer	90 mM Tris pH 6.8
	1.5% SDS

RIPA lysis buffer	50 mM Tris-HcL pH 8.0
	150 mM NaCl
	2 mM EDTA pH 8.0
	0.1% SDS
	1% IGEPAL
	0.5% sodium deoxycholate
L1 buffer (ChIP)	50 mM Tris-HCl pH 8.0
	2 mM EDTA pH 8.0
	0.1% IGEPAL
	10% (v/v) glycerol
	10 mM sodium butyrate
	10 mM NAM
	1 x PIC
L2 buffer (ChIP)	50 mM Tris-HCl pH 8.0
	10 mM EDTA
	1% SDS
	10 mM sodium butyrate
	10 mM NAM
	1 x PIC
ChIP dilution buffer	50 mM Tris-HCl
	200 mM NaCl
	0.5% IGEPAL
Low salt wash buffer (ChIP)	20 mM Tris-HCl pH 8.0
	150 mM NaCl
	2 mM EDTA
	1% Triton X-100
	0.1% SDS
High salt wash buffer (ChIP)	20 mM Tris-HCl pH 8.0
	500 mM NaCl
	2 mM EDTA
	1% Triton X-100
	0.1% SDS
LiCl wash buffer (ChIP)	10 mM Tris-HCl
	1 mM EDTA
	1% sodium deoxycholate
	1% IGEPAL
	250 mM LiCl
TE buffer	10 mM Tris-HCl pH 8.0
	1 mM EDTA
ChIP elution buffer	100 mM NaHCO3
	1% SDS

Fast IP buffer (ChIP)	50 mM Tris-HCl pH 7.5
	150 mM NaCl
	5 mM EDTA
	0.5% (v/v) IGEPAL
	1% (v/v) Triton X-100
	10 mM sodium butyrate
	10 mM NAM
	1 x PIC
Shearing buffer (ChIP)	50 mM Tris-HCl pH 8.0
	10 mM EDTA
	1% SDS
	10 mM sodium butyrate
	10 mM NAM
	1 x PIC
SOC medium	0.5% (w/v) yeast extract
	2% (w/v) tryptone
	10 mM NaCl
	2.5 mM KCl
	1 mM MgCl2
	10 mM MgSO4
	20 mM glucose
Horiuchi buffer	50 mM Tris-HCl pH 8.5
	5 mM $MgCl_2$
	1 mM DTT
	1 mM PMSF
	1% (v/v) DMSO

5.9. Chemicals

Name	Supplier
1-Methylpropyl-2-imidazolyl disulfide (PX-12)	Sigma-Aldrich
2-Deoxy-D-glucose	Sigma-Aldrich
2-Propanol	Merck Millipore
^{3}H-labelled acetyl-CoA	Hartmann Analytic
^{3}H-labelled S-adenosylmethionine (SAM)	American Radiolabeled Chemicals
4-(2-Aminoethyl)benzenesulfonyl fluoride hydrochloride (AEBSF)	Sigma-Aldrich
Acetic acid	VWR
Acrylamide/Bis Solution, 29:1(40 % w/v)	Serva
Agarose	Lonza
Albumin fraction V	Carl Roth
Ammonium persulfate (APS)	Carl Roth
Ampicillin sodium salt	Carl Roth
Antimycin A	Sigma-Aldrich

Brilliant Blue R-250	Carl Roth
Bromophenol Blue	Carl Roth
BSA molecular biology grade	New England Biolabs
Carbonyl cyanide-4-(trifluoromethoxy)phenylhydrazone (FCCP)	Sigma-Aldrich
Chloramphenicol	Merck Millipore
Chloroform	VWR
cOmplete Protease Inhibitor Cocktail EDTA-free (PIC)	Roche
D(+)-glucose	Sigma-Aldrich
Diethyl maleate (DEM)	Sigma-Aldrich
Dimethylsulfoxid (DMSO)	Carl Roth
Disuccinimidyl suberate (DSS)	Thermo Fisher Scientific
Dithiotreitol (DTT)	AppliChem
Ethanol	Merck Millipore
Ethylenediaminetetraacetic acid (EDTA)	Carl Roth
Formaldehyde 37%	Sigma-Aldrich
Geneticin disulphate (G418)	Carl Roth
Glycerol	Merck Millipore
Glycine	Serva
HEPES	Carl Roth
Hexadimethrine bromide (polybrene)	Sigma-Aldrich
Hydrochloric acid (HCl) 37%	Carl Roth
IGEPAL	Sigma-Aldrich
Isopropyl-ß-D-thiogalactopyranosid (IPTG)	VWR
Kanamycin	Carl Roth
LB	Sigma-Aldrich
LB-Agar	AppliChem
Lithium chloride (LiCl)	Alfa Aesar
Magnesium chloride ($MgCl_2$)	Sigma-Aldrich
Magnesium sulfate ($MgSO_4$)	Sigma-Aldrich
Methanol	Merck Millipore
N,N,N′,N′-Tetramethyl ethylenediamine (TEMED)	Carl Roth
Nicotinamide (NAM)	Carl Roth
Nonfat-dried milk	AppliChem
Oligomycin	Sigma-Aldrich
Phenylmethanesulfonyl fluoride (PMSF)	AppliChem
Poly-L-Lysine 70000 · HBr	Serva
Polyethylene glycol 8000 (PEG 8000)	Promega
Polyethylenimine (PEI)	Polysciences
Ponceau S	Carl Roth
Potassium chloride (KCl)	Carl Roth
Potassium dihydrogen phosphate (KH_2PO_4)	Carl Roth
Potassium hydroxide (KOH)	Carl Roth

Puromycin dihydrochloride	Sigma-Aldrich
Rotenone	Sigma-Aldrich
Roti nanoquant	Carl Roth
Shikonin	Sigma-Aldrich
Sodium acetate	Carl Roth
Sodium butyrate	Alfa Aesar
Sodium chloride (NaCl)	Carl Roth
Sodium deoxycholate	Sigma-Aldrich
Sodium dodecyl sulfate (SDS), 20% solution	Sigma-Aldrich
Sodium hydrogen carbonate ($NaHCO_3$)	Carl Roth
Tris-HCl	Sigma-Aldrich, AppliChem
Triton X-100	Carl Roth
Trypan Blue 0.4%	Thermo Fisher Scientific
Tryptone	BD Biosciences
Tween 20	Carl Roth
UltraPure DNase/RNase-Free Distilled Water	Thermo Fisher Scientific
Yeast extract	BD Biosciences

6. Methods

6.1. Molecular biology methods

6.1.1. Heat shock transformation of chemically competent *E. coli*

Chemically competent *E. coli* cells were thawed on ice. Plasmid DNA (50-100 ng) or cloning mixture (amount depending on the application) was added, mixed gently by flicking the tube and incubated for 30 min on ice. Next, bacteria were placed at 42°C in a thermoblock and incubated for 45 s followed by 2 min on ice. 1 mL of LB or SOC medium without antibiotic was added and bacteria were incubated at 37°C for 1h with shaking. After recovery, bacteria were plated on an LB-agar plate with appropriate antibiotic.

6.1.2. Polymerase chain reaction (PCR)

6.1.2.1. Standard PCR

DNA fragments used for cloning were amplified from the template DNA by PCR using Q5 High Fidelity Polymerase (NEB) or Phusion High Fidelity Polymerase (NEB) according to manufacturer's protocol. Standard components of a PCR reaction were:

- template DNA 1-50 ng
- 1 x reaction buffer (Q5 buffer for Q5 polymerase, HF or GC for Phusion polymerase)
- dNTP mix 200 μM
- forward primer 0.5 μM
- reverse primer 0.5 μM
- polymerase 0.02 U / μL

- optionally: 1 x Q5 High GC enhancer (for Q5 polymerase)
- optionally: DMSO up to 5% reaction volume (for Phusion polymerase)

Standard PCR program involved the following steps:

Initial denaturation	2 min	98°C
Denaturation	5-10 s	98°C
Annealing	10-30 s	48-72°C
Elongation	20-30 s / kb	72°C
Final extension	2 min	72°C
Hold	∞	4°C

Denaturation, annealing and elongation were repeated 25-35 times.

6.1.2.2. Quantitative PCR (qPCR)

To quantify the amount of specific transcript in cells quantitative reverse transcription PCR (RT-qPCR) method was used. First, the cells were lysed and the total RNA was extracted using Quick-RNA Miniprep Kit (Zymo Research). Then 0.3-1 μg of total RNA was reverse transcribed into complementary cDNA using RevertAid First Strand cDNA Synthesis Kit (Thermo Fisher Scientific). cDNA was used as a template in the qPCR reaction. The following components were mixed in each of the wells on a 96-well qPCR plate in a total reaction volume of 20 μL: 1 x ABsolute Blue qPCR Sybr Green (Thermo Fisher Scientific), 100 nM forward primer, 100 nM reverse primer, 2 μL of cDNA solution diluted in water in the proportion of 1 : 1. The plate was sealed and centrifuged at 1000 rpm for 1 min. The reaction was performed in a LightCycler 96 system (Roche). The qPCR program involved the following steps:

Step name	Number of cycles	Step ramp [°C / s]	Duration [s]	Target [°C]	Acquisition mode
Preincubation	1	4.4	600	95	None
3-step amplification	40-50	4.4	10	95	None
		2.2	30	60	None
		4.4	30	72	Single
Melting	1	4.4	5	95	None
		2.2	60	65	None
		-		97	Continuous 5 readings / °C
Cooling	1	1	30	37	None

The quantification cycle (Cq) was automatically calculated by the machine and used for further calculations to quantify the amount of the specific sequence based on the standard curve. The expression levels were normalised to the β2-microglobulin (*B2M*) housekeeping gene.

qPCR after ChIP was performed according to the same protocol. As a template, ChIP elution fraction was used. Total HEK293 genomic DNA was used for preparation of the standard curve.

6.1.3. Cloning

6.1.3.1. gRNA cloning

All gRNAs were cloned into vectors initially carrying BbsI or BsaI restriction sites. For linearisation of every construct, 1 μg of plasmid was used. For digestion with BbsI (Thermo Fisher Scientific) plasmid was incubated in 1 x G Buffer (Thermo Fisher Scientific) at 37°C for 1h. For digestion with BsaI-HF (NEB) plasmid was incubated in 1 x CutSmart Buffer (NEB) at 37°C overnight.

Sense and antisense DNA strands encoding each gRNA were mixed equimolarly at the final concentration of 10 μM in 1 x T4 Ligase Buffer (Thermo Fisher Scientific). The annealing was performed according to the following program:

From 95°C to 65°C: ΔT = 5°C, 5 min incubation at each step

From 65°C to 27°C: ΔT = 3°C, 3 min incubation at each step

10 min incubation at 25°C

1 μL of the annealed oligonucleotides, 2.5 μL of 10 x T4 Ligase Buffer and 1 U T4 Ligase were added directly to the digested plasmid and incubated at 37°C for 1h. 5 μL of the reaction was used for transformation of chemically competent *E. coli* strain DH5α.

6.1.3.2. Site-directed mutagenesis

To introduce point mutations and deletions in DNA constructs, strategy of blunt-end joining was used. Briefly, the back-to-back primers carrying the desired point mutation or amplifying the plasmid without the deletion fragment were used in a standard PCR reaction. Next, 1 μL of FastDigest DpnI (Thermo Fisher Scientific) per 50 μL of PCR reaction mixture was added. The specificity of the PCR product was assessed by performing agarose gel electrophoresis. DNA fragments were purified either from preparative agarose gel after electrophoresis using GelElute Gel Extraction Kit (Sigma-Aldrich) or directly from the reaction mixture using QIAquick PCR purification kit (Qiagen). The concentration and purity of DNA fragments was calculated from the absorbance at 260 nm and 280 nm. The blunt-end-joining reaction mixture consisted of the following components:

- 1 x T4 Ligase Buffer (Thermo Fisher Scientific)
- ATP 1 mM
- plasmid DNA 100 ng / 5 kbp
- T4 PNK (Thermo Fisher Scientific) 10 U / μL
- T4 Ligase (Thermo Fisher Scientific) 5 U / μL

The reaction mixture was incubated at 37°C for 1h. 5 μL was used for transformation of chemocompetent *E. coli* strain DH5α.

Alternatively, for site-directed mutagenesis, QuikChange strategy was used. In this method two overlapping primers containing the desired mutation were used for the vector amplification what resulted in generation of a nicked plasmid in a PCR reaction using Pfu Turbo DNA polymerase (Agilent). PCR reaction components in QuikChange method were as follows:

- 1 x Turbo buffer (Agilent)
- DNA template 5-50 ng
- forward primer 125 ng
- reverse primer 125 ng
- dNTP mix 200 μM
- Pfu Turbo polymerase 0.05 U / μL

PCR program in QuikChange method involved the following steps:

Segment 1	30 s	95°C
Segment 2	30 s	95°C
	1 min	55°C
	1 min / kb	68°C

Segment 2 was repeated 12-18 times depending on the type of introduced mutation according to the manufacturer's protocol. Subsequent digestion with FastDigest DpnI and bacterial transformation was done as previously described.

6.1.3.3. Gibson Assembly

DNA fragments used for the Gibson Assembly method were obtained using standard PCR and purified using GelElute Gel Extraction Kit (Sigma-Aldrich) or QIAquick PCR purification kit (Qiagen). 50-200 ng of vector DNA was mixed with 3-7 x molar excess of insert DNA and GA Mix 1 in the proportion that guaranteed that the DNA solution in water did not constitute more than 25% of a total reaction volume. The reaction mixture was incubated at 50°C for 20, 40 and 60 min and 2 μL was used for transformation of minimum 100 μL chemocompetent *E. coli* strain DH5α.

6.1.4. Agarose gel electrophoresis

Sample containing DNA was mixed with 1 x TriTrack DNA Loading Dye (Thermo Fisher Scientific) and separated in 0.8-2% agarose gel containing SYBR Safe DNA Gel Stain (Thermo Fisher Scientific) in 1 x TAE buffer and subsequently visualised using UV transilluminator.

6.1.5. Sanger sequencing of purified DNA molecules

For the sequencing of PCR products or plasmid fragments, GATC / Eurofins Genomics service was used.

6.2. Biochemical methods

6.2.1. Dual luciferase assay

HEK293 5xUAS-luc were seeded on a 96-well plate and transfected with plasmid DNA of choice mixed with pRL plasmid encoding *Renilla* luciferase (ca. 1 molecule of pRL per 50 molecules of the plasmid of choice) using Lipofectamine 3000 according to the procedure described in chapter 6.3.2. Dual luciferase assay was performed with Dual-Luciferase Reporter Assay System (Promega) 24 h after transfection. The medium was aspirated and 100 μL of 1 x Passive Lysis Buffer was added to each well. Cells were lysed at room temperature for 15 min with intense shaking. Next, the plate was centrifuged to pellet cell debris at 4000 rpm for 5 min. 5 μL of clear lysate was transferred to each well on the OptiPlate (Perkin Elmer). The assay protocol was performed using Varioskan LUX microplate reader according to the following program:

Apply 40 μL Luciferase Assay Reagent II

Mix 1 s at 300 rpm

Measure the firefly luminescence signal for 500 ms

Apply 40 μL Stop&Glo Reagent II

Mix 1 s at 300 rpm

Measure the *Renilla* luminescence signal for 500 ms

Each experiment was performed in 3 biological and 3 technical replicates.

6.2.2. Preparative recombinant protein production in bacterial expression system

Expression strain of *E. coli* was chemically transformed with expression plasmid and grown overnight at 37°C on the selection LB-agar plate. The next day, a small-scale culture (5 mL) was grown overnight in LB medium and in the morning the culture was diluted 1:100. From this point, the optical density (OD600) of the culture was monitored every 30 min. When the OD600 of the culture reached 0.8-1.5 (i.e. when bacteria were in the exponential growth phase), protein production was induced by adding 1M IPTG to the final concentration of 1 mM. From this point, bacteria were grown at 18°C for 12-20 h. The culture was centrifuged at 3000 x g, 4°C for 20 min. Bacterial pellet was resuspended in IPH buffer in the proportion of 13.3 mL buffer / 1 g pellet. Bacteria were disrupted by 3 rounds of sonication on ice using Branson Digital Sonifier with the following parameters: 50% amplitude, 0.5 s ON, 0.5 s OFF, 1 min ON time. The suspension was centrifuged at 20000 x g, 4°C for 20 min and the crude extract (supernatant) was collected. The crude extract was mixed with 2 x volume of MBP column buffer supplemented with 1 mM DTT. 50 μL of amylose resin (NEB) per 1.33 mL of crude extract was added and the suspension was incubated at 4°C for 2 h with rotation. The mixture was centrifuged at 4000 x g, 4°C for 2 min and the resin was washed 3 times with MBP column buffer. After the final wash, the resin with immobilised MBP-protein was gently resuspended in 50% glycerol in MBP column buffer and stored at -20°C until further processing.

6.2.3. HeLa nuclear extract preparation

Nuclear extract for in vitro histone methyltransferase assay was prepared according to the published protocol with slight modifications [208]. HeLa S3 cells were grown in suspension to a cell density of 0.5-0.8 x 10^6 cells / mL and harvested by centrifugation

at 1000 x g, 4°C for 10 min. Cells were washed twice with ice-cold PBS. Cell pellet volume (CV) was estimated, resuspended in 5 x CV of hypotonic buffer A and incubated on ice for 10 min. The CV after cell swelling was estimated and resuspended in 1 x CV of cold buffer A supplemented with 0.2% IGEPAL, 1 mM DTT and 1 x PIC. Cells were mechanically lysed using a dounce homogeniser with a tight pestle until more than 90% cells were stained by trypan blue. The suspension was centrifuged at 3000 x g, 4°C for 15 min. The supernatant containing the cytoplasmic fraction was gently removed. The pellet was resuspended in 10 x volume of cold buffer A supplemented with 150 mM NaCl and 1 mM DTT and centrifuged at 3000 x g, 4°C for 5 min. The nuclear pellet was thoroughly resuspended in 2 x volume of cold Buffer C and incubated with rotation at 4°C for 1 h. The nuclear suspension was centrifuged at 25000 x g, 4°C for 20 min. The clear supernatant was collected, aliquoted, snap frozen in liquid nitrogen and stored at -80°C.

6.2.4. HEK293 nuclear fraction preparation

Nuclear fraction for IP was prepared according to the modified REAP protocol [209]. HEK293 cells were washed twice with ice-cold PBS, scraped from the dishes in residual (2-4 mL) PBS and centrifuged at 300 x g, 4°C for 5 min. The pellet was washed with ice-cold PBS supplemented with 1 x PIC, 0.5 mM AEBSF and 1 mM DTT and a small fraction of the suspension was collected for the whole cell lysate preparation. The cell pellet volume was estimated and the aliquots of 100 μL were distributed into 1.5 mL protein low binding tubes. After the pop-spin centrifugation (at 10000 rpm, 4°C for 5 s) the supernatant was decanted and the cells were resuspended in 9 x volume (900 μL) of PBS supplemented with 0.1% IGEPAL and 1 x PIC (PBS/IGEPAL/PIC),

triturated 5 times using P1000 pipette and immediately pop-spun like previously. The supernatant was quickly decanted and the pellet was resuspended in another 9 x volume of PBS/IGEPAL/PIC and triturated 3 times like previously. After the final pop-spin, the nuclei were gently washed with ice-cold PBS by pipetting it slowly into the wall of the tube without disrupting the pellet. The content of each tube was filled to 100 μL with PBS and 278 μL buffer C (MV) supplemented with 0.1% IGEPAL and 1 x PIC was added to each tube. The nuclei were immediately resuspended and incubated for 4-14 h at 4°C with rotation. After the incubation, the samples were centrifuged at 17000 x g, 4°C for 1 h. The supernatant was collected and the protein concentration was measured by Roti Nanoquant.

6.2.5. Quantification of protein concentration by Roti Nanoquant

The concentration of protein samples was measured by Roti Nanoquant (Carl Roth), that is a modification of the Bradford method [210], according to manufacturer's protocol. Before the measurements, samples were diluted 1 : 100 (for nuclear extracts) or 1 : 40 – 1 : 80 depending on the expected protein content. The absorbance at 590 nm and 450 nm was measured using Varioskan LUX or Multiskan GO microplate reader (Thermo Fisher Scientific).

6.2.6. Immunoprecipitation from nuclear fraction

To immunoprecipitate FLAG-tagged proteins from the nuclear fraction 1 mg of nuclear extract (prepared according to the modified REAP protocol, chapter 6.2.4) was mixed with 30 μL 50% Anti-FLAG M2 Affinity Agarose Gel slurry equilibrated with buffer

C* (MV) and the volume was brought to 1.8 mL with buffer C* (MV). 1 µL of Benzonase (Sigma-Aldrich) was added to each IP tube and the samples were incubated overnight at 4°C with rotation. After the incubation, the beads were centrifuged (at 6000 x g, 4°C for 1 min) and washed (5 min each wash, at 4°C with rotation) according to the following scheme: 2 times with buffer C* (MV) supplemented with 0.2% IGEPAL, 2 times with PBS supplemented with 0.2% IGEPAL and 1 x PIC, 1 time with PBS. The bound proteins were eluted from the beads with 2 portions of 30 µL 1.5 x MS elution buffer. Each elution was performed in a thermoshaker at 70°C for 20 min with shaking at 12000 rpm. Both elution fractions were pooled and stored at -20°C until further processing.

6.2.7. RIPA total cell lysate preparation

For preparation of total cell lysate, the cells were washed twice with ice-cold PBS and resuspended in ice-cold 1 x RIPA lysis buffer supplemented with 1 x PIC in the proportion of ~100 µL buffer per 1 x 10^6 cells. The cells were lysed at 4°C for 30 min with rotation followed by centrifugation of cellular debris at 17000 x g, 4°C for 30 min. The supernatant was collected and the protein concentration was measured by Roti Nanoquant.

6.2.8. Sodium dodecyl sulfate-polyacrylamide gel electrophoresis (SDS-PAGE)

SDS-PAGE was performed following the Laemmli protocol [211]. The percentage of acrylamide was chosen from the range 8-18.6% based on the size of the separated protein of interest. The protein samples were mixed with 6 x Laemmli sample loading

buffer in the proportion of 5 : 1 and incubated at 98°C for 5 minutes before loading on the gel. Electrophoresis was performed in 1 x SDS-PAGE running buffer at 150-180V for approximately 60-90 min.

6.2.9. Protein staining with Coomassie Brilliant Blue

Proteins after SDS-PAGE were stained with Coomassie Brilliant Blue solution (2% Coomassie Brilliant Blue, 40% methanol, 10% acetic acid) for 20-40 min with rocking. The time of staining depended on the gel thickness and percentage of acrylamide in the gel. The background was destained in destaining solution (50% water, 40% methanol, 10% acetic acid) until the protein bands were clearly visible. The destaining solution was changed up to 3 times.

6.2.10. Immunostaining (Western Blotting)

To perform immunostaining of proteins separated by SDS-PAGE, proteins were transferred to nitrocellulose membrane with 0.45 μm pore size. Transfer was performed in 1 x transfer buffer at 230 mA for 1 h. The efficiency of transfer was monitored by reversible staining of the membrane with ponceau S solution (0.1% (w/v) Ponceau S in 1% acetic acid) followed by destaining with water. Membrane was incubated in blocking solution at room temperature for 1 h. The choice of blocking solution was made depending on the guidelines provided by the supplier of used antibody. Albumin fraction V or nonfat-dried milk at the concentration of 4-5%, dissolved in TBS-T (TBS, 0.1-0.2% Tween 20) was used as a blocking agent. After blocking, primary antibody diluted in blocking solution according to the supplier's guidelines was applied and the membrane was incubated at 4°C overnight with gentle

rotation or rocking. After incubation with primary antibody, the membrane was washed with TBS-T (TBS, 0.1-0.2% Tween 20) 3 times, 5 minutes per wash and the secondary antibody conjugated to horseradish peroxidase (HRP) diluted in blocking solution was applied. The membrane was incubated at room temperature for 1 h with rocking. After incubation with secondary antibody, the membrane was washed as previously and incubated with ECL substrate (Bio Rad) for 5 minutes at room temperature. The chemiluminescence signal was detected and visualised using ChemiDoc imager (Bio Rad).

6.2.11. Co-purification of the histone writing activity from HeLa nuclear fraction with MBP-enzyme fusions

MBP-enzyme fusions immobilised on the amylose resin were washed 3 times with MBP column buffer to remove 50% glycerol in which the slurry was stored. Next, MBP-enzyme slurry was mixed with 'empty' amylose resin so that the volume of the beads was constant across all the experimental conditions. The volume of each MBP-enzyme slurry used for the assay was previously determined by separating various volumes of MBP-enzyme slurry by SDS-PAGE followed by staining the proteins with Coomassie Brilliant Blue solution and destaining the background with destaining solution. MBP-enzyme/amylose mixture was mixed with HeLa nuclear extract (20-100 μL depending on the batch) in 1 x IPH buffer. The mixture was rotated at 4°C for 1 h. After the incubation, the slurry was washed 3 times with 1 x IPH buffer and subjected to in vitro methyltransferase assay.

6.2.12. In vitro methyltransferase assay

MBP-enzyme fusions immobilised on amylose resin after incubation with HeLa nuclear extract were mixed with 30 μg calf thymus histones (Sigma-Aldrich) and 1 μL ^{3}H-labelled SAM (1 mCi / mL) in 1 x Horiuchi buffer [212]. The reaction mixture was incubated at 30°C for 1h with gentle shaking. The reaction was terminated by adding 6 μL of 6 x Laemmli sample loading buffer and incubating at 95°C for 5 min. The whole sample was separated in 18.6% SDS-PAGE gel and blotted to the nitrocellulose membrane. The radioactivity signal was detected on Kodak BioMax MS Film Maximum Sensitivity-Radioisotope with intensifying screen and / or by cutting the ponceau S stained histone bands from the membrane, dissolving the membrane in Filter-Count liquid scintillation counter cocktail (Perkin Elmer) and measured using liquid scintillation counter (Hidex).

6.2.13. Chromatin immunoprecipitation (ChIP)

6.2.13.1. Blocking protein A / protein G-coupled beads for ChIP-qPCR

Protein A sepharose- and protein G sepharose suspensions (A/G beads) were mixed in a 3 : 1 ratio and washed twice with 1 mL ChIP dilution buffer (DB) with centrifugation at 1500 x g after each wash. BSA (NEB) and deoxyribonucleic acid sodium salt from salmon testes (Sigma-Aldrich) were added to the beads to the final concentration of 62.5 μg / mL and 50 μg / mL, respectively in a total volume of 2 mL per 666.7 μL initial A/G beads. The beads were blocked at room temperature for 2 h with rotation. After blocking, the beads were centrifuged at 2000 x g for 1 min and the supernatant was discarded. The beads were resuspended in DB to make 50% slurry.

6.2.13.2. Blocking protein A / protein G-coupled beads for ChIP-seq

Protein A sepharose- and protein G sepharose suspensions (A/G beads) were mixed in a 3 : 1 ratio and washed twice with 1 mL ChIP dilution buffer (DB) with centrifugation at 1500 x g after each wash. BSA (NEB) and tRNA from *Saccharomyces cerevisiae* (Sigma-Aldrich) were added to the beads to the final concentration of 500 μg / mL and 650 μg / mL, respectively in a total volume of 2 mL per 666.7 μL initial A/G beads. The beads were blocked at room temperature for 2 h and then overnight at 4°C with rotation. After blocking, the beads were centrifuged at 2000 x g for 1 min and the supernatant was discarded. The beads were resuspended in DB to make 50% slurry.

6.2.13.3. Preparation of chromatin from HEK293

Human HEK293 cells were grown on 15-cm dishes to ~80% confluency and crosslinked by adding formaldehyde to the cell growth medium to the final concentration of 1%. The cells were fixed at room temperature for 5 minutes (histone and transcription factor ChIP) or 10 minutes (FLAG-2HA-dCas9 ChIP) with gentle rocking. The crosslinking was quenched by adding glycine to the final concentration of 125 mM. The cells were washed 3 times (5 min per wash) with ice-cold PBS. 2.5 mL ice-cold PBS supplemented with 1 x PIC, 10 mM sodium butyrate and 10 mM nicotinamide (NAM) was added to each dish and the cells were collected by scraping. The cells were pelleted at 500 x g, 4°C for 5 min, resuspended in L1 buffer at the density of 10^7 cells / mL and incubated on ice for 5 min. Next, the suspension was centrifuged at 800 x g, 4°C for 5 min and the nuclear pellet was resuspend in L2 buffer at the density of 10^7 cells at the starting point / mL. Nuclear suspension was distributed

into 300-μL aliquots in the sonication tubes and the chromatin was sheared using QSonica sonicator for 5 min (sonication ON time) at 80% amplitude in 20 s ON / 40 s OFF cycles. The cellular debris were centrifuged at 10000 rpm for 1 min and the clear supernatant was collected. 10 μL of sheared chromatin was collected for checking sonication efficiency and 10 μL – for overnight de-crosslinking to measure the chromatin DNA concentration. For checking sonication efficiency, 10 μL sample was mixed with 90 μL L2 buffer and 8.4 μL 5 M NaCl, incubated at 95°C for 10 min and cooled down on ice for 2 min. 2 μL RNase A 10 mg / mL (Thermo Fisher Scientific) and 2 μL proteinase K 20 mg / mL (Roche) were added and the sample was incubated at 55°C for 45 min with shaking. The DNA fragments were purified using QIAquick PCR purification kit and eluted from the column with 50 μL water. DNA concentration was measured using Varioskan LUX or Multiskan GO microplate reader and 400-500 ng DNA was separated in 1% agarose gel. For measuring the chromatin DNA concentration, 10 μL sample was mixed with 40 μL L2 buffer, 2 μL RNase A 10 mg / mL (Thermo Fisher Scientific) and 2 μL proteinase K 20 mg / mL (Roche) and de-crosslinked overnight at 65°C with shaking. The DNA fragments were purified using QIAquick PCR purification kit, eluted from the column with 100 μL water and the DNA concentration was measured using Varioskan LUX or Multiskan GO microplate reader. If the DNA fragments were of correct size (200-700 bp) the chromatin was processed to immunoprecipitation or aliquoted and snap-frozen in liquid nitrogen. Otherwise more sonication cycles were performed.

6.2.13.4. Preparation of *Drosophila* chromatin

For crosslinking of *Drosophila* S2 cells, growth medium was aspirated and 1% formaldehyde solution in PBS was added to the cells. The cells were fixed at room temperature for 5 min with gentle rocking. The crosslinking was quenched by adding glycine to the final concentration of 130 mM for 10 min. The cells were scraped from the plate, pelleted at 1000 x g and washed twice with ice-cold PBS. Next, the cells were resuspended in ice-cold fast IP buffer at the density of 2 x 10^7 cells / mL and incubated 10 min on ice. During the incubation, the cells were pulled through the syringe with a 27G needle. The cells were centrifuged at 12000 rpm, 4°C for 1 min. The homogenisation cycle was repeated once. 1 mL of the shearing buffer was added to the pellet from 2 x 10^7 cells. The nuclear suspension was distributed into 200-μL aliquots in the sonication tubes and the chromatin was sheared using QSonica sonicator for 13 min 20 s (sonication ON time) at 80% amplitude in 20 s ON / 40 s OFF cycles. From this point *Drosophila* chromatin was treated according to the same procedures as described in chapter 6.2.13.3.

6.2.13.5. Immunoprecipitation

Chromatin samples were diluted 10 times with ChIP dilution buffer (DB). Before IP, chromatin samples were pre-cleared with pre-blocked A/G beads at 4°C for 1-2 h in the proportion of 80 μL A/G beads per 25 μg chromatin DNA. The beads were centrifuged and the clear supernatant was further processed. The IP samples were prepared by diluting pre-cleared chromatin in DB and adding relevant antibodies. If spike-in ChIP was performed, *Drosophila* and human chromatins were mixed at this step. Equivalent of 10% total input was collected and stored at 4°C until the final ChIP samples were eluted. The ChIP samples were incubated with antibodies overnight at

4°C with rotation. Next, 40 μL of pre-blocked A/G beads were added and incubated at 4°C with rotation for 2 h. The ChIP samples were subjected to washes according to the following scheme: 2 x 1 mL low salt buffer, 2 x 1 mL high salt buffer, optionally: 2 x 1 mL LiCl wash buffer, 1 x TE buffer. Each wash was performed at 4°C with rotation for 5 min followed by centrifugation at 2000 x g, 4°C for 1 min. Chromatin was eluted from the beads with two 100-μL portions of freshly prepared ChIP elution buffer at 30°C in a thermoblock with shaking at 800 rpm. Each elution lasted 15 min. Both fractions were pooled and (together with the 10% input sample saved before the IP) subjected to overnight de-crosslinking, like previously described.

6.2.14. Preparing ChIP samples for Next Generation Sequencing (NGS)

6.2.14.1. DNA library preparation

To prepare libraries for ChIP-seq NEBNext Ultra II DNA Library Prep Kit, NEBNext Multiplex Oligos for Illumina (96 Unique Dual Index Primer Pairs) and AMPure XP beads (Beckman Coulter) were used. First, the DNA concentration of ChIP elution fractions were measured using Qubit dsDNA HS (High Sensitivity) Assay Kit (Thermo Fisher Scientific). By default, the starting mass of DNA for the library preparation was 5 ng. If the concentration of DNA was too low, the samples were previously concentrated using miVac concentrator (SP Scientific). The best efficiency of the library preparation was obtained with the following adjustments to the protocol: adaptor dilution 1 : 25, 11 cycles of PCR amplification, 5 μl of pre-mixed forward/reverse primer solution. The size distribution of obtained DNA fragments was checked on the Bioanalyzer 1000 or Bioanalyzer High Sensitivity Chip (Agilent).

6.2.14.2. Size selection of DNA fragments

Double size selection of DNA fragments after preparation of DNA libraries for NGS was performed using magnetic AMPure XP beads (Beckman Coulter). The whole procedure was performed at room temperature. Half the volume of the DNA library sample was diluted in water to the final volume of 50 μL. 0.65 x volume of beads was added and triturated 10 times to bind to the beads fragments shorter than desirable (left side size selection). The suspension was incubated 1 min and the beads were separated with the magnet for 5 min. The supernatant was collected and 1.15 x volume of beads was added and triturated 10 times to prevent bigger fragments than desirable from binding to the beads (right side size selection). The suspension was incubated and separated with the magnet like previously. The supernatant was discarded and the beads with immobilised fragments of desirable size were washed with 180 μL 85% ethanol and air dried. The DNA fragments were eluted from the beads by adding 20 μL water, triturating 10 times and incubating 1 min. Finally, the beads were separated with the magnet and the clear supernatant with eluted DNA fragments was collected and transferred to a new vessel. The size distribution of obtained DNA fragments was checked on the Bioanalyzer High Sensitivity Chip (Agilent) and DNA concentration of the final library was measured using Qubit dsDNA HS (High Sensitivity) Assay Kit (Thermo Fisher Scientific). The final pool of libraries for NGS was prepared by equimolarly mixing all library samples to reach the concentration of 5 nM.

6.2.15. Preparing RNA samples for Next Generation Sequencing (NGS)

Total RNA was extracted using Quick-RNA Miniprep Kit (Zymo Research). The concentration was measured using Qubit RNA BR (Broad Range) Assay Kit (Thermo

Fisher Scientific). The integrity of RNA was checked on the Bioanalyzer 6000 Nano Chip (Agilent). The samples were diluted in nuclease-free water to the concentration of 100 ng / μL. 1 μg RNA was submitted to the Helmholtz Zentrum München NGS Core Facility.

6.2.16. Preparation of genomic DNA for MS analysis

Genomic DNA for MS analysis was prepared using Quick-DNA Miniprep Plus kit (Zymo Research) with modifications. HEK293 cells were washed 3 times with ice-cold PBS, trypsinised and distributed into aliquots containing 5 x 10^6 cells each. Cell pellets were snap-frozen in liquid nitrogen and stored at -80°C. On the day of extraction, frozen cell pellets were resuspended thoroughly in 200 μL BioFluid&Cell Buffer (Zymo Research) and 200 μL PBS. From this point the whole procedure was performed at room temperature unless indicated otherwise. All the centrifugation steps were performed at 12000 x g for 1 min unless indicated otherwise. 20 μL proteinase K (20 mg / mL, Zymo Research) was added, the sample was vortexed for 15 s and incubated at 55°C for 10 min. Next, 1.8 μL RNase A (100 mg / mL, Qiagen) was added, the sample was mixed by pipetting and incubated at 37°C for 30 min. After the digestion, 1 volume of Genomic Binding Buffer (Zymo Research) was added, the sample was briefly vortexed, applied to the spin column (Zymo Research) and centrifuged. 1.6 μL RNase A (100 mg / mL, Qiagen) was resuspended in 400 μL Genomic Binding Buffer (Zymo Research), applied to the column and incubated at room temperature for 30 min. After the incubation, the column was centrifuged at 200 x g for 2 min followed by 1000 x g for 1 min. The flowthrough and the collection tube were discarded. The column was washed with 400 μL Pre-Wash Buffer (Zymo Research), 700 μL g-DNA Wash Buffer

(Zymo Research) and finally with 200 μL g-DNA Wash Buffer (Zymo Research). To elute DNA, 50 μL water at 60°C was added to the column and the column was incubated at 60°C for 5 min. The column was centrifuged, the elution fraction was collected and re-applied to the same column. The sample was incubated at 60°C for 3 min, centrifuged and stored at -20°C. The concentration of DNA and RNA (as a control for sample purity) was measured using Qubit DNA BR (Broad Range) and Qubit RNA BR (Broad Range) Assay Kits (Thermo Fisher Scientific).

6.2.17. Intracellular crosslinking with disuccinimidyl suberate (DSS)

The whole procedure of intracellular crosslinking was performed at room temperature. HEK293 cells were washed 3 times with PBS pH 8.0 and resuspended at the density of 2.5 x 10^7 cells / mL in PBS pH 8.0. The working stock of DSS at the concentration of 25 mM was prepared and added to the cell suspension to the final concentration of 5 mM. The mixture was thoroughly resuspended by gentle trituration and incubated for 30 min. The reaction was stopped by adding 1 M Tris-HCl pH 7.5 to the final concentration of 20 mM for 15 min. Laemmli sample loading buffer was added to the final concentration of 1 x. Samples of the volume 2 μL, 10 μL and 30 μL (equivalent of 3.3 x 10^4, 1.67 x 10^5 and 5 x 10^5 cells) were separated in the SDS-PAGE gel and immunoblotted with relevant antibody.

6.3. Cell culture methods

6.3.1. Eukaryotic cell growth conditions

All human cell cultures were maintained at 37°C under a humidified atmosphere with 5% CO_2. HEK293 cells were cultured in low glucose DMEM medium supplemented with 10% Foetal Bovine Serum (FBS), 200 mM L-Glutamine (L-Glu), 1% Pen/Strep (unless stated otherwise), 1 mM sodium pyruvate (NaPyr) and 1 x Non-Essential Amino Acid Solution (NEAA). HEK293T cells were cultured in high glucose DMEM medium supplemented with 10% FBS, 200 L-Glu, 1% Pen/Strep (unless stated otherwise), 1 mM NaPyr and 1 x NEAA. HeLa S3 cells previously adapted to grow in suspension were cultured in RPMI-1640 medium supplemented with 5% Neonatal Calf Serum (NCS), 200 mM L-Glu, 1% Pen/Strep and 50 μM β-mercaptoethanol in a spinner flask. *Drosophila* Schneider 2 cells (S2) were cultured at 27°C under a humidified atmosphere without CO_2 supply, in Schneider medium supplemented with 10% heat-inactivated FBS and 0.5% Pen/Strep. All the experiments involving the culture of mESC were done in the Stricker Lab according to the protocols routinely used in the lab.

6.3.2. Human cell standard transfection with plasmid DNA – small scale

For the small-scale transfection experiments, mammalian cells were transfected using Lipofectamine 3000 reagent (Thermo Fisher Scientific) according to the manufacturer's protocol with slight modifications. The cells were seeded one day before in order to be 70-90% confluent at the time of transfection. On the day of transfection, the growth medium was exchanged. The plasmid DNA was mixed with P3000 reagent and diluted in serum-free DMEM. In a separate tube, a dilution of Lipofectamine 3000 in serum-free DMEM was prepared. Diluted DNA was mixed with diluted Lipofectamine 3000, incubated at room temperature for 15 min and added dropwise to the cell medium. Transfection medium was exchanged with a fresh

medium 12-20 h after transfection. For experiments requiring transient transfection the cells were harvested 3 days after transection. For establishing stable HEK293 cell lines, selection medium with 400 μg / mL G418 was applied 48 hours after transfection.

For the trial HEK293T transfection with Lipofectamine 2000, the same protocol as for Lipofectamine 3000 was used. The only exception was the lack of P3000 reagent. For the trial transfection with TurboFect (Thermo Fisher Scientific) the plasmid DNA was diluted in serum-free medium and the transfection reagent was added directly to the mixture. The solution was vortexed immediately, incubated at room temperature for 15-20 min and added dropwise to the cell medium.

6.3.3. Human cell transfection with plasmid DNA – large scale

For the large-scale transfection experiments, mammalian cells were transfected using polyethylenimine (PEI). One day before transfection, cells from 1 confluent 15-cm dish were split 1 : 4. On the day of transfection, 9 μg of plasmid DNA per 15-cm dish was diluted in 900 μL pre-warmed serum-, L-Glu- and Pen/Strep-free medium. 75 μL of a 1 mg / mL PEI solution in water (pH 7.0) was added, the sample was gently mixed by shaking the tube and the transfection mixture was incubated at room temperature for 20 min. After the incubation, the solution was gently mixed again by pipetting up and down and added dropwise to the cell medium. The dish was gently rocked and the cells were incubated with the transfection medium overnight.

6.3.4. Coating cell growth surface with poly-L-lysine

For lentiviruses production in HEK293T, 6-well plates coated with poly-L-lysine (poly-L-Lys) were used. 0.1 mg / mL solution of poly-L-Lys in sterile water was poured into each well of the plate so that the liquid covered the whole well surface (~1 mL per well) and incubated in the cell culture hood for 5 min. Next, the wells were washed twice with sterile water with 5 min incubation time per wash. The plates were left open in the cell culture hood to dry. The dried coated plates were sealed with parafilm and stored at 4°C until needed (up to 14 days).

6.3.5. Lentiviral vector production using LENTI-Smart (Invivogen)

Lentiviral particles were produced in HEK293T cell line grown in Pen/Strep-free medium. The cells were seeded one day before transfection on poly-L-Lys coated 6-well plates in order to be 70-90% confluent at the time of transfection. On the day of transfection, the growth medium was exchanged. LENTI-Smart was transferred from -20°C to the room temperature and pre-warmed for 10 min. The lyophilised reagent was resuspended in 400 μL sterile water and incubated at room temperature for 15 min. 3 μg of pLKO.1-puro plasmid (kindly shared by Dr. Timo Dirk Müller and Dr. Marc Walter) was prepared in a low DNA binding tube. 100 μL resuspended LENTI-Smart was added per 3 μg of plasmid DNA and the mixture was incubated at room temperature for 15 min. Next, total mixture volume was added to the cell medium for 14-18 h. After the incubation, the transfection medium was discarded and the fresh medium was added for 24 h. At this point the medium with lentiviral particles was collected (first collection fraction) and the fresh medium was added for the next 24 h after which the second collection fraction was harvested. The first collection fraction was kept for 24 h at 4°C before the second harvesting took place. Both collection

fractions were pooled, centrifuged at 2000 rpm for 5 min, filtered through 0.45 μm PVDF syringe filter and immediately used for target cell transduction.

6.3.6. Human cell transduction with lentiviral particles

HEK293 cells were transduced with lentiviruses on 96-well plates or 6 cm dishes. During the transduction procedure, the cells were grown in Pen/Strep-free medium. The cells were seeded one day before transduction at the density of 1.4 x 10^5 cells / cm^2. On the day of transduction, the growth medium was exchanged. Growth medium and the working solution with 8 μg / mL and 80 μg / mL hexadimethrine bromide (polybrene), respectively were prepared by mixing 8 mg / mL polybrene stock with growth medium. Growth medium with polybrene was mixed with polybrene working solution and lentiviral supernatant so that the final liquid volume reached ~100 μL per well on a 96-well plate or 5-7 mL on a 6-cm dish and the final polybrene concentration was 8 μg / mL. Lentiviral supernatant was incubated on the cells for 14-18 h. After the transduction, the supernatant was removed from the cells and fresh medium was added for 24 h of recovery. Next, selection medium with 2.5 μg / mL puromycin was applied and the cell viability was assessed under the microscope 48 h later.

6.3.7. Harvesting cells for metabolomic analysis

HEK293 cells for metabolomic analysis were seeded one day before harvesting on 10 cm dishes at the density of 1.24 x 10^6 cells / dish. On the day of harvesting, the cells were washed twice with ice-cold PBS, scraped from the plates in residual PBS

and transferred to 1.5 mL protein low-binding tube. The cells were centrifuged at 300 x g, 4°C for 3 min, resuspended in 100 μL ice-cold PBS, snap-frozen in liquid nitrogen and stored at -80°C. The metabolites extraction was performed by the Yanes Lab.

6.3.8. siRNA transfection of human cells

HEK293 cells were transfected with ON-TARGETplus SMARTpool or Non-targeting Pool (Dharmacon) using Lipofectamine RNAiMAX (Thermo Fisher Scientific). Lyophilised siRNA was resuspended in 1 x siRNA Buffer (Dharmacon) to the concentration of 100 μM, aliquoted and stored at -80°C until use. One day before transfection, HEK293 cells were seeded at the density of 2.5 x 10^5 cells per well in a 6-well plate format. On the day of transfection, siRNA was diluted to the 10 μM working stock and used for 'forward transfection' according to the manufacturer's protocol with modifications. Briefly, the siRNA working stock was diluted in 250 μL serum-free medium in a DNA low-binding tube so that the final concentration of siRNA duplex in the well was 20 nM. Lipofectamine RNAiMAX was diluted in 250 μL serum-free medium in a separate tube. The solutions were mixed, incubated for 15-20 min at room temperature and added dropwise to the cell medium.

For the sequential transfection procedure, 'reverse transfection' protocol with the final concentration of siRNA duplex 10 nM was used 3 days after the first transfection. Briefly, 1.77 μL of 100 μM siRNA stock was diluted in 2.9 mL serum-free medium in a 10 cm dish, mixed gently and incubated at room temperature for 10-20 min. The cells from one well in a 6-well plate were trypsinised and 50% of the cells diluted in 8 mL of

growth medium were transferred to the dish with transfection reagent for another 3 days.

6.3.9. Measurements of extracellular acidification rate (ECAR) and oxygen consumption rate (OCR)

Extracellular acidification rate (ECAR) and oxygen consumption rate (OCR) were measured using Seahorse XF96 Analyzer (Agilent) according to the manufacturer's instructions. One day before the assay, the cells were seeded on the Seahorse XF96 cell culture microplates at the density of 2 x 10^4 cells per well. Before the assay, the cells were washed twice with the assay medium (Seahorse XF Base Medium without phenol red supplemented with 10 mM glucose and 2 mM L-glutamine) and incubated at 37°C without CO_2 supply for 1 h. The assay was performed according to the following protocol:

Initialisation		Calibration Equilibration	 12 min
Baseline	3 cycles:	Mix Wait Measure	3 min 3 min
Oligomycin injection – 20 μL, 10 μM			
	3 cycles:	Mix Wait Measure	3 min 3 min
FCCP injection – 20 μL, 6 μM			
	3 cycles:	Mix Wait Measure	1 min 30 s 3 min
Rotenone + antimycin A injection – 20 μL, 4 μM each			
	3 cycles:	Mix Wait Measure	3 min 3 min
2-DG injection – 20 μL, 1 M			

	5 cycles:	Mix	3 min
		Wait	
		Measure	3 min

7. Abbreviations

1C	one carbon metabolism
2-HG	2-hydroxyglutarate
2-OGDO	2-oxoglutarate-dependent dioxygenase
5-fC	5-formylcytosine
5-hmC	5-hydroxymethylcytosine
5-mC	5-methylcytosine
5-mTHF	5-methylentetrahydrofolate
α-KG	α-ketoglutarate
ac	acetyl
ACL(Y)	ATP-citrate lyase
ACSS2	acyl-coenzyme A synthetase short-chain family member 2
ADP	adenosine diphosphate
AHCY	adenosylhomocysteinase
AML	acute myeloid leukaemia
ARRDC4	arrestin domain-containing protein 4
ATP	adenosine triphosphate
AU	arbitrary units
B2M	ß-2-microglobulin
BCAA	branched-chain amino acid
BER	base excision repair
BHMT1/2	betaine-homocysteine methyltransferase 1 / 2
bp	base pairs
°C	degree Celsius
CBS	cystathionine-beta synthase
ChIP	chromatin immunoprecipitation
ChIP-seq	chromatin immunoprecipitation sequencing
ChoRE	carbohydrate response element
CoA	coenzyme A
Cox-2	cyclooxygenase 2
CPM	counts per million
CV	cell pellet volume
Cys	cysteine
DBD	DNA-binding domain
dCas9	catalytically deactivated Cas9
DEM	diethyl maleate
DHRS2	dehydrogenase / reductase SDR family member 2
dm6	*Drosophila melanogaster* genome version 6
DMG	dimethylglycine
DNA	deoxyribonucleic acid
DNMT	DNA methyltransferase
DSS	disuccinimidyl suberate

DTU	differential transcript usage
ECAR	extracellular acidification rate
EGR1	early growth response 1
ENO	enolase
EZH1/2	enhancer of zeste 1 / 2
FBP	fructose-1,6-bisphosphate
FDR	false discovery rate
FH	fumarate hydratase
FLAD1	flavin adenine dinucleotide synthetase 1
G6P	glucose-6-phosphate
GAPDH	glyceraldehyde 3-phosphate dehydrogenase
GFP	green fluorescent protein
GLP	G9a-like protein
GO	gene ontology
gRNA	guide RNA
GSH	reduced glutathione
h	hour
H	histidine
H1, H2A, H2B, H3, H4	histone H1, H2a, H2B, H3, H4
HAT	histone acetyltransferase
HBP	hexosamine biosynthesis pathway
hCys	homocysteine
HDAC	histone deacetylase
HEK293(T)	human embryonic kidney 293 (containing the SV40 T-antigen)
hg38	human genome version 38
hGenDes	human gene desert
hLINE	human long interspersed nuclear element
HP1	heterochromatin protein 1
IDH1/2	isocitrate dehydrogenase 1 / 2
IGBMC	Institut de Génétique et de Biologie Moléculaire et Cellulaire
iMEF	immortalised mouse embryonic fibroblasts
IP	immunoprecipitation
JmjC	jumonji C
K	lysine
KAT	lysine acetyltransferase
kb	kilobase
kd	knockdown
kDa	kilodalton
K_m	Michaelis constant
LC-MS	liquid chromatography – mass spectrometry
LiCl	lithium chloride
lncRNA	long noncoding RNA
LSD1/2	lysine-specific demethylase 1 / 2
LTR	long terminal repeats

m	metre
MAT	methionine adenosyltransferase
MBP	maltose-binding protein
MCF-7	Michigan cancer foundation 7
me	methyl
mESC	mouse embryonic stem cell
min	minute
MLX	Max-like protein X
MLXIP	MLX interacting protein
MLXIPL, MLXPL	MLX interacting protein like
MS	mass spectrometry
MTR	methionine synthase
MTRR	methionine synthase reductase
NAD^+ / NADH	nicotinamide adenine dinucleotide oxidised / reduced
NADSYN1	NAD synthetase 1
NAM	nicotinamide
NAMPT	NAM phosphoribosyltransferase
NE	nuclear extract
NMN	nicotinamide mononucleotide
NMNAT1/2	NMN adenylyltransferase 1 / 2
NTF3	neurotrophin 3
OCR	oxygen consumption rate
OD	optical density
OGDH	oxoglutarate dehydrogenase
ORF	open reading frame
OX	oxidative phase
PA	propionic acidemia
PARP	poly-ADP-ribose polymerase
PCC	propionyl-coenzyme A carboxylase
PCCA	propionyl-coenzyme A carboxylase subunit α
PCCB	propionyl-coenzyme A carboxylase subunit β
PCR	polymerase chain reaction
PDC	pyruvate dehydrogenase complex
PDH	pyruvate dehydrogenase
PDHA1	pyruvate dehydrogenase subunit E1a
PEP	phosphoenolpyruvate
PIC	protease inhibitor cocktail
PKLR	pyruvate kinase isozymes L / R
PKM	pyruvate kinase
PKM1/2	pyruvate kinase isozymes M1 / M2
PPP	pentose phosphate pathway
PRC2	polycomb repressive complex 2
PTM	post-translational modification
Pyk1	pyruvate kinase 1

R	arginine
RB	reductive-building phase
RC	reductive-charging phase
RFK	riboflavin kinase
RNA	ribonucleic acid
RNA-seq	RNA sequencing
rpm	revolutions per minute
RRE	*rev*-response element
RT-qPCR	quantitative reverse transcription PCR
s	second
SAH	S-adenosylhomocysteine
SAM	S-adenosylmethionine
SD	standard deviation
SDHA	succinate dehydrogenase complex flavoprotein subunit A
SDHB	succinate dehydrogenase complex flavoprotein subunit B
SDR	short chain dehydrogenase / reductase
SESAME	serine-responsive SAM-containing metabolic enzyme complex
SETDB1	SET domain bifurcated histone lysine methyltransferase 1
shRNA	short hairpin RNA
SIRT	sirtuin
SUV39H1/H2	suppressor of variegation 3-9 homolog 1 / 2
TAF	TBP-associated factor
TATA	TATA box
TBP	TATA-binding protein
TCA	tricarboxylic acid
Tdh	threonine dehydrogenase
TET	ten-eleven translocation
THF	tetrahydrofolate
Thr	threonine
tk	thymidine kinase
TXN(1)	thioredoxin (1)
TXNIP	thioredoxin-interacting protein
UAS	upstream activation sequence
VEGFA	vascular endothelial growth factor A
VP16/48/64	herpes simplex virus protein vmw65 one / three / four copies
VSV-G	G protein of vesicular stomatitis virus
WB	western blot
WT	wild type
x g	times gravity
YMC	yeast metabolic cycle

8. Acknowledgements

It would not be possible to carry out this work without help and support of many people. I wish to express my sincere gratitude to:

- my supervisor, Robert Schneider, for giving me the chance to work in his lab, for the scientific guidance through my whole PhD on one hand and freedom and trust in the parts that went beyond the initial plan of the project on the other, for sharing his scientific expertise and overall knowledge and creating unforgettable atmosphere in the lab,

- my thesis committee members, for invaluable comments, suggestions and feedback during my TAC meetings. I would like to thank especially Hei Sook Sul for sharing her metabolic expertise and J. Andrew Pospisilik for the always motivating and constructive 'look from the outside' that helped me to set the future scientific directions,

- my collaborators: Oscar Yanes and Joan Miró Blanch for metabolomic analysis and Mirko Wagner for analysis of DNA modifications,

- all the members of the Schneider Lab for their help, advice, discussions and constructive criticism. Special thanks to:
    - Adam Kebede for being my first line of help and a very patient teacher at the beginning of my PhD,
    - Andrey Tvardovskiy for his help with histone extraction and MS analysis,
    - Simona Nasiscionyte, my dearest friend, for her support, care and all the wine that we drank together,
    - Saulius Lukauskas, for all the bioinformatic analysis, help with statistics, looking from outside of the box and countless discussions; for his patience, believing in me and providing encouragement and incredible moral support.

- Finally, my very special thanks go to my parents and brother for their constant support and always reminding me what is the most important.

9. Bibliography

[1] C. H. Waddington, “The epigenotype,” *Endeavour*, pp. 18–20, 1942.

[2] C. Dupont, D. R. Armant, and C. A. Brenner, “Epigenetics: Definition, mechanisms and clinical perspective,” *Semin. Reprod. Med.*, vol. 27, no. 5, pp. 351–357, 2009.

[3] C. T. Wu and J. R. Morris, “Genes, genetics, and epigenetics: A correspondence,” *Science*, vol. 293, no. 5532, pp. 1103–1105, 2001.

[4] W. Flemming, *Zellsubstanz, Kern und Zelltheilung*. Leipzig: F.C.W. Vogel, 1882.

[5] D. E. Olins and A. L. Olins, “Chromatin history: our view from the bridge,” *Nat. Rev. Mol. Cell Biol.*, vol. 4, no. 10, pp. 809–814, 2003.

[6] F. Miescher, “Ueber die chemische Zusammensetzung der Eiterzellen,” *Med. Untersuchungen*, no. 4, pp. 441–460, 1871.

[7] A. Kossel, “Ueber die chemische Beschaffenheit des Zellkerns,” *Münchener Med. Wochenschrift*, no. 2, pp. 65–69, 1911.

[8] O. T. Avery, C. M. Macleod, and M. Mc Carty, “Studies on the chemical nature of the substance inducing transformation of pneumococcal types: Induction or transformatioby A Desoxyribonucleic acid fraction isolated from pneumococcus type III,” *J. Exp. Med.*, vol. 179, no. 2, pp. 137–159, 1944.

[9] V. G. Allfrey, R. Faulkner, and A. E. Mirsky, “Acetylation and methylation of histones and their possible role in the regulation of RNA synthesis.,” *Proc. Natl. Acad. Sci. U. S. A.*, vol. 51, no. 1938, pp. 786–794, 1964.

[10] A. L. Olins and D. E. Olins, “Spheroid chromatin units (v bodies),” *Science*, vol. 183, no. 4122, pp. 330–332, 1974.

[11] T. J. Richmond, J. T. Finch, B. Rushton, D. Rhodes, and A. Klug, “Structure of the nucleosome core particle at 7Å resolution,” *Nature*, vol. 311, no. 5986, pp. 532–537, 1984.

[12] M. Wakamori *et al.*, “Intra- and inter-nucleosomal interactions of the histone H4 tail revealed with a human nucleosome core particle with genetically-incorporated H4 tetra-acetylation,” *Sci. Rep.*, vol. 5, pp. 1–16, 2015.

[13] A. P. Wolffe, “Histone Genes,” in *Encyclopedia of Genetics*, 2001, pp. 948–952.

[14] K. Luger, A. W. Mäder, R. K. Richmond, D. F. Sargent, and T. J. Richmond, “Crystal structure of the nucleosome core particle at 2.8 Å resolution,” *Nature*, vol. 389, no. 6648, pp. 251–260, 1997.

[15] C. A. Davey, D. F. Sargent, K. Luger, A. W. Maeder, and T. J. Richmond, “Solvent mediated interactions in the structure of the nucleosome core particle at 1.9 Å resolution,” *J. Mol. Biol.*, vol. 319, no. 5, pp. 1097–1113, 2002.

[16] C. L. van Emmerik and H. van Ingen, “Unspinning chromatin: Revealing the dynamic nucleosome landscape by NMR,” *Prog. Nucl. Magn. Reson. Spectrosc.*, vol. 110, pp. 1–19, 2019.

[17] G. Felsenfeld and M. Groudine, “Controlling the double helix,” *Nature*, vol. 421, no. 6926, pp. 448–453, 2003.

[18] D. J. Tremethick, “Higher-order structures of chromatin: the elusive 30 nm fiber,” *Cell*, vol. 128, no. 4, pp. 651–654, 2007.

[19] E. Heitz, “Das Heterochromatin der Moose.,” *Jahrb. Wiss. Bot.*, no. 69, pp. 762–818, 1928.

[20] T. Straub, “Heterochromatin dynamics,” *PLoS Biol.*, vol. 1, no. 1, pp. 23–24, 2003.

[21] P. A. Grant, A. Eberharter, S. John, R. G. Cook, B. M. Turner, and J. L. Workman, “Expanded lysine acetylation specificity of Gcn5 in native complexes,” *J. Biol. Chem.*, vol. 274, no. 9, pp. 5895–5900, 1999.

[22] R. L. Schiltz, C. A. Mizzen, A. Vassilev, R. G. Cook, C. D. Allis, and Y. Nakatani, “Overlapping but distinct patterns of histone acetylation by the human coactivators p300 and PCAF within nucleosomal substrates,” *J. Biol. Chem.*, vol. 274, no. 3, pp. 1189–1192, 1999.

[23] E. P. Rogakou, D. R. Pilch, A. H. Orr, V. S. Ivanova, and W. M. Bonner, “DNA double-stranded breaks induce histone H2AX phosphorylation on serine 139,” *J. Biol. Chem.*, vol. 273, no. 10, pp. 5858–5868, 1998.

[24] H. Goto, Y. Yasui, E. A. Nigg, and M. Inagaki, “Aurora-B phosphorylates Histone H3 at serine 28

with regard to the mitotic chromosome condensation," *Genes to Cells*, vol. 7, no. 1, pp. 11–17, 2002.

[25] T. Kouzarides, "Histone methylation in transcriptional control," *Curr. Opin. Genet. Dev.*, vol. 12, no. 2, pp. 198–209, 2002.

[26] M. D. Shahbazian and M. Grunstein, "Functions of site-specific histone acetylation and deacetylation," *Annu. Rev. Biochem.*, vol. 76, no. 1, pp. 75–100, 2007.

[27] D. Rossetto, N. Avvakumov, and J. Côté, "Histone phosphorylation: A chromatin modification involved in diverse nuclear events," *Epigenetics*, vol. 7, no. 10, pp. 1098–1108, 2012.

[28] E. L. Greer and Y. Shi, "Histone methylation: a dynamic mark in health, disease and inheritance," *Nat. Rev. Genet.*, vol. 13, no. 5, pp. 343–357, 2012.

[29] V. M. Weake and J. L. Workman, "Histone ubiquitination: triggering gene activity," *Mol. Cell*, vol. 29, no. 6, pp. 653–663, 2008.

[30] Y. Chen *et al.*, "Lysine propionylation and butyrylation are novel post-translational modifications in histones," *Mol. Cell. Proteomics*, vol. 6, no. 5, pp. 812–819, 2007.

[31] L. Dai *et al.*, "Lysine 2-hydroxyisobutyrylation is a widely distributed active histone mark," *Nat. Chem. Biol.*, vol. 10, no. 5, pp. 365–370, 2014.

[32] S. Rousseaux and S. Khochbin, "Histone acylation beyond acetylation: terra incognita in chromatin biology," *Cell J.*, vol. 17, no. 1, pp. 1–6, 2015.

[33] K. Zhang, Y. Chen, Z. Zhang, and Y. Zhao, "Identification and verification of lysine propionylation and butyrylation in yeast core histones using PTMap software.," *J. Proteome Res.*, vol. 8, no. 2, pp. 900–906, 2009.

[34] R. Martinez-Zamudio and H. C. Ha, "Histone ADP-ribosylation facilitates gene transcription by directly remodeling nucleosomes," *Mol. Cell. Biol.*, vol. 32, no. 13, pp. 2490–2502, 2012.

[35] D. Zhang *et al.*, "Metabolic regulation of gene expression by histone lactylation," *Nature*, vol. 574, pp. 575–580, 2019.

[36] L. K. Durrin, R. K. Mann, P. S. Kayne, and M. Grunstein, "Yeast histone H4 N-terminal sequence is required for promoter activation in vivo," *Cell*, vol. 65, no. 6, pp. 1023–1031, 1991.

[37] M. H. Kuo, J. Zhou, P. Jambeck, M. E. A. Churchill, and C. D. Allis, "Histone acetyltransferase activity of yeast Gcn5p is required for the activation of target genes in vivo," *Genes Dev.*, vol. 12, no. 5, pp. 627–639, 1998.

[38] M. Shogren-Knaak, H. Ishii, J.-M. Sun, M. J. Pazin, J. R. Davie, and C. L. Peterson, "Histone H4-K16 acetylation controls chromatin structure and protein interactions," *Science*, vol. 311, no. 5762, pp. 844–848, 2006.

[39] V. Di Cerbo *et al.*, "Acetylation of histone H3 at lysine 64 regulates nucleosome dynamics and facilitates transcription," *Elife*, vol. 3, pp. 1–23, 2014.

[40] P. Tropberger *et al.*, "Regulation of transcription through acetylation of H3K122 on the lateral surface of the histone octamer," *Cell*, vol. 152, no. 4, pp. 859–872, 2013.

[41] K. L. Yap and M. M. Zhou, "Keeping it in the family: diverse histone recognition by conserved structural folds," *Crit. Rev. Biochem. Mol. Biol.*, vol. 45, no. 6, pp. 488–505, 2010.

[42] P. Byvoet, G. R. Shepherd, J. M. Hardin, and B. J. Noland, "The distribution and turnover of labeled methyl groups in histone fractions of cultured mammalian cells," *Arch. Biochem. Biophys.*, vol. 148, no. 2, pp. 558–567, 1972.

[43] K. Murray, "The Occurrence of ϵ-N-Methyl Lysine in Histones," *Biochemistry*, vol. 3, no. 1, pp. 10–15, 1964.

[44] N. D. Heintzman *et al.*, "Histone modifications at human enhancers reflect global cell-type-specific gene expression," *Nature*, vol. 459, no. 7243, pp. 108–112, 2009.

[45] H. Santos-Rosa *et al.*, "Active genes are tri-methylated at K4 of histone H3," *Nature*, vol. 419, no. 6905, pp. 407–411, 2002.

[46] M. P. Creyghton *et al.*, "Histone H3K27ac separates active from poised enhancers and predicts developmental state," *Proc. Natl. Acad. Sci. U. S. A.*, vol. 107, no. 50, pp. 21931–21936, 2010.

[47] B. E. Bernstein *et al.*, "A bivalent chromatin structure marks key developmental genes in embryonic stem cells," *Cell*, vol. 125, no. 2, pp. 315–326, 2006.

[48] G. Pan *et al.*, "Whole-genome analysis of histone H3 lysine 4 and lysine 27 methylation in human embryonic stem cells," *Cell Stem Cell*, vol. 1, no. 3, pp. 299–312, 2007.

[49] A. H. F. M. Peters *et al.*, “Partitioning and plasticity of repressive histone methylation states in mammalian chromatin,” *Mol. Cell*, vol. 12, no. 6, pp. 1577–1589, 2003.

[50] K. J. Ferrari *et al.*, “Polycomb-dependent H3K27me1 and H3K27me2 regulate active transcription and enhancer fidelity,” *Mol. Cell*, vol. 53, no. 1, pp. 49–62, 2014.

[51] A. Mattout and E. Meshorer, “Chromatin plasticity and genome organization in pluripotent embryonic stem cells,” *Curr. Opin. Cell Biol.*, vol. 22, no. 3, pp. 334–341, 2010.

[52] B. Schuettengruber and G. Cavalli, “Recruitment of Polycomb group complexes and their role in the dynamic regulation of cell fate choice,” *Development*, vol. 136, no. 21, pp. 3531–3542, 2009.

[53] J. A. Simon and R. E. Kingston, “Mechanisms of Polycomb gene silencing: Knowns and unknowns,” *Nat. Rev. Mol. Cell Biol.*, vol. 10, no. 10, pp. 697–708, 2009.

[54] R. Margueron *et al.*, “Role of the polycomb protein Eed in the propagation of repressive histone marks,” *Nature*, vol. 461, no. 7265, pp. 762–767, 2009.

[55] R. Margueron and D. Reinberg, “The Polycomb complex PRC2 and its mark in life,” *Nature*, vol. 469, no. 7330, pp. 343–349, 2011.

[56] C. Xu *et al.*, “Binding of different histone marks differentially regulates the activity and specificity of polycomb repressive complex 2 (PRC2),” *Proc. Natl. Acad. Sci. U. S. A.*, vol. 107, no. 45, pp. 19266–19271, 2010.

[57] N. Saksouk, E. Simboeck, and J. Déjardin, “Constitutive heterochromatin formation and transcription in mammals,” *Epigenetics and Chromatin*, vol. 8, no. 1, pp. 1–17, 2015.

[58] M. Gauchier *et al.*, “SETDB1-dependent heterochromatin stimulates alternative lengthening of telomeres,” *Sci. Adv.*, vol. 5, no. 5, pp. 1–14, 2019.

[59] J. H. A. Martens *et al.*, “The profile of repeat-associated histone lysine methylation states in the mouse epigenome,” *EMBO J.*, vol. 24, no. 4, pp. 800–812, 2005.

[60] J. Nakayama, J. C. Rice, B. D. Strahl, C. D. Allis, and S. I. S. Grewal, “Role of histone H3 lysine 9 methylation in epigenetic control of heterochromatin assembly,” *Science*, vol. 292, no. 5514, pp. 110–113, 2001.

[61] S. Rea *et al.*, “Regulation of chromatin structure by site-specific histone H3 methyltransferases,” *Nature*, vol. 406, no. 6796, pp. 593–599, 2000.

[62] M. Tachibana, K. Sugimoto, T. Fukushima, and Y. Shinkai, “SET Domain-containing protein, G9a, is a novel lysine-preferring mammalian histone methyltransferase with hyperactivity and specific selectivity to lysines 9 and 27 of histone H3,” *J. Biol. Chem.*, vol. 276, no. 27, pp. 25309–25317, 2001.

[63] M. Tachibana *et al.*, “Histone methyltransferases G9a and GLP form heteromeric complexes and are both crucial for methylation of euchromatin at H3-K9,” *Genes Dev.*, vol. 19, no. 7, pp. 815–826, 2005.

[64] M. Tachibana *et al.*, “G9a histone methyltransferase plays a dominant role in euchromatic histone H3 lysine 9 methylation and is essential for early embryogenesis,” *Genes Dev.*, vol. 16, no. 14, pp. 1779–1791, 2002.

[65] A. J. Bannister *et al.*, “Selective recognition of methylated lysine 9 on histone H3 by the HP1 chromo domain,” *Nature*, vol. 410, no. 6824, pp. 120–124, 2001.

[66] J. Zhu *et al.*, “Genome-wide chromatin state transitions associated with developmental and environmental cues,” *Cell*, vol. 152, no. 3, pp. 642–654, 2013.

[67] M. Gold, J. Hurwitz, and M. Anders, “The enzymatic methylation of RNA and DNA,” *Biochem. Biophys. Res. Commun.*, vol. 11, no. 2, pp. 107–114, 1963.

[68] A. P. Feinberg and B. Vogelstein, “Hypomethylation distinguishes genes of some human cancers from their normal counterparts,” *Nature*, vol. 301, no. 5895, pp. 89–92, 1983.

[69] W. Zhang and J. Xu, “DNA methyltransferases and their roles in tumorigenesis,” *Biomark. Res.*, vol. 5, no. 1, pp. 1–8, 2017.

[70] S. Feng *et al.*, “Conservation and divergence of methylation patterning in plants and animals,” *Proc. Natl. Acad. Sci. U. S. A.*, vol. 107, no. 19, pp. 8689–8694, 2010.

[71] M. Kaneda *et al.*, “Essential role for de novo DNA methyltransferase Dnmt3a in paternal and maternal imprinting,” *Nature*, vol. 429, no. 6994, pp. 900–903, 2004.

[72] M. Okano, S. Xie, and E. Li, “Cloning and characterization of a family of novel mammalian DNA (cytosine-5) methyltransferases,” *Nat. Am. Inc.*, vol. 19, no. 3, pp. 219–220, 1998.

[73] A. Hermann, R. Goyal, and A. Jeltsch, “The Dnmt1 DNA-(cytosine-C5)-methyltransferase methylates DNA processively with high preference for hemimethylated target sites,” *J. Biol. Chem.*, vol. 279, no. 46, pp. 48350–48359, 2004.

[74] M. A. Hahn *et al.*, “Dynamics of 5-hydroxymethylcytosine and chromatin marks in mammalian neurogenesis,” *Cell Rep.*, vol. 3, no. 2, pp. 291–300, 2013.

[75] Y. Zhang and C. Zhou, “Formation and biological consequences of 5-Formylcytosine in genomic DNA,” *DNA Repair (Amst).*, vol. 81, pp. 1–9, 2019.

[76] A. Nieborak and R. Schneider, “Metabolic intermediates – Cellular messengers talking to chromatin modifiers,” *Mol. Metab.*, vol. 14, pp. 39–52, 2018.

[77] *Manual of Clinical Enzyme Measurements*. Freehold, N.J. : Worthington Diagnostics, 1972.

[78] B. N. Albaugh, K. M. Arnold, and J. M. Denu, “KAT(ching) metabolism by the tail: insight into the links between lysine acetyltransferases and metabolism,” *ChemBioChem*, vol. 12, no. 2, pp. 290–298, 2011.

[79] F. Pietrocola, L. Galluzzi, J. M. Bravo-San Pedro, F. Madeo, and G. Kroemer, “Acetyl coenzyme A: a central metabolite and second messenger,” *Cell Metab.*, vol. 21, no. 6, pp. 805–821, 2015.

[80] R. W. Brownsey, A. N. Boone, J. E. Elliott, J. E. Kulpa, Lee, and W. M., “Regulation of acetyl-CoA carboxylase,” *Biochem. Soc. Trans.*, vol. 34, no. 2, pp. 223–227, 2006.

[81] J. D. Browning, J. Baxter, S. Satapati, and S. C. Burgess, “The effect of short-term fasting on liver and skeletal muscle lipid, glucose, and energy metabolism in healthy women and men,” *J. Lipid Res.*, vol. 53, no. 3, pp. 577–586, 2012.

[82] R. A. Harris, M. Joshi, N. H. Jeoung, and M. Obayashi, “Overview of the molecular and biochemical basis of branched-chain amino acid catabolism,” *J. Nutr.*, vol. 135, no. 6, pp. 1527S-1530S, 2005.

[83] D. G. Cotter, R. C. Schugar, and P. A. Crawford, “Ketone body metabolism and cardiovascular disease,” *Am. J. Physiol. - Heart Circ. Physiol.*, vol. 304, no. 8, pp. 1060–1076, 2013.

[84] F. Palmieri, “The mitochondrial transporter family (SLC25): Physiological and pathological implications,” *Pflugers Arch. Eur. J. Physiol.*, vol. 447, no. 5, pp. 689–709, 2004.

[85] P. Mews, G. Donahue, A. M. Drake, V. Luczak, T. Abel, and S. L. Berger, “Acetyl-CoA synthetase regulates histone acetylation and hippocampal memory,” *Nature*, vol. 546, no. 7658, pp. 381–386, 2017.

[86] G. Sutendra *et al.*, “A nuclear pyruvate dehydrogenase complex is important for the generation of acetyl-CoA and histone acetylation,” *Cell*, vol. 158, no. 1, pp. 84–97, 2014.

[87] K. E. Wellen, G. Hatzivassiliou, U. M. Sachdeva, T. V. Bui, J. R. Cross, and C. B. Thompson, “ATP-citrate lyase links cellular metabolism to histone acetylation,” *Science*, vol. 324, no. 5930, pp. 1076–1080, 2009.

[88] B. P. Tu *et al.*, “Cyclic changes in metabolic state during the life of a yeast cell.,” *Proc. Natl. Acad. Sci. U. S. A.*, vol. 104, no. 43, pp. 16886–16891, 2007.

[89] J. V. Lee *et al.*, “Akt-dependent metabolic reprogramming regulates tumor cell Histone acetylation,” *Cell Metab.*, vol. 20, no. 2, pp. 306–319, 2014.

[90] J. Wang, P. Alexander, L. Wu, R. Hammer, O. Cleaver, and S. L. McKnight, “Dependence of mouse embryonic stem cells on threonine catabolism,” *Science*, vol. 325, no. 5939, pp. 435–439, 2009.

[91] E. Seto and M. Yoshida, “Erasers of histone acetylation: the histone deacetylase enzymes,” in *Perspectives in Biology*, 2014.

[92] S. Imai, C. M. Armstrong, M. Kaeberlein, and L. Guarente, “Transcriptional silencing and longevity protein Sir2 is an NAD-dependent histone deacetylase,” *Nature*, vol. 403, no. 6771, pp. 795–800, 2000.

[93] P. Adamietz, “Poly(ADP-ribose) synthase is the major endogenous nonhistone acceptor for poly(ADP-ribose) in alkylated rat hepatoma cells,” *Eur. J. Biochem.*, vol. 169, no. 2, pp. 365–372, 1987.

[94] B. W. Durkacz, O. Omidiji, D. A. Gray, and S. Shall, “(ADP-ribose)n participates in DNA excision repair,” *Nature*, vol. 283, no. 5747, pp. 593–596, 1980.

[95] J. L. Sims, S. J. Berger, and N. A. Berger, “Effects of nicotinamide on NAD and poly(ADP-ribose) metabolism in DNA-damaged human lymphocytes,” *J. Supramol. Cell. Biochem.*, vol. 16, no. 3,

pp. 281–288, 1981.
[96] I. Gibbs-Seymour, P. Fontana, J. G. M. Rack, and I. Ahel, “HPF1/C4orf27 is a PARP-1-interacting protein that regulates PARP-1 ADP-ribosylation activity,” *Mol. Cell*, vol. 62, no. 3, pp. 432–442, 2016.
[97] J. C. Ame *et al.*, “PARP-2, A novel mammalian DNA damage-dependent poly(ADP-ribose)polymerase,” *J. Biol. Chem.*, vol. 274, no. 25, pp. 17860–17868, 1999.
[98] R. H. Houtkooper, C. Cantó, R. J. Wanders, and J. Auwerx, “The secret life of NAD+: an old metabolite controlling new metabolic signaling pathways,” *Endocr. Rev.*, vol. 31, no. 2, pp. 194–223, 2010.
[99] M. T. Borra, M. R. Langer, J. T. Slama, and J. M. Denu, “Substrate specificity and kinetic mechanism of the Sir2 family of NAD+-dependent histone/protein deacetylases,” *Biochemistry*, vol. 43, no. 30, pp. 9877–9887, 2004.
[100] E. Van Der Veer *et al.*, “Extension of human cell lifespan by nicotinamide phosphoribosyltransferase,” *J. Biol. Chem.*, vol. 282, no. 15, pp. 10841–10845, 2007.
[101] T. Zhang *et al.*, “Enzymes in the NAD+ salvage pathway regulate SIRT1 activity at target gene promoters,” *J. Biol. Chem.*, vol. 284, no. 30, pp. 20408–20417, 2009.
[102] S. Srivastava, “Emerging therapeutic roles for NAD+ metabolism in mitochondrial and age-related disorders,” *Clin. Transl. Med.*, vol. 5, no. 1, 2016.
[103] S. J. Mentch and J. W. Locasale, “One-carbon metabolism and epigenetics: understanding the specificity,” *Ann. N. Y. Acad. Sci.*, vol. 1363, no. 1, pp. 91–98, 2016.
[104] C. E. Clare, A. H. Brassington, W. Y. Kwong, and K. D. Sinclair, “One-carbon metabolism: linking nutritional biochemistry to epigenetic programming of long-term development,” *Annu. Rev. Anim. Biosci.*, vol. 7, no. 1, pp. 263–287, 2018.
[105] N. Shyh-Chang *et al.*, “Influence of threonine metabolism on S-adenosylmethionine and histone methylation,” *Science*, vol. 339, no. 6116, pp. 222–226, 2013.
[106] S. J. Mentch *et al.*, “Histone methylation dynamics and gene regulation occur through the sensing of one-carbon metabolism,” *Cell Metab.*, vol. 22, no. 5, pp. 861–873, 2015.
[107] S. A. Christopher, S. Melnyk, S. J. James, and W. D. Kruger, “S-adenosylhomocysteine, but not homocysteine, is toxic to yeast lacking cystathionine β-synthase,” *Mol. Genet. Metab.*, vol. 75, no. 4, pp. 335–343, 2002.
[108] F. Li *et al.*, “Human betaine-homocysteine methyltransferase (BHMT) and BHMT2: common gene sequence variation and functional characterization,” *Mol. Genet. Metab.*, vol. 94, no. 3, pp. 326–335, 2008.
[109] Y.-I. Kim, “Nutritional epigenetics: impact of folate deficiency on DNA methylation and colon cancer susceptibility,” *J. Nutr.*, vol. 135, no. 11, pp. 2703–2709, 2005.
[110] B. A. Garcia, Z. Luka, L. V. Loukachevitch, N. V. Bhanu, and C. Wagner, “Folate deficiency affects histone methylation,” *Med. Hypotheses*, vol. 88, pp. 63–67, 2016.
[111] Y. Kera, Y. Katoh, M. Ohta, M. Matsumoto, T. Takano-Yamamoto, and K. Igarashi, “Methionine adenosyltransferase II-dependent histone H3K9 methylation at the COX-2 gene locus,” *J. Biol. Chem.*, vol. 288, no. 19, pp. 13592–13601, 2013.
[112] W. Ding, L. J. Smulan, N. S. Hou, S. Taubert, J. L. Watts, and A. K. Walker, “S-adenosylmethionine levels govern innate immunity through distinct methylation-dependent pathways,” *Cell Metab.*, vol. 22, no. 4, pp. 633–645, 2015.
[113] B. D. Towbin *et al.*, “Step-wise methylation of histone H3K9 positions heterochromatin at the nuclear periphery,” *Cell*, vol. 150, no. 5, pp. 934–947, 2012.
[114] S. Li *et al.*, “Serine and SAM responsive complex SESAME regulates histone modification crosstalk by sensing cellular metabolism,” *Mol. Cell*, vol. 60, no. 3, pp. 408–421, 2015.
[115] Y. Shi *et al.*, “Histone demethylation mediated by the nuclear amine oxidase homolog LSD1,” *Cell*, vol. 119, no. 7, pp. 941–953, 2004.
[116] A. Karytinos *et al.*, “A novel mammalian flavin-dependent histone demethylase,” *J. Biol. Chem.*, vol. 284, no. 26, pp. 17775–17782, 2009.
[117] N. Wu, M. Yang, U. Gaur, H. Xu, Y. Yao, and D. Li, “Alpha-ketoglutarate: physiological functions and applications.,” *Biomol. Ther.*, vol. 24, no. 1, pp. 1–8, 2016.
[118] A. Salminen, A. Kauppinen, and K. Kaarniranta, “2-Oxoglutarate-dependent dioxygenases are

sensors of energy metabolism, oxygen availability, and iron homeostasis: potential role in the regulation of aging process," *Cell. Mol. Life Sci.*, vol. 72, no. 20, pp. 3897–3914, 2015.

[119] B. W. Carey, L. W. S. Finley, J. R. Cross, C. D. Allis, and C. B. Thompson, "Intracellular α-ketoglutarate maintains the pluripotency of embryonic stem cells," *Nature*, vol. 518, no. 7539, pp. 413–416, 2015.

[120] M. Xiao *et al.*, "Inhibition of α-KG-dependent histone and DNA demethylases by fumarate and succinate that are accumulated in mutations of FH and SDH tumor suppressors," *Genes Dev.*, vol. 26, no. 12, pp. 1326–1338, 2012.

[121] P. J. Pollard *et al.*, "Accumulation of Krebs cycle intermediates and over-expression of HIF1α in tumours which result from germline FH and SDH mutations," *Hum. Mol. Genet.*, vol. 14, no. 15, pp. 2231–2239, 2005.

[122] P. S. Ward *et al.*, "The common feature of leukemia-associated IDH1 and IDH2 mutations Is a neomorphic enzyme activity converting α-ketoglutarate to 2-hydroxyglutarate," *Cancer Cell*, vol. 17, no. 3, pp. 225–234, 2010.

[123] M. E. Figueroa *et al.*, "Leukemic IDH1 and IDH2 mutations result in a hypermethylation phenotype, disrupt TET2 function, and impair hematopoietic differentiation," *Cancer Cell*, vol. 18, no. 6, pp. 553–567, 2010.

[124] J. W. Kim and C. V. Dang, "Multifaceted roles of glycolytic enzymes," *Trends Biochem. Sci.*, vol. 30, no. 3, pp. 142–150, 2005.

[125] N. A. Demarse *et al.*, "Direct binding of glyceraldehyde 3-phosphate dehydrogenase to telomeric DNA protects telomeres against chemoteratpy-induced rapid degradation," *J. Mol. Biol.*, vol. 394, no. 4, pp. 789–803, 2009.

[126] W. Wang, L. Wang, A. Endoh, G. Hummelke, C. L. Hawks, and P. J. Hornsby, "Identification of α-enolase as a nuclear DNA-binding protein in the zona fasciculata but not the zona reticularis of the human adrenal cortex," *J. Endocrinol.*, vol. 184, no. 1, pp. 85–94, 2005.

[127] C. M. Haraguchi, T. Mabuchi, and S. Yokota, "Localization of a mitochondrial type of NADP-dependent isocitrate dehydrogenase in kidney and heart of rat: an immunocytochemical and biochemical study," *J. Histochem. Cytochem.*, vol. 51, no. 2, pp. 215–226, 2003.

[128] Y. Jiang *et al.*, "Local generation of fumarate promotes DNA repair through inhibition of histone H3 demethylation," *Nat. Cell Biol.*, vol. 17, no. 9, pp. 1158–1168, 2015.

[129] P. De and R. Chatterjee, "Nucleolar localization of succinic dehydrogenase in human malignant cells with MTT," *Experientia*, vol. 18, no. 12, p. 562, 1962.

[130] P. Madiraju, S. V. Pande, M. Prentki, and S. R. M. Madiraju, "Mitochondrial acetylcarnitine provides acetyl groups for nuclear histone acetylation," *Epigenetics*, vol. 4, no. 6, pp. 399–403, 2009.

[131] T. Wang *et al.*, "O-GlcNAcylation of fumarase maintains tumour growth under glucose deficiency," *Nat. Cell Biol.*, vol. 19, no. 7, pp. 833–843, 2017.

[132] J. P. Guilinger, D. B. Thompson, and D. R. Liu, "Fusion of catalytically inactive Cas9 to FokI nuclease improves the specificity of genome modification," *Nat. Biotechnol.*, vol. 32, no. 6, pp. 577–582, 2014.

[133] A. W. Cheng *et al.*, "Multiplexed activation of endogenous genes by CRISPR-on, an RNA-guided transcriptional activator system," *Cell Res.*, vol. 23, no. 10, pp. 1163–1171, 2013.

[134] E. V. Wasmuth and C. D. Lima, "Efficient targeted DNA methylation with chimeric dCas9–Dnmt3a–Dnmt3L methyltransferase," *Nucleic Acids Res.*, vol. 45, no. 4, pp. 1703–1713, 2016.

[135] M. L. Maeder, S. J. Linder, V. M. Cascio, Y. Fu, Q. H. Ho, and J. K. Joung, "CRISPR RNA-guided activation of endogenous human genes," *Nat. Methods*, vol. 10, no. 10, pp. 977–979, 2013.

[136] D. G. Gibson, L. Young, R. Y. Chuang, J. C. Venter, C. A. Hutchison, and H. O. Smith, "Enzymatic assembly of DNA molecules up to several hundred kilobases," *Nat. Methods*, vol. 6, no. 5, pp. 343–345, 2009.

[137] C. Ingram-Smith, B. I. Woods, and K. S. Smith, "Characterization of the acyl substrate binding pocket of acetyl-CoA synthetase," *Biochemistry*, vol. 45, no. 38, pp. 11482–11490, 2006.

[138] S. S. Szegedi, C. C. Castro, M. Koutmos, and T. A. Garrow, "Betaine-homocysteine S -methyltransferase-2 is an S -methylmethionine-homocysteine methyltransferase," *J. Biol. Chem.*, vol. 283, no. 14, pp. 8939–8945, 2008.

[139] A. Lorenzato, M. Olivero, M. Perro, J. J. Brière, P. Rustin, and M. F. Di Renzo, “A cancer-predisposing ‘hot spot’ mutation of the fumarase gene creates a dominant negative protein,” *Int. J. Cancer*, vol. 122, no. 4, pp. 947–951, 2008.

[140] J. D. Dombrauckas, B. D. Santarsiero, and A. D. Mesecar, “Structural basis for tumor pyruvate kinase M2 allosteric regulation and catalysis,” *Biochemistry*, vol. 44, no. 27, pp. 9417–9429, 2005.

[141] R. B. Kapust and D. S. Waugh, “Escherichia coli maltose-binding protein is effective in promoting solubility,” *Protein Sci.*, vol. 8, no. 8, pp. 1668–1674, 1999.

[142] G. R. Wagner and M. D. Hirschey, “Nonenzymatic protein acylation as a carbon stress regulated by sirtuin deacylases.,” *Mol. Cell*, vol. 54, no. 1, pp. 5–16, 2014.

[143] S. B. Baylin, M. Esteller, M. R. Rountree, K. E. Bachman, K. Schuebel, and J. G. Herman, “Aberrant patterns of DNA methylation, chromatin formation and gene expression in cancer,” *Hum. Mol. Genet.*, vol. 10, no. 7, pp. 687–692, 2001.

[144] G. Leroy *et al.*, “A quantitative atlas of histone modification signatures from human cancer cells,” *Epigenetics and Chromatin*, vol. 6, pp. 1–14, 2013.

[145] C. Alabert *et al.*, “Two distinct models for propagation of histone PTMs across the cell cycle,” *Genes Dev.*, vol. 29, no. 6, pp. 585–590, 2015.

[146] F. Comoglio and R. Paro, “Combinatorial modeling of chromatin features quantitatively predicts DNA replication timing in Drosophila,” *PLoS Comput. Biol.*, vol. 10, no. 1, pp. 1–14, 2014.

[147] Z. Wang *et al.*, “Combinatorial patterns of histone acetylations and methylations in the human genome,” *Nat. Genet.*, vol. 40, no. 7, pp. 897–903, 2008.

[148] D. G. Hardie, “AMP-activated protein kinase - an energy sensor that regulates all aspects of cell function,” *Genes Dev.*, vol. 25, no. 18, pp. 1895–1908, 2011.

[149] S. Trefely *et al.*, “Subcellular metabolic pathway kinetics are revealed by correcting for artifactual post harvest metabolism,” *Mol. Metab.*, vol. 30, pp. 61–71, 2019.

[150] P. Wongkittichote, N. Ah Mew, and K. A. Chapman, “Propionyl-CoA carboxylase – a review,” *Mol. Genet. Metab.*, vol. 122, no. 4, pp. 145–152, 2017.

[151] X. Zhang, M. Li, Y. Xu, J. Ren, and A. P. Zeng, “Quantitative study of H protein lipoylation of the glycine cleavage system and a strategy to increase its activity by co-expression of LplA,” *J. Biol. Eng.*, vol. 13, pp. 1–9, 2019.

[152] D. A. Orlando *et al.*, “Quantitative ChIP-seq normalization reveals global modulation of the epigenome,” *Cell Rep.*, vol. 9, no. 3, pp. 1163–1170, 2014.

[153] I. M. Boros, “Histone modification in Drosophila,” *Brief. Funct. Genomics*, vol. 11, no. 4, pp. 319–331, 2012.

[154] W. H. Shang *et al.*, “Acetylation of histone H4 lysine 5 and 12 is required for CENP-A deposition into centromeres,” *Nat. Commun.*, vol. 7, pp. 1–13, 2016.

[155] Y. Hayashi-Takanaka *et al.*, “Distribution of histone H4 modifications as revealed by a panel of specific monoclonal antibodies,” *Chromosom. Res.*, vol. 23, no. 4, pp. 753–766, 2015.

[156] Y. Zhou *et al.*, “Metascape provides a biologist-oriented resource for the analysis of systems-level datasets,” *Nat. Commun.*, vol. 10, pp. 1–10, 2019.

[157] P. Patwari and R. T. Lee, “An expanded family of arrestins regulate metabolism,” *Trends Endocrinol. Metab.*, vol. 23, no. 5, pp. 216–222, 2012.

[158] K. Bluemlein, N.-M. Grüning, R. G. Feichtinger, H. Lehrach, B. Kofler, and M. Ralser, “No evidence for a shift in pyruvate kinase PKM1 to PKM2 expression during tumorigenesis,” *Oncotarget*, vol. 2, no. 5, pp. 393–400, 2011.

[159] A. S. Divakaruni, A. Paradyse, D. A. Ferrick, A. N. Murphy, and M. Jastroch, “Analysis and interpretation of microplate-based oxygen consumption and pH data,” in *Methods in Enzymology*, vol. 547, Elsevier Inc., 2014, pp. 309–354.

[160] C. W. Peterson, C. A. Stoltzman, M. P. Sighinolfi, K. S. Han, and D. E. Ayer, “Glucose controls nuclear accumulation, promoter binding, and transcriptional activity of the MondoA-Mlx heterodimer,” *Mol. Cell. Biol.*, vol. 30, no. 12, pp. 2887–2895, 2010.

[161] P. Patwari, L. J. Higgins, W. A. Chutkow, J. Yoshioka, and R. T. Lee, “The interaction of thioredoxin with Txnip: Evidence for formation of a mixed disulfide by disulfide exchange,” *J. Biol. Chem.*, vol. 281, no. 31, pp. 21884–21891, 2006.

[162] M. Monge *et al.*, “Proteomic approach to ETV5 during endometrial carcinoma invasion reveals a link to oxidative stress,” *Carcinogenesis*, vol. 30, no. 8, pp. 1288–1297, 2009.
[163] I. V. Kulakovskiy *et al.*, “HOCOMOCO: Towards a complete collection of transcription factor binding models for human and mouse via large-scale ChIP-Seq analysis,” *Nucleic Acids Res.*, vol. 46, no. D1, pp. D252–D259, 2018.
[164] W. Yang *et al.*, “PKM2 phosphorylates histone H3 and promotes gene transcription and tumorigenesis,” *Cell*, vol. 150, no. 4, pp. 685–696, 2012.
[165] X. Gao, H. Wang, J. J. Yang, X. Liu, and Z. R. Liu, “Pyruvate kinase M2 regulates gene transcription by acting as a protein kinase,” *Mol. Cell*, vol. 45, no. 5, pp. 598–609, 2012.
[166] M. Xia *et al.*, “Novel function and intracellular localization of methionine adenosyltransferase 2β splicing variants,” *J. Biol. Chem.*, vol. 285, no. 26, pp. 20015–20021, 2010.
[167] A. Ben-Shem, N. Garreau de Loubresse, S. Melnikov, L. Jenner, G. Yusupova, and M. Yusupov, “The structure of the eukaryotic ribosome at 3.0 Å resolution,” *Science*, vol. 334, no. 6062, pp. 1524–1529, 2011.
[168] M. Taoka *et al.*, “Landscape of the complete RNA chemical modifications in the human 80S ribosome,” *Nucleic Acids Res.*, vol. 46, no. 18, pp. 9289–9298, 2018.
[169] S. Katada, A. Imhof, and P. Sassone-Corsi, “Connecting threads: epigenetics and metabolism,” *Cell*, vol. 148, no. 1–2, pp. 24–28, 2012.
[170] Y. Katoh *et al.*, “Methionine adenosyltransferase II serves as a transcriptional corepressor of Maf oncoprotein,” *Mol. Cell*, vol. 41, no. 5, pp. 554–566, 2011.
[171] K. Hyun, J. Jeon, K. Park, and J. Kim, “Writing, erasing and reading histone lysine methylations,” *Exp. Mol. Med.*, vol. 49, no. 4, pp. 1–22, 2017.
[172] S. Lanouette, V. Mongeon, D. Figeys, and J. F. Couture, “The functional diversity of protein lysine methylation,” *Mol. Syst. Biol.*, vol. 10, no. 4, pp. 1–26, 2014.
[173] P. Mosca, B. Leheup, and N. Dreumont, “Nutrigenomics and RNA methylation: role of micronutrients,” *Biochimie*, vol. 164, pp. 53–59, 2019.
[174] F. Frottin *et al.*, “The nucleolus functions as a phase-separated protein quality control compartment,” *Science*, vol. 365, no. 6451, pp. 342–347, 2019.
[175] S. Sharma, J. Yang, P. Watzinger, P. Kötter, and K. D. Entian, “Yeast Nop2 and Rcm1 methylate C2870 and C2278 of the 25S rRNA, respectively,” *Nucleic Acids Res.*, vol. 41, no. 19, pp. 9062–9076, 2013.
[176] G. Bourgeois *et al.*, “Eukaryotic rRNA modification by yeast 5- methylcytosine-methyltransferases and human proliferation-associated antigen p120,” *PLoS One*, vol. 10, no. 7, pp. 1–16, 2015.
[177] J. J. Gruber *et al.*, “HAT1 Coordinates Histone Production and Acetylation via H4 Promoter Binding,” *Mol. Cell*, vol. 75, no. 4, pp. 711–724, 2019.
[178] N. H. T. Nguyen *et al.*, “Propionate increases neuronal histone acetylation, but is metabolized oxidatively by glia. Relevance for propionic acidemia,” *J. Neurochem.*, vol. 101, no. 3, pp. 806–814, 2007.
[179] A. F. Kebede *et al.*, “Histone propionylation is a mark of active chromatin,” *Nat. Struct. Mol. Biol.*, vol. 24, no. 12, pp. 1048–1056, 2017.
[180] C. L. Quinlan *et al.*, “Targeting S-adenosylmethionine biosynthesis with a novel allosteric inhibitor of Mat2A,” *Nat. Chem. Biol.*, vol. 13, no. 7, pp. 785–792, 2017.
[181] C. Ye, B. M. Sutter, Y. Wang, Z. Kuang, and B. P. Tu, “A metabolic function for phospholipid and histone methylation,” *Mol. Cell*, vol. 66, no. 2, pp. 180–193, 2017.
[182] W. J. Israelsen and M. G. Vander Heiden, “Pyruvate kinase: function, regulation and role in cancer,” *Semin. Cell Dev. Biol.*, vol. 43, pp. 43–51, 2015.
[183] A. Groth, W. Rocha, A. Verreault, and G. Almouzni, “Chromatin challenges during DNA replication and repair,” *Cell*, vol. 128, no. 4, pp. 721–733, 2007.
[184] R. Zhao, T. Nakamura, Y. Fu, Z. Lazar, and D. L. Spector, “Gene bookmarking accelerates the kinetics of post-mitotic transcriptional re-activation,” *Nat. Cell Biol.*, vol. 13, no. 11, pp. 1295–1304, 2011.
[185] G. Deblois *et al.*, “Metabolic adaptations underlie epigenetic vulnerabilities in chemoresistant breast cancer.,” *bioRxiv*, 2018.

[186] F. Grimolizzi and L. Arranz, “Multiple faces of succinate beyond metabolism in blood,” *Haematologica*, vol. 103, no. 10, pp. 1586–1592, 2018.
[187] S. Herzig and R. J. Shaw, “AMPK: Guardian of metabolism and mitochondrial homeostasis,” *Nat. Rev. Mol. Cell Biol.*, vol. 19, no. 2, pp. 121–135, 2018.
[188] R. W. Friesen, E. M. Novak, D. Hasman, and S. M. Innis, “Relationship of dimethylglycine, choline, and betaine with oxoproline in plasma of pregnant women and their newborn infants,” *J. Nutr.*, vol. 137, no. 12, pp. 2641–2646, 2007.
[189] C. A. Stoltzman, C. W. Peterson, K. T. Breen, D. M. Muoio, A. N. Billin, and D. E. Ayer, “Glucose sensing by MondoA:Mlx complexes: a role for hexokinases and direct regulation of thioredoxin-interacting protein expression,” *Proc. Natl. Acad. Sci. U. S. A.*, vol. 105, no. 19, pp. 6912–6917, 2008.
[190] O. Warburg, F. Wind, and E. Negelein, “The metabolism of tumours,” *Br. Med. J.*, vol. 8, no. 6, pp. 519–530, 1927.
[191] L. Chen, Y. Shi, S. Liu, Y. Cao, X. Wang, and Y. Tao, “PKM2: The thread linking energy metabolism reprogramming with epigenetics in cancer,” *Int. J. Mol. Sci.*, vol. 15, no. 7, pp. 11435–11445, 2014.
[192] D. K. Dhar *et al.*, “Pyruvate kinase M2 is a novel diagnostic marker and predicts tumour progression in human biliary tract cancer,” *Cancer*, vol. 119, no. 3, pp. 575–585, 2013.
[193] W. Yang *et al.*, “ERK1/2-dependent phosphorylation and nuclear translocation of PKM2 promotes the Warburg effect,” *Nat. Cell Biol.*, vol. 14, no. 12, pp. 1295–1304, 2012.
[194] D. Anastasiou *et al.*, “Pyruvate kinase M2 activators promote tetramer formation and suppress tumorigenesis,” *Nat. Chem. Biol.*, vol. 8, no. 10, pp. 839–847, 2012.
[195] C. L. He *et al.*, “Pyruvate Kinase M2 Activates mTORC1 by Phosphorylating AKT1S1,” *Sci. Rep.*, vol. 6, pp. 1–14, 2016.
[196] S. Angiari *et al.*, “Pharmacological activation of pyruvate kinase M2 inhibits CD4+ T cell pathogenicity and suppresses autoimmunity.,” *Cell Metab.*, vol. 31, no. 2, pp. 391–405, 2019.
[197] N. M. Alhawiti, S. Al Mahri, M. A. Aziz, S. S. Malik, and S. Mohammad, “TXNIP in metabolic regulation: physiological role and therapeutic outlook,” *Curr. Drug Targets*, vol. 18, no. 9, pp. 1095–1103, 2017.
[198] D. Crean, L. Felice, C. T. Taylor, H. Rabb, P. Jennings, and M. O. Leonard, “Glucose reintroduction triggers the activation of Nrf2 during experimental ischemia reperfusion,” *Mol. Cell. Biochem.*, vol. 366, no. 1–2, pp. 231–238, 2012.
[199] M. R. Kaadige, J. Yang, B. R. Wilde, and D. E. Ayer, “MondoA-Mlx transcriptional activity is limited by mTOR-MondoA interaction,” *Mol. Cell. Biol.*, vol. 35, no. 1, pp. 101–110, 2015.
[200] J. L. Y. Chen *et al.*, “Lactic acidosis triggers starvation response with paradoxical induction of TXNIP through MondoA,” *PLoS Genet.*, vol. 6, no. 9, pp. 1–18, 2010.
[201] B. R. Wilde, Z. Ye, T.-Y. Lim, and D. E. Ayer, “Cellular acidosis triggers human MondoA transcriptional activity by driving mitochondrial ATP production,” *Elife*, vol. 8, pp. 1–25, 2019.
[202] H. Cha-Molstad, G. Saxena, J. Chen, and A. Shalev, “Glucose-stimulated expression of Txnip is mediated by carbohydrate response element-binding protein, p300, and histone H4 acetylation in pancreatic beta cells,” *J. Biol. Chem.*, vol. 284, no. 25, pp. 16898–16905, 2009.
[203] A. D. James *et al.*, “Cutting off the fuel supply to calcium pumps in pancreatic cancer cells: role of pyruvate kinase-M2 (PKM2),” *Br. J. Cancer*, vol. 122, no. 2, pp. 266–278, 2020.
[204] J. Chen, J. Xie, Z. Jiang, B. Wang, Y. Wang, and X. Hu, “Shikonin and its analogs inhibit cancer cell glycolysis by targeting tumor pyruvate kinase-M2,” *Oncogene*, vol. 30, no. 42, pp. 4297–4306, 2011.
[205] F. Meng, Z. Lu, and K. Chen, “Knockdown of PKM2 suppresses tumor progression in human cervical cancer by modulating epithelial–mesenchymal transition via Wnt/β-catenin signaling,” *Cancer Manag. Res.*, vol. 10, pp. 4191–4202, 2018.
[206] B. Chen, J. Chen, M. G. House, K. J. Cullen, K. P. Nephew, and Z. Guo, “Role of neurofilament light polypeptide in head and neck cancer chemoresistance,” *Mol. Cancer Res.*, vol. 10, no. 3, pp. 305–315, 2012.
[207] A. Shalev, “Minireview: Thioredoxin-interacting protein: regulation and function in the pancreatic β-cell,” *Mol. Endocrinol.*, vol. 28, no. 8, pp. 1211–1220, 2014.

[208] M. F. Carey, C. L. Peterson, and S. T. Smale, “Dignam and Roeder nuclear extract preparation,” *Cold Spring Harb. Protoc.*, vol. 4, no. 12, pp. 1–4, 2009.

[209] K. Suzuki, P. Bose, R. Y. Leong-Quong, D. J. Fujita, and K. Riabowol, “REAP: A two minute cell fractionation method,” *BMC Res. Notes*, vol. 3, pp. 1–6, 2010.

[210] M. Bradford, “A rapid and sensitive method for the quantitation of microgram quantities of protein utilizing the principle of protein-dye binding,” *Anal. Biochem.*, vol. 72, no. 1–2, pp. 248–254, May 1976.

[211] U. K. Laemmli, “Cleavage of structural proteins during the assembly of the head of bacteriophage T4,” *Nature*, vol. 227, no. 5259, pp. 680–685, 1970.

[212] K. Y. Horiuchi *et al.*, “Assay development for histone methyltransferases,” *Assay Drug Dev. Technol.*, vol. 11, no. 4, pp. 227–36, 2013.

10. Curriculum Vitae

Education

2016 - 2020	PhD studies: Helmholtz Zentrum München, Helmholtz Graduate School Environmental Health; Ludwig-Maximilians-Universität München; Germany
2015	PhD studies: Doctoral School of Life Sciences and Health; University of Strasbourg; France
2013 - 2015:	Graduate studies: Biotechnology; Faculty of Biochemistry, Biophysics and Biotechnology; Jagiellonian University; Kraków, Poland
2010 - 2013:	Undergraduate studies: Biotechnology; Faculty of Biochemistry, Biophysics and Biotechnology; Jagiellonian University; Kraków, Poland

Work experience

2015 – 2020	PhD student at Schneider Laboratory, Institut de Génétique et de Biologie Moléculaire et Cellulaire, Illkirch, France and Institute of Functional Epigenetics, Helmholtz Zentrum München, Germany
2014 - 2015 (12 months):	Master thesis experiments at the Department of Physical Biochemistry; Faculty of Biochemistry, Biophysics and Biotechnology; Jagiellonian University; Kraków, Poland
2014 – Internship (4 months):	Internship at Jaworski Laboratory (Laboratory of Molecular and Cellular Neurobiology); The International Institute of Molecular and Cell Biology; Warszawa, Poland
2013 – Summer internship (2 months):	Internship at Bukau Laboratory (Biogenesis and quality control of proteins); Zentrum für Molekulare Biologie der Universität Heidelberg; Germany
2013 (2 months):	Bachelor thesis experiments at the Department of Plant Physiology and Biochemistry; Faculty of Biochemistry, Biophysics and Biotechnology; Jagiellonian University; Kraków, Poland